UNIVERSITY OF SOUTHAMPTON

Engineering Faculty

Electronics and Computer Science Department

Optoelectronics Research Centre

Jose Alfredo Alvarez-Chavez

June 2003

UNIVERSITY OF SOUTHAMPTON

ABSTRACT

FACULTY OF ENGINEERING AND APPLIED SCIENCE
DEPARTMENT OF ELECTRONICS AND COMPUTER SCIENCE
OPTOELECTRONICS RESEARCH CENTRE

High-power Fibre Lasers

By Jose A. Alvarez-Chavez

This thesis reports on the experimental study of high-power, high-energy, cladding-pumped, rare-earth (Yb^{3+}, Er^{3+}/Yb^{3+})-doped fibre lasers. Some of the main capabilities of fibre lasers such as: High brightness and thermal properties were exploited for the development of a variety of continuous wave (CW) and Q-switched devices, whose characteristics also includes compactness. Our devices could already be considered an option for several applications.

The 25-year long scientific and commercial evolution that fibre lasers have experienced is discussed in the first two chapters. The invention of Erbium-doped fibre amplifiers (EDFA's) and Internet were two major breakthroughs, which launched the need of WDM systems and laser sources. Fibre lasers, are now considered a flexible and powerful device whose technology has finally reached its maturity.

Cladding pumping is the technique employed in these experiments in order to pump double clad fibre lasers using high power, broad stripes and bars. In this work, several inner cladding shapes have been used to overcome the normally high mismatch between diode laser beams and inner cladding areas of fibre lasers.

Chapter Three consists of a review of cladding-pumped fibre lasers. It describes how inner cladding geometry and pump absorption limits the output power scalability of these devices. Nonlinear effects and amplified spontaneous emission are also studied due to their implication they have over fibre lasers performance.

Results on conventional, continuous wave (CW) fibre lasers including fibre characterization and employed launching techniques are described in Chapter Four. A new method to obtain high intensity laser beam output from an Yb^{3+}-doped, cladding-pumped, highly multimode fibre laser has been proposed. In this experiment, we propose the use of fibre tapers to increase intensity and improve beam quality. In CW regime, our results show an intensity increase of ~3.5 times with a low power penalty of ~1 dB. Also, without tapering, a maximum output power of 21-W was reached with a slope efficiency of >80%.

Using a simple set of optic elements such as a $\lambda/2$ waveplate, a polarizing beam-splitter and a bulk grating, we investigated the polarization characteristics of an Yb^{3+} fibre laser, from which we obtained 6.5 W of single polarization tunable output in the

range of 1070 to 1106 nm. As a free running laser, the system produced 18 W at 1090 nm and showed a threshold of 1.8 Watts. The experiment is our first approach for developing a reliable high-power Yb^{3+}-doped fibre source, that could be used in conjunction with optical parametric oscillators (OPO) and amplifiers (OPA) to frequency convert to a broad band of wavelengths.

Using a new design of ytterbium-doped fibre made in-house with the conventional modified chemical vapor deposition (MCVD) process, we explored the possibilities of energy storage with such a large mode area (LMA) fibre. The fibre system was capable of delivering energetic pulses of >2 mJ, which could suggest the feasibility of a pulsed fibre laser in the region of tens of milli-Joules. The experiment is described in Chapter Six, on which the experiment that uses the tapered fibre laser in Q-Switched regime is also described and compared to LMA fibre laser. Gaussian-type pulses were obtained which reached pulse energies of 0.6 mJ at 4 kHz using a tapered fibre laser and 1.3 mJ at 500 Hz using conventional laser, corresponding to average powers of 2.1 Watts for the tapered laser and 0.8 watts for the conventional laser.

Er^{3+}/Yb^{3+}-doped fibre lasers were part of our experimental work. This co-doping technique allows pumping of Yb^{3+} ions using broad-stripe high-power pump sources to reach much higher output power levels. Efficient energy transfer from excited Ytterbium ions into Erbium is achieved. From a preliminary study, the fibre laser showed a threshold of 160 mW and a slope efficiency of 49% with respect to absorbed pump power. The maximum output power was 6.2 watts at 1535 nm and a linewidth of 1 nm. One of our co-doped fibre devices produced 16.8 W of continuous wave, multimode laser power at the interesting wavelength of operation of 1550 nm.

Finally, conclusions and future work are included in Chapter Eight.

CONTENTS

Chapter 1

Introduction

1.1 Introduction

The acronym LASER stands for Light Amplification by Stimulated Emission of Radiation. Basically, a laser consists of two reflective materials, which normally are high reflection mirrors and a gain medium. Many types of lasers have been developed since 1958 when A.L. Schawlow and C.H. Townes introduced the first theoretical description of the effect of light amplification via optical masers [1]. Among them, a fibre laser has an important role as a high-intensity source with applications in many areas such as telecommunications, laser ranging, materials processing, imaging and medicine.

Many things have evolved favourably since the first demonstration of laser action inside a fibre [2]. Fibre lasers have been under considerable scientific research and industrial activity for over 25 years. During that time, one of the events that made a big impact on the telecommunications area was the invention of the Erbium doped fibre amplifier (EDFA) in 1987 [3-4], which made possible the fifth generation of lightwave systems via optical fibres. At the same time, this invention led to the development of very high speed telecommunications systems that overcame the limit established by electronic repeaters.

A succession of milestones has followed and continues. The transmission of signals at 10 Gbits/s (using more than two hundred EDFAs) was reported in 1993 by researchers from KDD and AT&T Bell Laboratories [5]. From the other hand, another big step was made when the wavelength division multiplexing technique was introduced. This technique allows the multiplexing of more than 50 channels if considering the normal spectrum bandwidth of ~40 nm.

The International Telecommunication Union (ITU) sets the standard channel spacing to 100 GHz, which correspond to around 0.9 nm at 1.55 nm, the wavelength of operation of the fifth and sixth generations of lightwave telecommunication systems.

The explosion of Internet traffic has encouraged the development of WDM systems with an ever-increasing number of channels. Each channel needs around 1 mW of power [6]. Moreover, the power budget of actual systems continues to increase with the use of gain equalizers and dispersion compensators. Fibre lasers can solve this problem if used as amplifiers, although the typical optical signal obtained from Ytterbium-doped devices, at around 1 μm, has to be converted to the wavelength of operation of today's telecommunication systems, i.e. 1300 – 1600 nm.

References to Chapter One

1.1 A.L. Shawllow and C.H. Townes, "Infrared and optical masers", Phys. Rev., Vol. 112, No. 6, 1940 (1958)

1.2 E. Snitzer, "Proposed fibre cavities for optical masers", J. Appl. Phys., Vol. 32, No. 1, 36 (1961)

1.3 R. J. Mears, L. Reekie, S.B. Poole, and D. N. Payne, "Low-threshold, tunable continuous wave (CW) and Q-switched fibre laser operating at 1.55 μm", Electron. Lett., Vol. 22, No. 3, 159 (1986)

1.4 R. J. Mears, L. Reekie, I.M. Jauncey, and D. N. Payne, "Low-noise erbium-doped fibre amplifier operating at 1.54μm", Electron. Lett., Vol. 23, No. 19, 1026 (1987)

1.5 H. Taga et. al., "10 Gbit/s, 9000-km IM-DD transmission experiments using 274 Er^{3+}-doped fibre amplifiers", proc. Conference on Optical Fibre Communications, OFC'93, paper PD1, OSA (1993)

1.6 A. Girard, "Guide to WDM Technology", EXFO Electro-Optical Engineering Inc., Quebec Canada (2000)

Chapter 2

High Power Rare Earth Doped Fibre Lasers

2.1 Introduction

The wide variety of applications where high-power fibre lasers are used place them as a suitable alternative to traditional solid state lasers which operate mainly in two regions: 1 and 1.5 μm [1]. Among these, applications in telecommunications, medicinal technologies, material processing, graphic arts and defence are found. In this document results on experimental work on Yb^{3+}, Nd^{3+} and Er^{3+}/Yb^{3+}-doped, high-power, cladding pumped fibre lasers will be discussed.

2.1.1 Fiber materials, rare earth ions, characteristics and fabrication methods

In order to predict the characteristics and performance of rare-earth-doped fibre lasers and amplifiers we need to first investigate the sprectroscopic properties of glasses doped with rare-earths. Rare earths have important characteristics that distinguish them from other optical active ions: they emit and absorb over narrow wavelength ranges, these wavelength ranges are relatively insensitive to host material, the intensities of these transitions are weak, the lifetime of metastable states are long, and the quantum efficiencies tend to be high [2].

One of the most powerful tools for obtaining the necessary information from rare earths is optical spectroscopy related to both absorption and emission transitions. The Judd-Ofelt theory is one of the basis for spectroscopic analysis from which one can obtain stimulated emission cross sections for laser transitions, the suitability of new laser hosts, to understand the performance limitations imposed on active media, and to evaluate parasitic transitions [3].

The rare earths are divided into two groups of 14 elements each. The lanthanides begin with Cerium, with an atomic number Z equal to 58, with their 4f shell filled as their main characteristic and end with Lutetium(Lu, Z=71). The actinides have their 5h shell filled and start with Thorium (Z=90) to Lawrencium (Z=103). Only lanthanides are used for optical fibre lasers and amplifiers so, only them will be considered here, due to the lanthanide contraction. This leads to an increase in effective nuclear charge as the atomic number increases, due to the imperfect screening by the 4f electrons. So, with increasing Z, the 4f electrons become more tightly bound [4].

In condensed matter the trivalent (3+) state is the most stable for rare-earth ions, that is why most optical devices use trivalent ions. The electronic configuration of a trivalent rare-earth is given by equation 2.1:

$$1s^2 2s^2 2p^6 3s^2 3p^6 3d^{10} 4s^2 4p^6 4d^{10} 4f^N 5s^2 5p^6 \quad (N=1, \ldots.14) \qquad 2.1$$

Ionisation preferentially removes the 6s and 5d electrons, and the electronic configuration for these ions, is that of the xenon structure plus a certain number (1-14) of 4f electrons. Now, because the 4f electrons interact only weakly with electrons on other ions, the Hamiltonian can be written and decomposed as:

$$H = H_{freeion} + V_{ion-staticlattice} + V_{ion-dynamiclattice} + V_{EM} + V_{ion-ion} \qquad 2.2$$

Where $H_{free\ ion}$ is the Hamiltonian of the isolated ion, $V_{ion\text{-}static\ lattice}$ and $V_{ion\text{-}dynamic\ lattice}$ represent the static and dynamic interactions of ion with the host, V_{EM} contains the interaction of the ion with the electromagnetic field and $V_{ion\text{-}ion}$ describes the interaction between rare earth ions. After using the central field approximation [2, 3], the solutions to H are products of one-electron states that are antisymmetric under the intercharge of a pair of electrons, as required by the Paulis exclusion principle. Total orbital angular momentum L and total spin S are considered to be good quantum numbers, or exact eigenvalues of the Hamiltonian. The total orbital angular moment is specified by the letters S, P, D, F, G, H, I, K…etc to represent L = 0, 1, 2, 3, 4, 5, 6, 7, …etc. respectively and each $4f^N$ state splits into several ^{2S+1}L states due to the

Coulomb interaction between the 4f electrons. L and S are vectorially added to form the total angular momentum J and the states are labelled $^{2S+1}L_J$. In the central field approximation all L, S, J and M (the azimuthal quantum number) are considered to be degenerate and define the terms of the configuration, as shown in figure 2.1

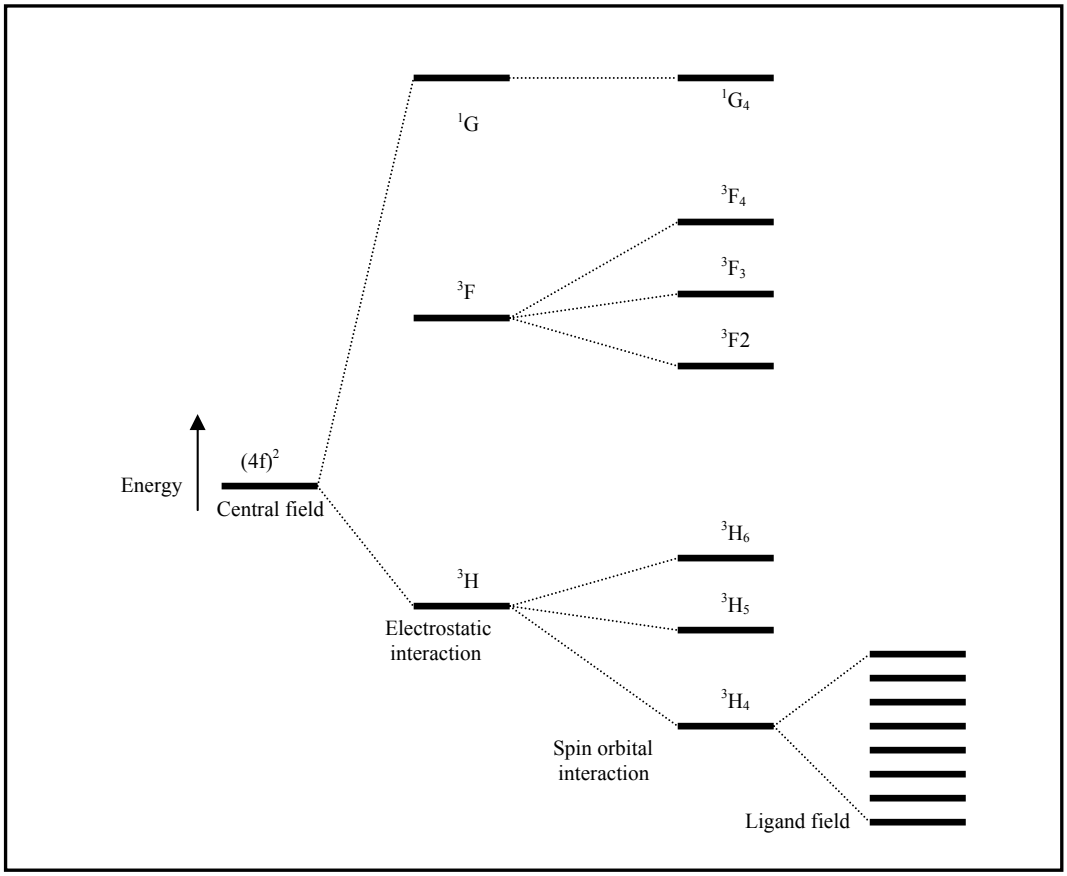

Fig 2.1 Energy level splitting hierarchy that results from various interactions[3]

Knowledge of the transition intensities of 4f-4f transitions and of absorption and emission cross sections is the first step in investigating the performance of rare-earth-doped fibre lasers and amplifiers. These transitions can be estimated using the Judd-Ofelt theory [3]. It is not my objective to provide an extensive description of the mentioned theory so, I will only briefly describe some interesting processes that take place within a fibre laser.

Although both the electrostatic and spin orbit interactions increase with increasing atomic, number, spin-orbit increases more rapidly, and LS is more significant for the high-Z rare earths.

The dynamic interaction terms in equation 2.2 are time dependant, therefore they do not lead to stationary states of the system. For luminescent devices the most important term is V_{EM}, the interaction with the electromagnetic field, which give rise to the emission and absorption of photons. This involves both the interaction between the electron charge and the electric field and the interaction between the electron spin and the magnetic field. On the other hand, the branching ratio, which has an important influence on the performance of a device based on a particular transition, appears often in the discussion of specific ions. It has a significant effect on the threshold of a laser and the efficiency of an amplifier. Other important properties that must be know to describe a luminescent device are the cross sections, which essentially represent the interaction of light and the ion as a function of frequency or wavelength of the light.

The oscillator strength $f_{a,b}$ for the transition $a \rightarrow b$ is proportional to the spectral integral of the corresponding cross section $\sigma_{a,b}$.

Useful relations for determining stimulated emissions cross sections from measurements of the excited state lifetime and emission spectrum are as follows [2]:

$$\frac{B_{a,b}}{\sigma_a} = A_{a,b} = \frac{8\pi n^2}{c^2}\int \upsilon^2 \sigma_{a,b}(\upsilon) d(\upsilon) = \int I_{a,b}(\upsilon) d\upsilon \qquad 2.3$$

$$\frac{B_{a,b}}{\sigma_a} = A_{a,b} = 8\pi n^2 c \int \frac{\sigma_{a,b}(\lambda)}{\lambda^4} d(\lambda) = \int I_{a,b}(\lambda) d\lambda \qquad 2.4$$

In these expressions $I_{a,b}(\nu)$ is the spontaneous emission rate per unit bandwidth and $I_{a,b}(\lambda)$ is the spontaneous emission rate per unit wavelength interval. $I_{a,b}$ is proportional to the emission spectrum (that could be measured). $\beta_{a,b}$ is the branching ratio, which is the fraction of all spontaneous decay processes that occur through the a, b channel or transition.

The crystal field interaction is responsible for the observed shape of the emission and absorption spectra. Considering a transition between two J multiplets, the even k terms determine the position of the Stark components for each multiplet; therefore the

wavelengths at which emission and absorption occurs. The odd k-terms determine the intensity of the process for each pair of the components involved. The crystal field terms vary from material to material, and this is the most important factor affecting the host dependence of the spectra [2].

In principle, it is possible for us to calculate the intensity and shapes of the bands if the $V_{\text{ion-static lattice}}$ is known. In practice, crystal field theory is only qualitative. Nevertheless, Judd and Offelt [2] developed a semi-empirical technique for calculating the strength of rare-earth transitions. This techniques relies on the on the assumption that the energy range occupied by the $(4f)^n$ multiplets as well as that spanned by the opposite parity states are small compared to the separation theses two sets of states.

There are some *non radiative transitions* that occur in rare earth systems. We will not cover them in here and would refer the reader to [2, 3, 5] for a complete review of processes involving emission and absorption of phonons such as: non radiative relaxation oscillation.

Now we will discuss the interaction between rare earth ions described by the $V_{\text{ion-ion}}$ term in equation 2.2. The most important manifestation of this interaction is the transfer or sharing of energy between ions. Techniques such as Yb→Er since the early days of solid state lasers to improve the pumping efficiency of devices. In contrast Er→Er energy transfer is an important dissipative mechanism for fiber amplifiers and 1550nm.

Cross relaxation is a process in which an ion in an excited state transfers part of its excitation to a neighboring ion, is generally accepted as the primary quenching mechanism for Nd^{3+}. This is illustrated in figure 2.2.

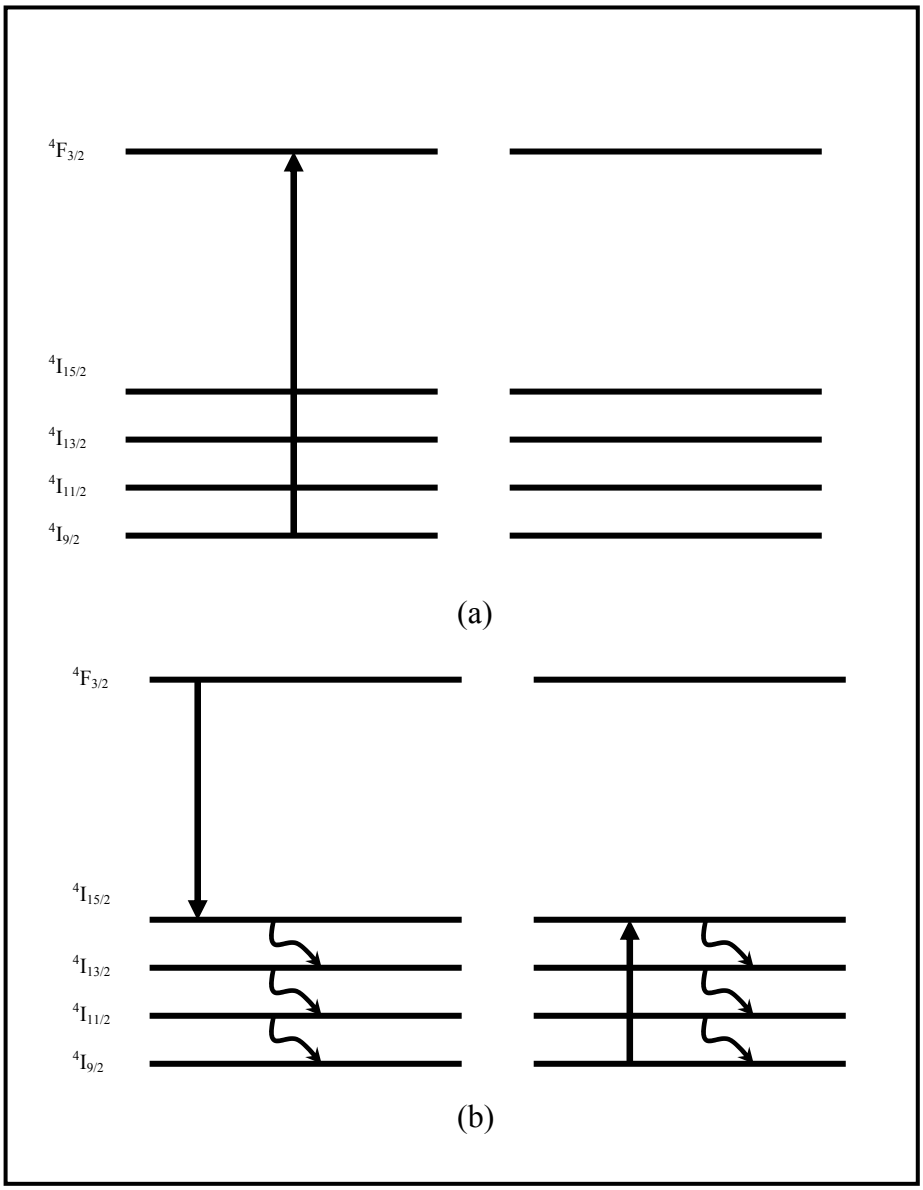

Figure 2.2 Cross relaxation process in rare-earth ions: (a) One of a pair of interacting ions is excited to the $^4F_{3/2}$ metastable state. (b) First ion transfers part of its energy to the second ion, exciting it to the $^4I_{15/2}$ state while decaying to the same level

As cooperative up-conversion requires two excited ions, it is not evident at low pumping levels. At high pump powers it appears as accelerated and non-exponential decay, the latter owing to variations in the distance or interaction strength between excited ions.

In Figure 2.2(a), if an ion excited into the metastable $^4F_{3/2}$ level interacts with a nearby ion in the ground state, the first ion can transfer part of its energy to the second, leaving both in the intermediate $^4I_{15/2}$ state. Since the energy gaps to the lower states are small, both ions quickly decay non-radiatively to the ground state. This quenching process manifests itself as a non-exponential decay that is independent of pump power, for only one excited ion is required for cross-relaxation.

The cooperative upconversion process or energy transfer is another aspect to study. It is believed to be the major cause of inefficiency for Er^{3+} devices. In references [3, 5] this process has been reviewed. Er^{3+} has no no levels between the important $^4I_{13/2}$ metastable state and the ground state, therefore cross-relaxation between an excited ion and one at the ground state can not occur. However, when two excited ions interact, one can transfer its energy to the other, leaving itself in the ground state and the other in the higher $^4I_{9/2}$ state, which in oxide glasses quickly relaxes through multiphonon emission back to the $^4I_{13/2}$. The net result of that process being to convert one unit of excitation into heat. In fluoride glasses, both excitations can be lost since radiative relaxation from the $^4I_{9/2}$ to the ground state may dominate.

This process is shown in figure 2.3 and could be compared to 2.2 to note that up-conversion is the inverse of cross-relaxation.

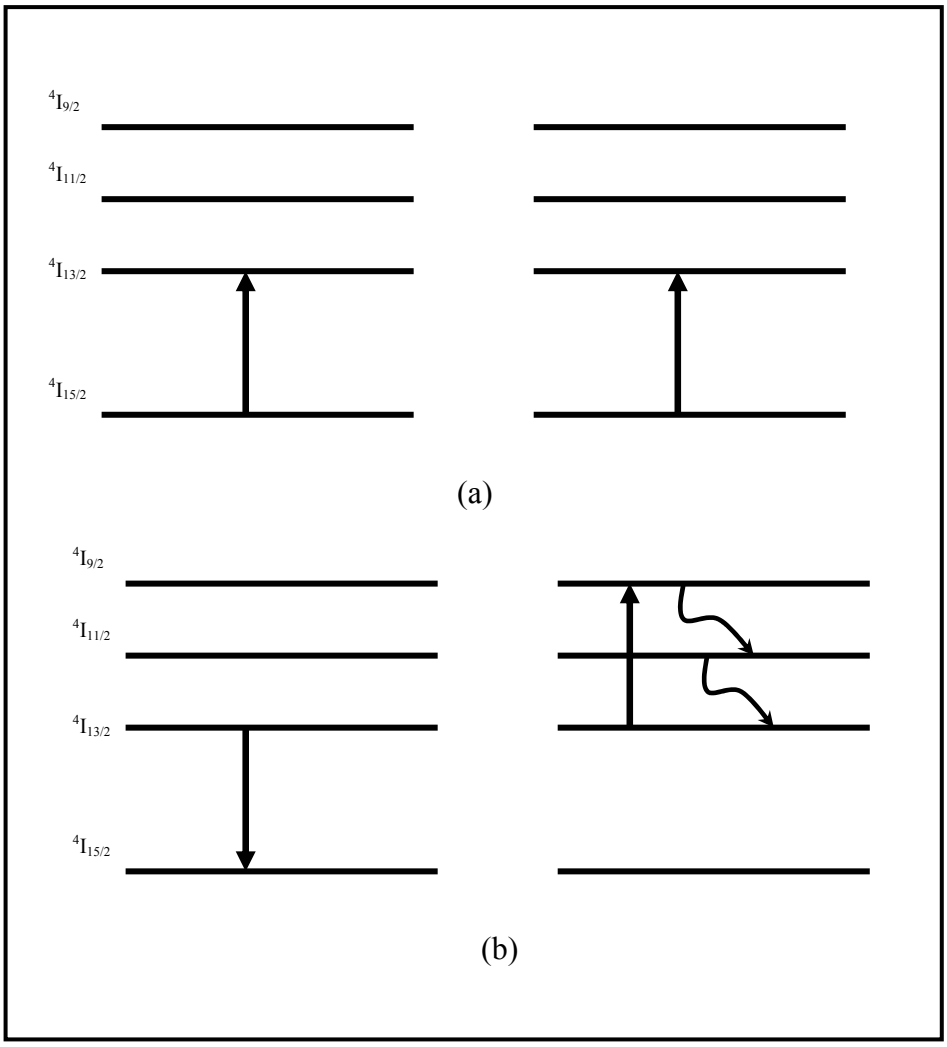

Figure 2.2 Cross relaxation process in rare-earth ions: (a) both interacting ions are excited to the metastable $^4I_{13/2}$ level. (b) The donor ion transfers all its energy to the acceptor, leaving itself in the ground state and the acceptor in the $^4I_{9/2}$ state.

The reduction of quantum efficiency of an ion with increasing concentration of that ions is known as *concentration quenching*. It manifests itself as a shortening of the excited state lifetime, although it may not be observable under all conditions. Taking data from ref. [2] Table 2.1 is shown below.

Glass Type	*Quenching concentration ($10^{20}cm^{-3}$)*
Silicate	3.9 - 6.0
Phosphate	3.9 – 8.6
Fluorophosphate	3.4 – 4.0
Fluorozirconate	4.2
Fluoroberyllate	3.8 5.3

Table 2.1 Nd^{3+} concentrations resulting in a factor of 2 reduction in $^4F_{3/2}$ lifetime

There is empirical equation that describes the observed lifetime τ_{obs} to the ion concentration ρ is the following:

$$\tau_{obs} = \frac{\tau}{1+\left(\frac{\rho}{Q}\right)^{P}} \qquad 2.5$$

In equation 2.5, τ_0 is the lifetime in the limit of zero concentration and Q is the quenching concentration given in table 2.1. The typical value of concentration for Nd^{3+} is ρ=2.

There are other deleterious processes such as the one that involves energy transfer to the OH^- complex and excited state absorption . And they will not be studied in deep in this thesis since excited state absorption is not present in Yb^{3+}-doped fibre lasers.

2.1.2 Fibre lasers description

Lasing takes place in a fibre due to the amplification of the stimulated emission that is observed when pumping a rare-earth (RE) doped material. Among the most common active materials that have been used for this purpose are: Erbium (Er^{3+}) emitting at 1.55 μm, Neodymium (Nd^{3+}), Ytterbium (Yb^{3+}), with an output wavelength in the

region of 1 μm and Praseodymium (Pr^{3+}) lasing at 1.3 μm [6, 7], all of them. Work on fibre lasers doped with Yb^{3+} constitutes the basis of this thesis.

Basically, a fibre laser consists of a RE-doped core with dimensions in the order of several microns or tens of microns depending on the pumping scheme. A cladding that can be either a phosphosilicate or germanosilicate-doped glass surrounds the doped core. It can have different shapes: circular, rectangular, or a more complex geometric form [8]. The coating material is normally a low-index ultra-violet-curable polymer, which provides the necessary numerical aperture for the pump light in the so- called inner cladding.

In Figure 2.3 the basic structure of a fibre laser is showed.

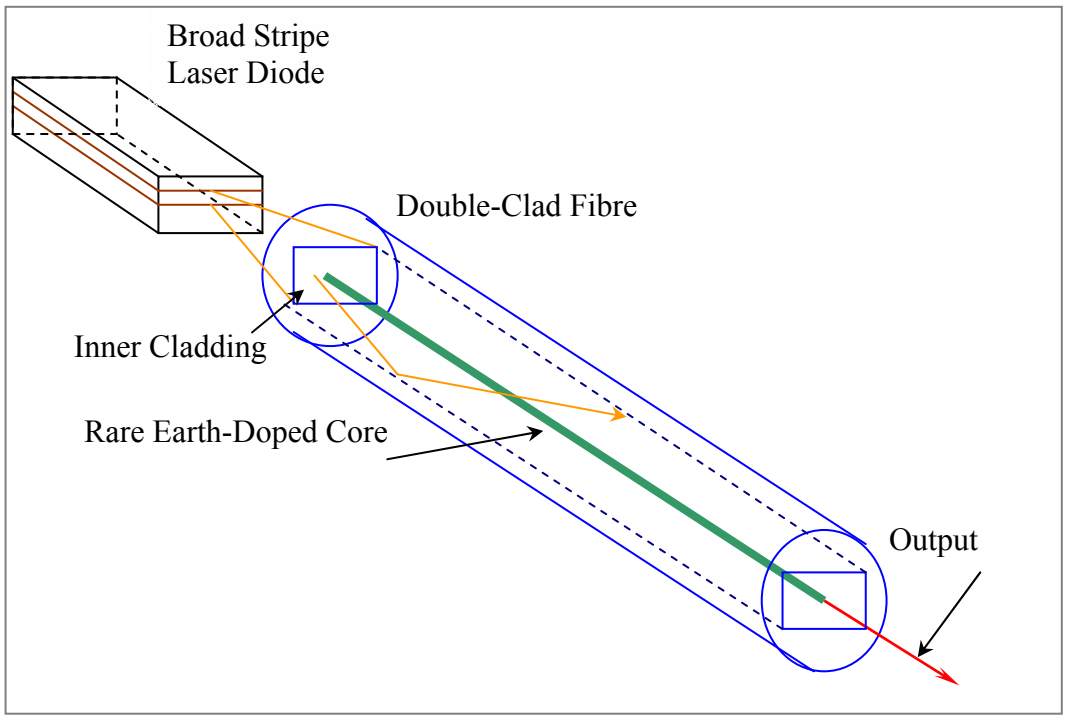

Fig. 2.3 Rare earth-doped fibre laser

The necessary feedback for the photo multiplication process is normally provided by the 4% Fresnel reflection from the flat cleaved ends. After pumping the device, reflection from the facets helps create the laser cavity. The fibre lasers developed for this work were fabricated in-house using the MCVD technique.

The main characteristics such as gain, optical efficiency, device length, pump absorption, output power and wavelength will be discussed in the following chapters.

Ytterbium is a relatively simple material in terms of absorption and emission [9]. It shows broad spectral bands for both emission and absorption. Laser operation is typical at 1 μm. The use of efficient frequency discrimination can be introduced to suppress lasing at the natural emission wavelengths. These discrimination is performed by introducing fibre Bragg gratings (FBG) inside the laser cavity. FBG can be written directly into the RE-doped core to avoid splice losses. Absorption and emission spectral characteristics of Ytterbium ions in silicate glass are shown in figure 2.4.

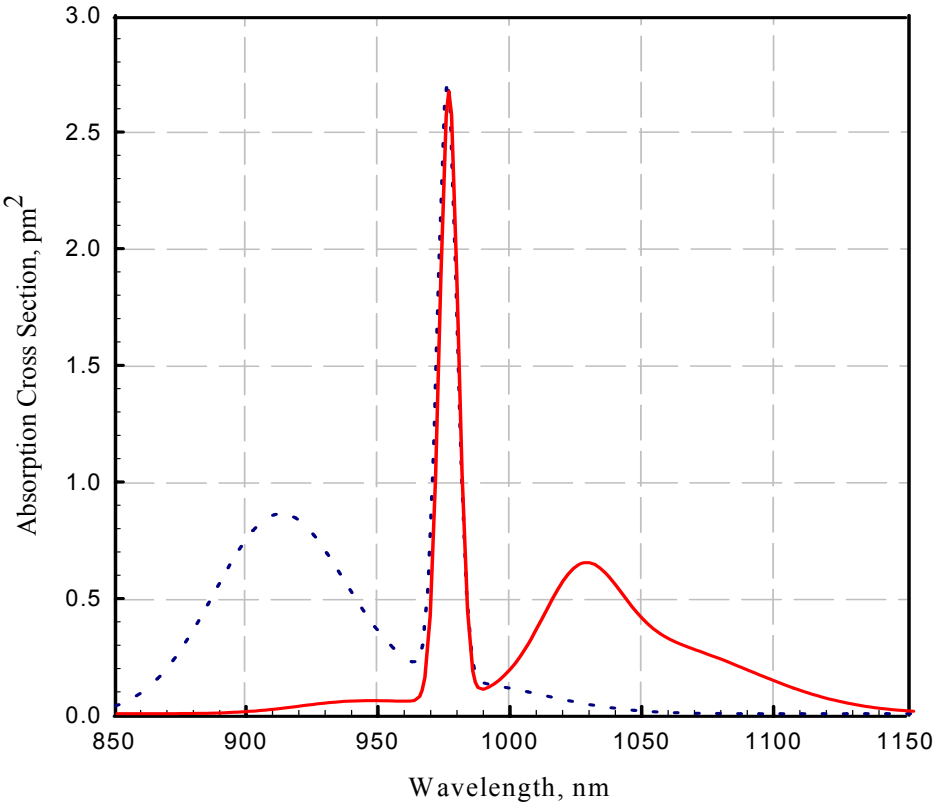

Figure 2.4 Absorption and emission characteristics of Ytterbium [5]

The cross section of a rare earth is a useful concept for understanding how these materials absorb the pump and emit laser signal. Cross section will be defined in Chapter 3.

2.1.3 Evolution of fibre lasers

Maiman made the first demonstration of laser action in ruby in the early 1960's [10]. The first fibre laser was reported in 1962 by Koester and Snitzer [1]. In their experiment they used 1-m, neodymium-doped, glass core surrounded by a lower index clear glass and pumped using a flashtube. In general the paper outlines the advantages of incorporating a laser gain medium into a dielectric waveguide. The use of glass-made waveguides for laser resonators led to the development of neodymium-doped fibre lasers, initially multi-moded and side-pumped [12]. Although the side pumping of the first fibre lasers was inefficient and only low energy Q-switched lasers could be implemented, increased pump efficiency was achieved when longitudinal pumping was proposed by Stone and Burrus in 1973 [13]. Moreover, advances in fibre fabrication techniques, leading to efficient rare-earth doping of single mode fibres, and the development of high power laser diodes as pump sources have increased the interest in fibre laser technology.

Since its invention in 1985 by D.N. Payne and his group [14], the Erbium-doped fibre amplifier (EDFA) has attracted great interest principally because of its major applications in the Telecommunications industry. Nevertheless, the applications of EDFA's have not been confined to that area and there has been growing interest in the amplification of pulses for development of a source that can provide very high peak output powers. In that context, where the specific wavelength of operation is no longer critical, amplifiers based on other RE dopants appear to be a suitable option.

Yb3+-doped fibres are an example of these relatively new rare-earth dopants. After the first report of laser action in Yb^{3+}-doped silicate glass by Etzel, Gandy and Ginther in 1962 [15], it had until recently attracted relatively little interest as a laser-active ion. It had in part been overshadowed by the Nd^{3+} ion with its important advantage of a 4-level transition, whereas Yb^{3+} has only three levels and quasi 4-level

transition although this can also be considered as an advantage that is going to be discussed later.

Ytterbium offers high output power and excellent power conversion efficiency. The atomic level structure of Ytterbium is simple [16]. As can been seen in figure 2.3 only two energy levels are relevant. It consists of two manifolds; the ground level manifold $^2F_{7/2}$ which contains three Stark levels and a well separated excited manifold $^2F_{5/2}$ with two Stark levels at 10000 cm^{-1} above the ground level. It is for that reason that excited state absorption (ESA) is negligible at both pump (915 nm) and laser (1 μm) wavelengths. This energy gap also prevents concentration quenching and non-radiative decay via multi-phonon emission from $^2F_{5/2}$ [16].

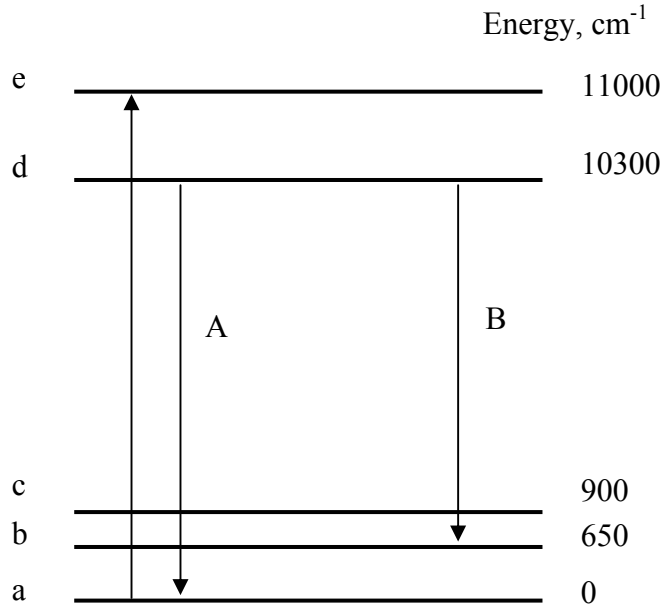

Fig. 2.5 Atomic level structure of Ytterbium

The closeness of the pump and laser wavelengths in combination with features described above contribute to the normally high efficiency (as high as 75% with respect to incident diode pump power) that can be obtained from Yb^{3+}-doped fibre lasers.

Some of the important characteristics of Yb^{3+}-doped fibre lasers to be discussed in this thesis are:

- High efficiency: >70% with respect to incident pump power
- High CW power; 110W so far but even much higher powers can be expected with the use of novel pumping techniques
- Immunity from thermal lensing and beam steering
- Simplicity of cooling due to high surface: volume ratio; no water-cooling system required
- Flexibility in terms of pump wavelength required
- Broadly tuneable
- Fibre coupled output

2.1.4 Cladding pumped fibre lasers (CPFL)

Given the fact that stimulated emission is the process through which both lasers and amplifiers operate, they show a similar behaviour. A laser without feedback constitutes an amplifying medium or amplifier, and any amplifier can be converted into a laser through a suitable feedback mechanism which could be a ring cavity or, as it has been done often in our experiments, by flat cleaving the fibre facets. The optical gain achieved after lasers and amplifiers are pumped to reach high population inversion is the way of operation of these devices. Both of them can be classified depending on the number of levels involved in lasing action. In general, there are three-level and four-level lasers and amplifiers [17]. The dopant ions are excited to a higher energy level via absorption of photons from the pump source. Rapid relaxation oscillation of the excited ions then takes place into a lower energy excited level. The stored energy is then used for amplification of the signal beam through stimulated

emission. The energy state occupied by the de-excited photons after stimulated emission is the difference between three and four-level systems.

The fibre devices described in this work are normally end-pumped by a laser source, usually a semiconductor diode. In order to do that, an imaging system is needed between the pump source and the fibre facet. The imaging system is designed to achieve the maximum launched power in the fibre. Numerical aperture (NA) and physical dimensions of both the fibre and semiconductor diode are the two main factors that have to be taken into account for the design of the imaging system. If a match of these two parameters is achieved for both the doped core and pump source, good launching efficiency should be expected.

Launching efficiency cannot be improved by using an imaging system when a single-mode fibre is pumped by high-power laser diodes. This is in part due to what brightness fundamental theorem states. It says that the brightness of a source is an invariant quantity, unchangeable by a lens or any other passive optical system [18]. The concept of brightness is useful to explain how important it is to achieve a high launching efficiency. Brightness of a source is defined as the power emitted per unit area per unit solid angle. So, the larger the divergence (solid angle), the lower the brightness of an emitter is.

Moreover, in order to increase the output power of laser diodes the diode facet area must be increased, because the damage threshold of the semiconductor material also limits diode brightness. This limits some industrial applications since light from large area diodes shows poor beam quality and cannot be focused to doped core dimensions. To overcome this problem, a new type of fibre device had to be developed as it also was limiting applications in Telecommunications field, which only use light coupled into the single mode core.

The power of conventional fibres could also be increased by polarization and wavelength combination of multiple diodes onto a single fibre. Practical implementation of this approach is limited by the size, complexity and losses of the components that can increase in number exponentially.

Double clad fibres offer a solution for increasing the amount of pump power from diode lasers into rare-earth doped fibre lasers. As can be seen in figure 2.6, a second cladding that surrounds the doped core constitutes a second larger waveguide on which the pump can be launched. High power, low brightness sources can then be used as pump for fibre lasers.

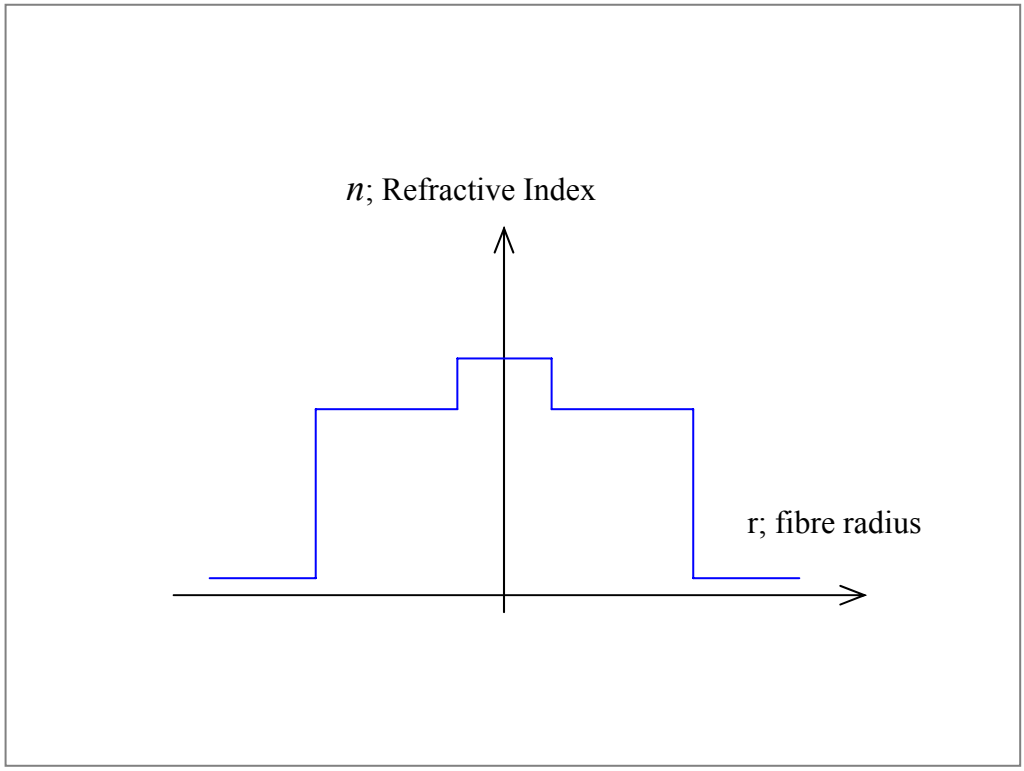

Fig. 2.6 Refractive index profile of a double clad fibre

Since the light overlaps with the doped core to some degree, it pumps the core as it propagates down the fibre. Depending on the shape of the inner cladding the pump power absorption could be higher as more skew modes can cross the core and be absorbed by the rare earth.

Achieving high laser efficiency depends on optimising the coupling of the pump radiation from the inner cladding to the core. As this coupling is relatively weak due to the small area ratio $A_{core}/A_{cladding}$, one needs to determine the optimising condition for available cladding shapes. Because a shape that increases the intensity in one region would violate the brightness theorem, the ideal situation is that the pump

remains uniform along the fibre, so that the initial effective absorption coefficient is maintained.

To determine whether this is the case or not, one needs to unfold the multiple reflections experienced by pump rays as viewed from an end of the fibre. For instance, fibres with the core centred within a circular inner cladding have a weak absorption because the skew rays miss the core and only the doped region absorbs the meridional rays.

Cross sections of some of the inner cladding shapes used in cladding-pumped fibre lasers are shown in figure 2.7.

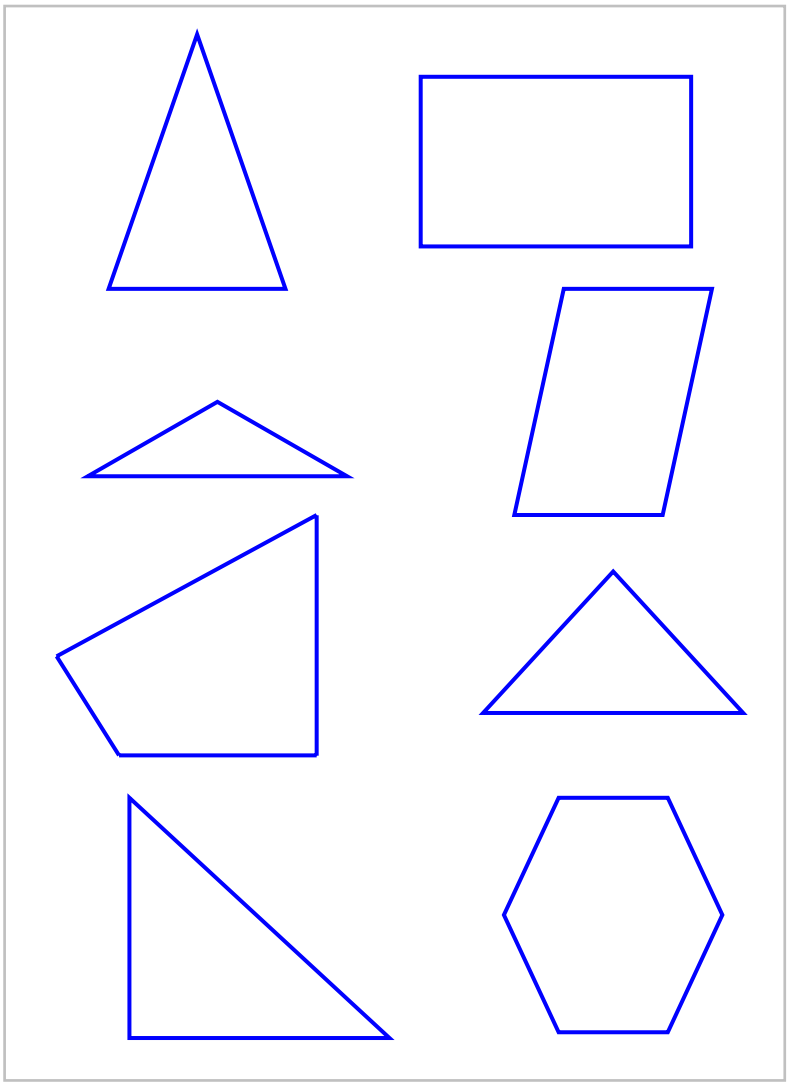

Figure 2.7 Inner cladding cross sections [4]

The initial effective absorption coefficient in this case is $\alpha_{core}A_{core}/A_{cladd}$ [8], i.e. the same as in any other shape although during propagation the meridional rays are depleted, the intensity around the core is decreases, and the overall absorption increases.

On the other hand and depending on the cladding shape, if the pump power is reflected infinitely in all directions and fills the cross section of the inner cladding uniformly (with no overlaps or voids) then all rays will experience equal absorption, the pump field will remain unchanged and the overall absorption coefficient does not drop throughout the length of the fibre. If non-uniform filling of the cladding is present, the overall absorption will drop because of the unequal absorption that pump rays will experience. Practical shapes that provide uniform absorption (up to a certain degree) are shown in figure above.

As previously mentioned, one of the difficulties encountered when the first cladding is circular is that only few pump modes will cross the doped core and be converted into signal. A first solution to this was to offset the core from the centre of the first cladding. This solution typically provides an increase in absorption of 28% in an Nd^{3+}-doped fibre. This estimation emphasizes the importance of a high dopant concentration that is also uniformly distributed across the first cladding.

As a consequence of low and non-uniform dopant concentration, the length of a fibre laser could be of a few hundred meters, with high scattering losses and high laser threshold.

A second solution to increase pump absorption is shown in figure 2.7. Almost any shape but circular supports modes that can fill the multimode cladding. As was mentioned above, a rectangular shape is particularly attractive because it matches the output pattern of a multi-stripe laser diode, thereby minimizing the area of the first cladding and thus the required fibre length. As will be discussed later, another design parameter involves bending the fibre with a certain radius that is determined by limiting bend losses.

In figure 2.8, one can see the variation of absorption versus dopant concentration. It can be seen that absorption tends to saturation along with the increasing length, for circular double clad fibres.

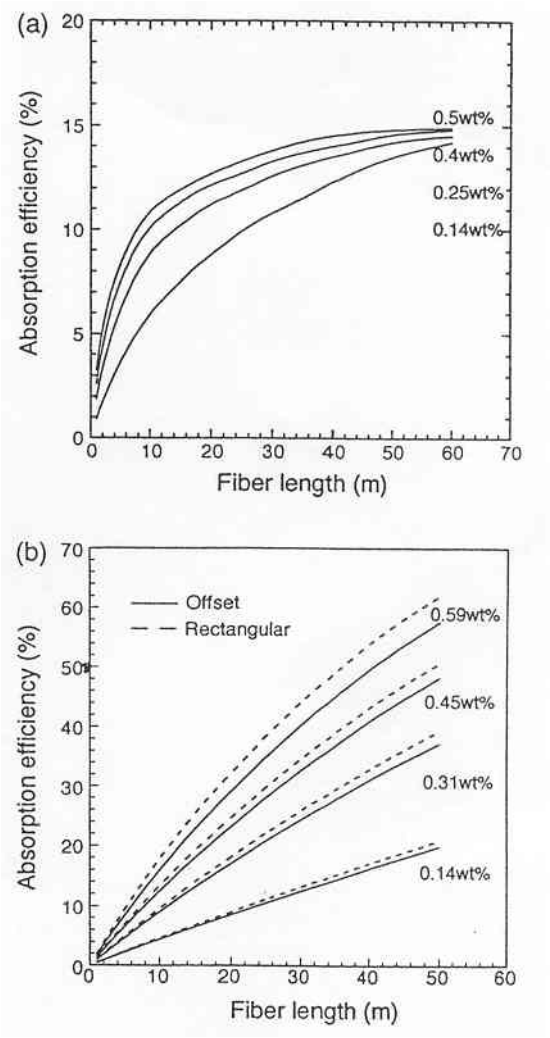

Figure 2.8 Absorption efficiency versus doped concentrations for (a) circular, (b) offset and rectangular double cladding fibres. From Liu and Ueda [19].

The fibre parameters are core diameter = 12 μm; bend radius R = 150 mm; cladding size = ϕ400μm for circular and offset, 210x600μm for rectangular and offset distance ρ=150μm. It can be seen that at the beginning of the fibre (figure 2.6) the absorption

increases with length sharply. The increase becomes smaller and smaller after a certain distance. The phenomenological explanation and original discussion of absorption versus fibre length was performed by Bedo et. al. in [20]. In that paper, they report the calculation of absorption (in figure 2.8) using a rectangular double clad fibre with dimensions *a* and *b* for the horizontal and vertical axis respectively, core radius *r*, a group of pump rays that have the same projection direction on the entrance face of the fibre and which are launched into the fibre at a given point P(x_0, y_0) with an angle θ and then reflected by the four surfaces A_1, A_2, B_1, B_2, as discussed in section 3.3 and figure 3.5 of this thesis.

It could have been possible to think about improving launching efficiency by increasing the core size that could be adapted to the emitter size of a high power pump source. But, the increased fibre diameter results in reduced beam quality and multimode operation. The degree to which a laser beam is highly collimated and spatially coherent is referred to as the beam quality of the laser beam. It is also sometimes phrased as the times diffraction limited value of the beam. The spatial beam quality is a critical parameter in the performance of a laser in a wide range of applications, as well as a critical design parameter in designing optical beam trains and focusing and imaging systems for such lasers. This is because the spatial beam quality determines how tightly the laser beam can be focused, or how little it will spread while propagating to the far field.

As a practical consideration, the observation of a Gaussian intensity profile in the output beam from an experimental laser is often taken as a sign that the laser is indeed producing a high quality beam. From theoretical point of view, it is known that laser oscillators using stable resonators will typically oscillate in the lowest and perhaps higher-order Hermite-Gaussian or Laguerre-Gaussian transverse modes. It is well recognized that the lowest order or TEM_{00} mode from such cavity provides an ideal beam profile. Nevertheless, this assumption is not always valid. For instance, one can perform a superposition of five high-order Laguerre-Gaussian modes, which could include some percentage of every one of theses modes: LG_{01}, LG_{10}, LG_{11}, LG_{20}, and LG_{21}. The M^2 value of this mixture of modes would approximately be 3.5, so the

beam would be 3.5 times diffraction limited as compared to a genuinely Gaussian beam.

From a physical interpretation, the beam quality factor M^2 is a measure of the near field times far-field space-beamwidth product of any arbitrary real beam normalized to the space-beamwidth product of an ideal TEM_{00} Gaussian beam.

The propagation of a real beam depends on the beam quality factors M^2_x and M^2_y defined by [21]:

$$W_x(x) \cong M_x^2\left(\frac{\lambda}{\pi W_{0x}}\right) \qquad (2.6)$$

$$W_y(z) \cong M_y^2\left(\frac{\lambda}{\pi W_{0y}}\right) \qquad (2.7)$$

Where W_x and W_y are the real beam spot sizes and W_{0x} and W_{0y} are the waist spot sizes at waist locations z_{0x} and z_{0y}.

Furthermore, one can also note that the spot size ω as conventionally defined for a Gaussian beam is related to the transverse variance σ^2 or standard deviation σ of a TEM_{00} beam by $\omega=2\sigma$. Then, we can propose that the "real beam spot sizes" W_x and W_y for any arbitrary non-Gaussian beam at any place z could be defined as $W_x(z)=2\sigma_x(z)$ and $W_y(z)=2\sigma_y(z)$, where $\sigma_x(z)$ and $\sigma_y(z)$ are the time-averaged standard deviations of x and y evaluated on the real beam intensity profile I (x, y, z) at that plane z.

The propagation of the real beam in addition to being dependent on the inverse waist size also depends on the so-called beam quality factors M_x^2 and M_y^2 in each transverse direction. This beam quality factor as we have defined it, is always $M^2>1$, with M=1 only for the ideal TEM_{00} Gaussian beam.

Thus, one can say that the use of an inner cladding to pump the fibre laser is the origin of the so-called cladding pumping technique [22]. With this technique, the laser emission generated in the core can have brightness thousands of times higher than that of the laser diodes. Powers exceeding 150 W have been coupled from four polarization combined laser diodes into high NA fibres with a 250 μm diameter. Using cladding pumping technique, SDL Corporation has achieved up to 110 W of single mode lasing signal at 1064 nm by using tens of meters of Yb3+-doped fibre [23]. Commercial fibre laser devices working in continuous wave regime and output powers of 5, 10 and 20 W at ~1 μm have a lifetime of several thousands of hours [24].

2.1.5 Main results

The work that has been carried out for the development of rare-earth fibre lasers involved continuous experimentation on Yb^{3+} and Er^{3+}/Yb^{3+}-doped fibre lasers. We have adopted the cladding-pumping technique to improve launching efficiency compared to core-pumping technique. Initially, cladding pumping allowed us to launch up to ~40 watts of pump power at 915 nm in a ~200 μm double clad fibre. The fibre was pumped from both ends with 2 x 60 Watt broad stripe diode bars. With this fibre laser we obtained a stable, 21 watts of continuous wave laser signal at 1060 nm.

Beam quality is an important characteristic for fibre lasers if we want to find applications in telecommunications. The small overlap between the pump and the rare-earth-doped core leads to a small pump absorption, e.g., 1 dB/m. Larger core and absorption is often desirable, especially if we want to maintain single-mode operation. The insertion of a tapered section inside the laser cavity constitutes an option for increasing the intensity and consequently enhances the beam quality at the output of a fibre laser by suppressing high-order modes. We tapered-down sections of our Ytterbium-doped fibres and measured their beam quality, compared them with normal, un-tapered fibre lasers. Tapered fibre lasers showed an increase in intensity by a factor of 3. The power penalty was only ~1 dB. In general, the high-power, cladding-pumped fibre lasers with tapered region results in significant selection of transverse modes, increasing the brightness. A low power penalty had to be paid for a nearly diffraction limited output beam.

With respect to pulsed fibre lasers, some experiments were performed with fibres especially designed to increase the energy storage capacity that is normally limited by gain volume. This parameter was increased in our fibres (fabricated in-house) by designing the doping profile, reducing the numerical aperture of the core and by increasing the NA of the inner cladding that allowed cladding pumping of the fibre.
After fabricating the fibre pre-form, a Q-switched, cladding pumped, large mode area fibre laser was set-up. The device was capable of generating up to ~2.3 mJ of output pulse energy and more than 5 watts of output average power in a beam with an M^2 =3. At the time of publication, this was the highest energy per pulse reported for a fibre laser.

A high-power, linear-polarization, narrow-linewidth, single-mode laser source at 1064 nm can be used to pump an optical parametric oscillator (OPO) for generating broad-band sources. In our experiment, we developed an Ytterbium-doped fibre laser capable of delivering 6.6 Watts at 1090 nm with linearly polarized output beam. It has a 0.2 nm linewidth. The laser showed a tuning range of ~40 nm, from 1070 nm to 1100 nm, with a good power and polarization stability.

In summary, the main results reported in this thesis include:

- Cladding-pumped, Yb^{3+}-doped fibre laser with 21 Watts CW output at 1060 nm

- High-power, cladding-pumped, Yb^{3+}-doped fibre laser with tapered region inside the laser cavity. Intensity increase by a factor of 3 with power penalty of ~1 dB with respect to un-tapered fibre laser

- High-energy, cladding-pumped, large-mode area fibre laser capable of delivering 2.3mJ of pulsed energy at ~500 Hz. 5 Watts of CW average output power

- 6.6 Watts output power, single polarization, narrow-linewidth (~0.2nm) and widely tuneable (~40 nm) cladding-pumped fibre laser.

- Development of high-power, cladding pumped, Er^{3+}/Yb^{3+}-doped fibre laser with different configurations. Highest output power reported for this type of co-doped lasers: 16.8 W with a slope efficiency of up to 50%.

2.1.6 Objectives of the work

The main objectives of the work are the following:

- Development of reliable, compact, efficient, high-power, Ytterbium (Yb^{3+}), and Er^{3+}/Yb^{3+}-doped fibre lasers pumped by broad stripe lasers diodes

- To study the effects and limits of power scaling in high-power Yb^{3+}-doped fibre lasers

- To develop reliable Yb^{3+} and Er^{3+}/Yb^{3+}-doped fibre lasers and to study their operation in both continuous and Q-switched (pulsed) regime

- To employ cladding-pumping technique for the development of efficient fibre lasers with the highest possible output power taking into account the pumping diode bars available in-house

- Development of stable, single polarization, Yb^{3+}-doped fibre lasers that can be used in conjunction with optical parametric oscillators for frequency-convert into a broad wavelength range.

2.2 Outline of the thesis

This thesis reports on the research work I have done in the development of high-power, cladding pumped fibre lasers and amplifiers doped mainly with ytterbium and neodymium. It is organized in 8 Chapters. The first two chapters provide the reader with a brief introduction to the topic. A description of fibre laser devices including their evolution is contained in second chapter. The cladding pumping technique is also

discussed in this chapter. The objectives of this work are also listed in Chapter Two along with the main experimental results.

Chapter 3 describes how the process of amplified spontaneous emission (ASE) can, for instance, limit the maximum energy obtained from a fibre laser operating in Q-switched regime. Some basic calculations of gain and ASE power in cladding-pumped fibre lasers are also included. This chapter also discusses the advantages of cladding pumped fibre lasers over the end pumping of single mode fibres. Several cladding shapes have been proposed to increase pump power absorption by the normally ytterbium-doped and neodymium-doped core of our fibre lasers. The fibres that have been used in the experiments were fabricated in-house with circular, D-shaped, rectangular and other cladding shapes. A comparison between cladding pumping and core pumping 3 is also included in this chapter. The power scaling that has been obtained in fibre lasers via the use of the cladding pumped technique is also reported.

In Chapter Four the initial experiments on conventional, continuous wave (CW), Ytterbium-doped fibre lasers are described. The cut-back technique that is used to determine optimal laser cavity, slope efficiency, launching techniques and threshold power are introduced. Results on a CW Yb^{3+}-doped fibre laser with 21 Watts of output power at 1064 nm are discussed. Also, a technique to improve brightness of an otherwise highly multimode fibre laser was proposed. It includes a tapered section inside the laser cavity, which resulted in an increase of this parameter by a factor of 3 with a low power penalty of 1 dB. A description of the beam-shaped diode bar used in the experiment as a pump source at 915 nm is included.

A single polarization, high-power ytterbium-doped fibre laser was studied and is reported on Chapter Five. Using a simple set of passive optical elements such as $\lambda/2$ wave-plates, polarizing beam-splitters and bulk gratings the polarization characteristics of an Yb^{3+}-doped fibre laser were studied. 6.5 Watts at 1060 nm of single polarization laser signal were generated. The laser demonstrated a tuneable operation in a range from 1070 nm to 1106 nm. As a free-running laser, the system generated 18 W at 1090 nm. The experiment is an option for developing a reliable high-power, Ytterbium-doped, single polarization fibre source that can be set-up in

conjunction with optical parametric oscillators (OPO) for a frequency-conversion system capable of generating laser signal of a broad range of wavelength.

The rapid build-up of amplified spontaneous emission (ASE) and the onset of lasing due to the high gains achievable within single mode lasers limit the energy storage to a few tens of micro-Joules. In chapter 6, an experiment with a large mode area fibre laser that allows maximum overlap and preferential gain to the fundamental mode is discussed. With this fibre, a q-switched, cladding pumped, Yb^{3+}-doped fibre laser that is capable of generating high energy pulses, in the order of a few milli Joules at repetition rates under ~500 Hz.

Chapter Eight reports on experimental work on Er^{3+}/Yb^{3+}-doped fibre lasers. The co-doping technique allows pumping Ytterbium ions into excited energy levels using for instance, high-power broad-stripe diode bars. These excited ions then transfer their energy to Er ions via cross relaxation between adjacent ions of Er and Yb, providing another option for pumping fibre lasers or amplifiers.

Finally, conclusions and future work are included in chapter 9.

References to Chapter Two

2.1 Muendel M. et al, "High power fibre lasers", in Proc. Conference on Lasers and Electro-optics, paper CthD1, Baltimore USA (1999)

2.2 Miniscalco W.J., "Optical and electronic properties of rare-earth ions in glasses", in Rare-earth-doped fibre lasers and amplifiers, Marcel-Dekker, USA (1993), Michel Digonnet ed.

2.3 Sudo S., Optical fiber amplifiers: materials, devices and applications, Artech House Inc., USA (1997)

2.4 Wybourne B.G., "Spectroscopic properties of rare earths", Wiley-Interscience, USA, 1965

2.5 France P.W., "Optical fibre lasers and amplifiers", Blackie and Son Ltd. UK, (1991)

2.6 Desurvire E., "Erbium-doped fibre amplifiers", Wiley Inter-Science, USA (1994)

2.7 Digonnet M., "Rare-earth doped fibre lasers and amplifiers", Marcel-Dekker, USA (1993)

2.8 Muendel M., "Optimal inner cladding shapes for double-clad fibre lasers", in Proc. Conference on Lasers and Electro-optics, paper CTuU2, USA (1996)

2.9 Zou X., Toratani H., "Evaluation of spectroscopic properties of Yb^{3+}-doped glasses", Physical Review B, Vol. 52, No. 22, 15889-15897, (1995)

2.10 Maiman T.H., "Optical and microwave optical experiments in Ruby", Physical Review Letters, Vol.4 No. 11, 564-566, (1960)

2.11 Snitzer E., "Proposed fibre cavities for optical masers", Journal of Applied Optics, Vol. 32, No. 1, 36-39 (1961)

2.12 Snitzer E., "Optical maser action in Nd^{3+} in a Barium crown glass", Physics Review Letters, Vol. 7, No. 12, 444-446, (1961)

2.13 Burrus C.A., Stone J., "Nd^{3+}-doped SiO_2 lasers in an end-pumped fibre geometry", Applied Physics Letters, Vol. 23, No. 7, 388-389, (1973)

2.14 Mears R.J., Reekie L., Juancey I.M., Payne D.N., "Low-noise Erbium-doped fibre amplifier operating at 1.54 μm", Electronics Lett., Vol. 23, No. 19, 1026-1028, (1987)

2.15 Etzel, H.W., Gandy H.W., Ginther R.J., "Stimulated emission of infrared radiation from ytterbium-activated silica glass", Applied Optics, Vol. 1, 534, (1962)

2.16 Pask, H.M., Carman R.J., Hanna D.C., Tropper A.C., Mackechnie C.J., Barber P.R, Dawes J.M, "Ytterbium-doped silica fibre lasers: versatile sources for the 1-1.2 μm region", IEEE Journal of Selected Topics in Quantum Electronics, Vol. 1, No. 1, 2-13 (1995)

2.17 Yariv A., *Optical Electronics in Modern Communications*, 5th Ed., Oxford University Press, Chapter 6, 185-194, (1997)

2.18 Hecht E., *Optics*, 2nd Ed., Addison-Wesley, Oxford (1997)

2.19 Liu A., Ueda K., "The absorption characteristics of circular, offset, and rectangular double-clad fibres", Optics Communications Vol. 132, 511-518, (1996)

2.20 Bedo S., Luthy W., Weber H.P., Optics Communications, Vol. 99, p 331, (1993)

2.21 Siegman A.E., "Defining and measuring laser beam quality", in *Solid State Lasers: New Developments and Applications*, Inguscio M. and Wallenstein R. Eds., Plenum Press, USA (1993)

2.22 Snitzer E., Po H., Hakimi F., Tumminelli R., McCollum B.C., "Double clad, offset core Nd Fibre laser", in Tech. Digest Optical Fibre Sensors Conference, paper PD5, USA (1988)

2.23 Dominic V., MacComarck S., Waarts R., Sanders S., Bicknese S., Dohle R., Wolak E., Yeh P.S., Zucker E., "110-W fibre laser", Electronics Letters, Vol. 35 No. 14, 1158-1160, (1999)

2.24 SDL Corp. Catalogue

Chapter 3

Review of cladding-pumped fibre lasers

3.1 Introduction

We have already discussed basic characteristics of fibre lasers and mentioned their main applications. In this chapter we are going to discuss the evolution, advantages and disadvantages of cladding pumping technique applied to double clad fibre lasers. We also intend to compare cladding pumping with core pumping in order to justify the use of this technique for scaling the launched pump power available from broad stripe diode bars. Altogether, the advantages from higher power diode bars and the possibility of obtaining quasi-single mode operation from double clad fibres is a good combination that results in suitable high power sources for present needs in several fields.

3.2 Power scaling in cladding-pumped fibre lasers

Cladding pumping intends to increase the absorption of pump energy from broad stripe diode bars into rare earth doped cores of fibre lasers and amplifiers. The following discussion on power scaling will be divided in terms of the dopant inside the fibre laser. From the group of rare earths, only three dopants will be considered: Ytterbium, Neodymium, Erbium and the co-doped option of Er/Yb.

The existence of a cladding waveguide that surrounds the doped core is the key difference between conventional active fibres and double-clad ones. This inner cladding is often non-circular with the objective of inducing higher pump absorption. Double clad fibres are designed to provide single mode wave guiding for the signal inside the core while allowing highly multimode pump power to be launched and propagated along the inner cladding. Figure 3.1 illustrates the basic double clad fibre structure.

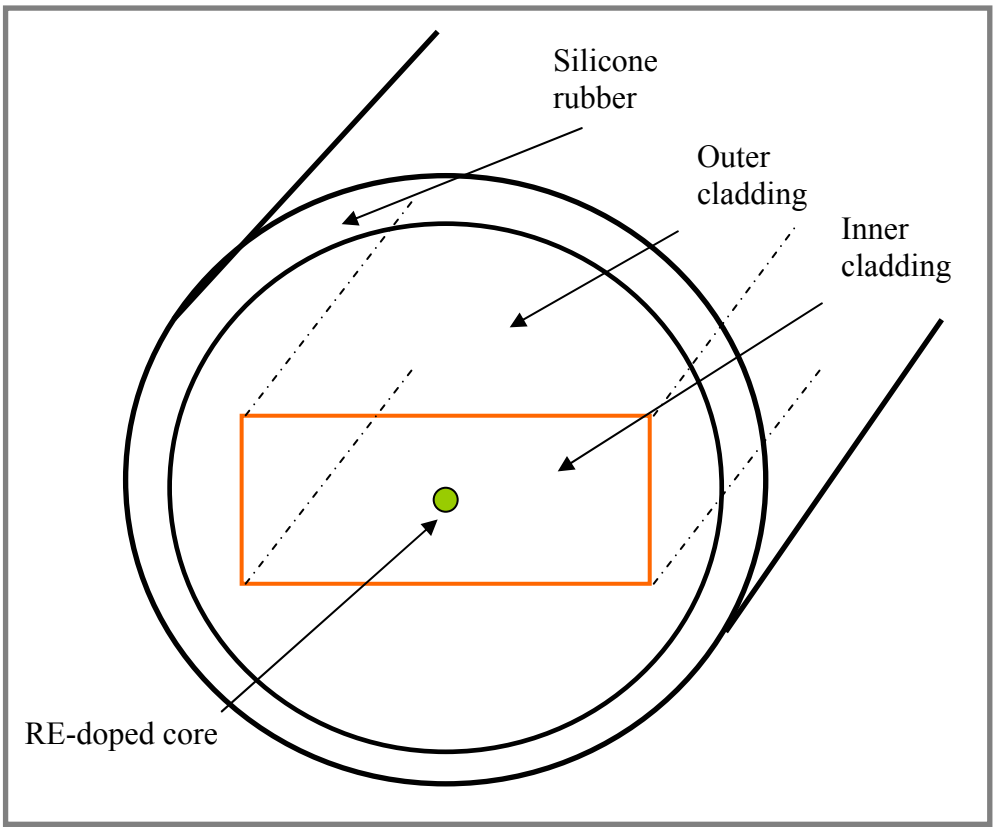

Figure 3.1 Double clad fibre

The inner cladding is large and has a high numerical aperture, which permits high launching efficiency for the pump. After every reflection at the boundary between inner cladding and the core, the pump rays cross the rare earth doped core and are absorbed by the active ion. This process takes place along the whole fibre. Thus, double clad structure makes it possible to use high power diode bars or diode arrays as pump sources (which today can provide hundreds of watts of pump energy) by making use of the large area and high NA of the inner cladding which in turn collects most of the pump power.

Snitzer et. al. proposed the first double clad structure for an Nd fibre in 1961 [1]. In their experiment they obtained an efficiency of 41% with respect to absorbed pump power with a total output power of 45 milli Watts. The active core of the Nd-doped fibre was off centre, it had a diameter of 5 μm and absorption rate of 1.3 dB/m. It was

doped with 1 wt% Nd_2O_3 and 3.8 wt% Al_2O_3. The NA of the inner cladding to the core was 0.14 and the NA of the same inner cladding with respect to the outer cladding was 0.1. Here we need to point out that at that time there were no high-power diode bars available.

Later on, from a fibre made by the MCVD process an experimental slope efficiency (with respect to incident pump power) of 66% was obtained [2] although the overall efficiency was 54%. The fibre (figure 3.2) had a clad to core diameter ratio of 22. The NA of the external cladding was 0.4. The efficiency mentioned above was obtained when pumping the fibre with a Krypton ion-dye laser combination, in comparison, the overall efficiency dropped to 24% while the slope efficiency also decreased to 29% when a diode array was used as the pump source.

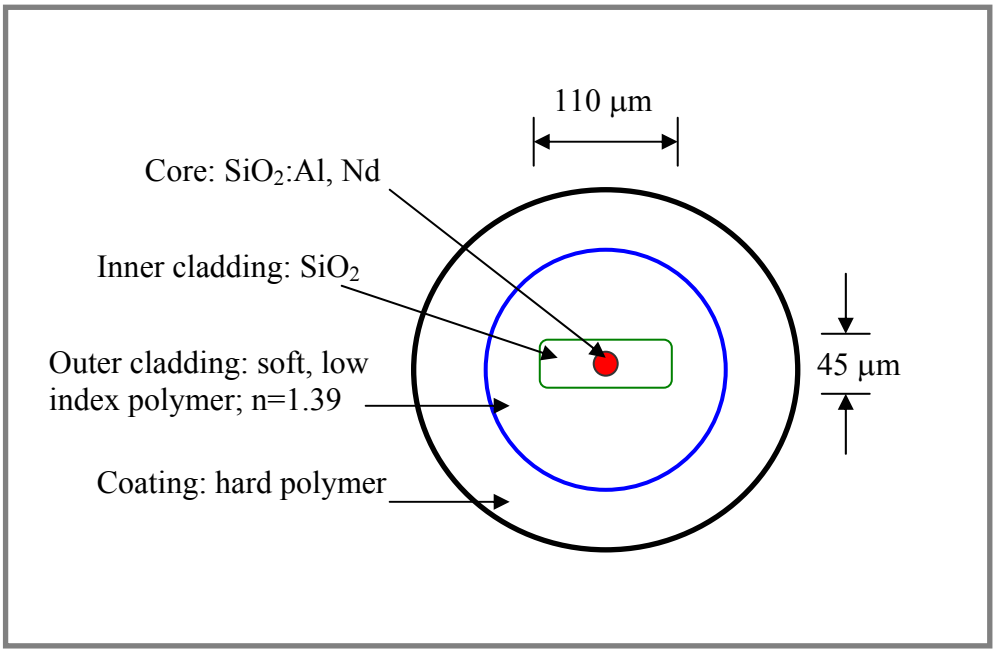

Figure 3.2 Cross section view of Nd-doped fibre taken from [2]

The highest output power from an Nd-dope fibre laser has been obtained by Zellmer and his colleagues [3]. They developed a 9.2 W, CW Neodymium-doped fibre laser by fabricating a low-loss Nd-doped fibre whose cross section is shown in figure 3.3, using the MCVD technique and solution doping of the Neodymium component to reach a concentration of 1300 ppm and co-doped with Al, P and Ge. The core diameter and NA were 12 µm and 0.18, respectively. Pure silica, 400-µm in diameter,

circular inner cladding surrounded the active core. The outer cladding consisted of a 50-μm-thick highly transparent polymer with low refractive index, which provided a NA of 0.38 with the inner cladding. The active core presented an absorption of 0.15 dB/m at 810 nm. A background loss of 6.4 dB/Km was measured at 1150 nm for the active core.

The output beams from nine 8-Watt diode bars were geometrically stacked into a single beam for a total available pump power of 50W, after lenses used for focusing. From the 50 W available, 35 W were launched into the fibre, from which in turn a two-times diffraction-limited multimode output power of 9.2 W was achieved. A slope efficiency of 26% was obtained when using an optimum out-coupling mirror with a signal transmission of 65%.

The emission spectrum of the fibre laser at 9 W was rather broad and ranged between 1065 and 1078 nm. In the paper, the authors mention the possibility of increasing the average absorption of the doped core by the periodic bending of the fibre. There are some implications for doing that such as bending losses, mode mixing and background losses. This is very interesting as in our experiments we also performed such bends to increase absorption and overall efficiency. This matter will be discussed further in following chapters.

From another report in the literature with respect to modelling of cladding pumped devices, the question over whether pump power in high-order anti-symmetric modes can be absorbed in the core arises [4]. In this paper, the authors recommend that a theoretical model of cladding-pumped fibre lasers should include intensity pattern evolution along the fibre, which would require substantial phase and amplitude information. However, after their modelling, they also conclude that after mode mixing takes place, the effective absorption is independent of launch conditions and that it is indeed proportional to the ratio of cladding and core areas.

Polaroid Corporation possesses the patent for double-clad fibre geometry. In one of their typical fibre structures, depicted in figure 3.3, the single mode circular core is situated in a rectangular silica inner cladding. They used a low-index polymer as the

outer cladding and a commercial polymer as the external coating. The core is 8 μm in diameter; it has an NA of 0.1 and is doped with 1.5 wt% Yb_2O_3 [5].

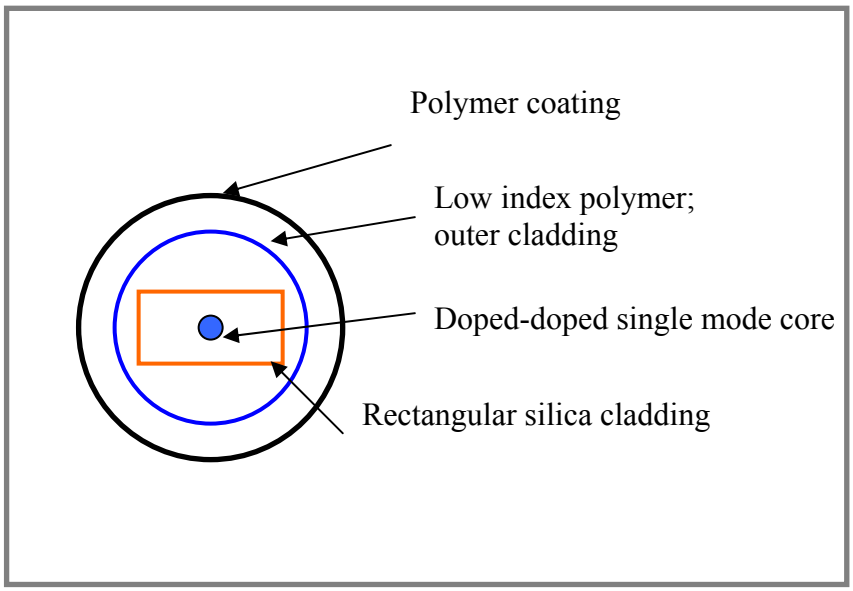

Figure 3.3 Typical cross section of a double-clad fibre from Polaroid [5]

The inner cladding has an NA of 0.45 and measures 170 x 330 μm, which provides suitable acceptance for the output of a 20 W laser diode bar. The total pump absorption was 13 dB for 50 metres of active fibre. It was reported in that work that the shape and size of the fibre strongly affects the coupling efficiency of the pump into the core.

It had already been reported that a rectangular inner cladding optimises the coupling as it provides a convenient shape for coupling in laser diode pump power and also increases absorption [6].

After 12 years of experimental work in Polaroid, they reported that the absorption into the core from the cladding is inversely proportional to the cladding area. Thus, is it beneficial to minimize the inner cladding area taking into account the availability of suitably bright pumps. This also would reduce the fibre length necessary to absorb the pump and losses in the core and cladding.

Muendel also reported an experiment to test the power-handling limits of their fibres [7]. In the experiment, a slope efficiency of 65% was obtained by coupling four SDL-P6 diodes to a double clad, Ytterbium-doped fibre. The total output power at 1.1μm was 35 W from an incident pump power of 55.4 W. It was also reported in this work that at full power, the CW intensity in the core is 140 MW/cm^2. Non-linear effects such as Stimulated Brillouin Scattering (SBS), Stimulated Raman Scattering (SRS) could be significant at these power levels [8], even in pulsed regimes as they approach fibre damage limits.

With respect to ytterbium-doped cladding pumped fibre lasers, the first cladding-pumping experiment at the ORC was performed by Pask et. al. [9]. The experiment was based on Yb-doped germano-silicate fibres fabricated in-house by the MCVD technique. Furthermore, the fibre had also the advantage of being photosensitive so that gratings were written directly into the doped core. Fibre gratings were also fabricated in un-doped fibres and then spliced to the active fibre to force operation at 1020 nm and 1140 when using pump light at 840 and 1047 nm.

For better efficiency, another fibre was fabricated. It had a single-mode inner core of 4.25 μm diameter, which produced a NA of 0.16 with the 12.75 μm inner cladding, which in turn produced a NA of 0.15 with the external coating. The concentration was measured to be 500 parts per million (ppm), obtained by solution doping. Very efficient performance, of up to 80% slope efficiency, was obtained at 1020, 1040 and 1140 nm. The pump source in this case was a Ti-sapphire laser operating at 974 nm.

Currently, the highest output power for a cladding pumped fibre laser in CW regime has been reported by researchers at SDL corporation who achieved 110 W output at 1120 nm. The Yb-doped fibre was fabricated by the former Fibre Laser Systems Division of Polaroid and had a rectangular 170 x 330 μm inner cladding with an NA of 0.46. The mode field diameter of the single mode core was 9 μm. The fibre length gave 13 dB of pump absorption at 915 nm. The pump source consisted of four 45-Watt, high-brightness diode bars. The output of each diode bar was a 10 x 10 mm beam with a 7-milli radians divergence in one direction and 10-milli radians in the orthogonal direction. The fibre was pumped on each end by polarization-combining

the four-diode bars and focussed into the inner cladding, which resulted in an incident spot size of 120 x 160μm with an NA of 0.3. At a drive current of 90 A for each bar, the maximum total output power of 110 W was obtained, which means that the average optical intensity on the active core was 300MW/cm^2.

The laser output was centred at 1120 nm and the optical efficiency was 58.3%, which was based on, pump power incident and output power after the collimating lens used for measuring M^2 parameter at the output. This parameter was measured at the output from the lower power beam generated by Fresnel reflection using a scanning razor-blade technique. An M^2 of 1.1 at low power was obtained which increased for higher powers up to 1.7 at 100 W believed to be due to thermal distortion in the output optics.

3.3 Geometry and pump absorption in CPFL

The amount of pump power affects directly the overall performance of the laser due to the fact that absorption of the pump is key to maintain a reasonable length. It is reported in the literature that pump absorption is directly proportional to the core to inner cladding area ratio multiplied by the absorption coefficient of the doped core [10]. This assumption is based on Beer's law. It was assumed in that work that the absorption coefficient has a constant value regardless the distance z from the front facet of the fibre where pump power is launched.

In contrast, Bedo undertook a theoretical analysis and reported experimental results as well [11]. In that paper the average effective absorption coefficient $\rho(z)$ decreases for increasing fibre length. The model suggests that the doped core absorbs each mode propagating in the inner cladding although the strength of the absorption depends on the field distribution of the mode at the position of the inner core.

In that sense, the better the overlap between the pump modes and inner cladding area, the higher the absorption. In his discussion the pump power P inside the fibre is separated in two sets of modes being P_a the total power that is absorbed at a constant absorption coefficient α_a, and P_n the amount of power that shows negligible field

distribution absorption at the position of the inner core and therefore not being absorbed. γ is the power coupling constant which describes the existing coupling between both P_a and P_n.

After an algebraic process also found in [11], P (z) can be described in terms of the effective absorption coefficient $\rho(z)$, the pump power P (0) at z=o and the position z at any point along the fibre by:

$$P(z) = P(0)e\left[-\rho(z)z\right] \qquad 3.1$$

Which for both limits give:

$$\lim_{z-0}\rho(z) = \alpha_a\left(1 - P_n^{'}\right) \qquad 3.2$$

And

$$\lim_{z-\infty}\rho(z) = \frac{\alpha_a + 2\gamma - \sqrt{\alpha_a^2 + 4\gamma^2}}{2} \qquad 3.3$$

In [11], experimentally determined average effective absorption coefficients were compared with theoretical results. From the comparison, several considerations appeared. First, the absorption coefficient $\rho(z)$ shows asymptotic behaviour with increasing of the length of the fibre. Thus, it should be considered that the longer the fibre the lower the absorption. The results also showed a large fraction of non-absorbing modes, which indicates that only a few modes were absorbed by the active core as absorption can only occur if there is a good overlap of the field distribution in the double clad fibre with the doped core.

In other words, the effective absorption coefficient is equivalent to the fraction formed by the ensemble of absorbing modes and the total power multiplied by the absorption coefficient of the same absorbing modes for short fibre lengths. The effective absorption coefficient results in a dynamic equilibrium between the coupling and the

absorption, and becomes independent of the z coordinate. With right fibre parameters, the effective absorption coefficient can be increased by the pump-coupling coefficient. For a higher effective absorption a stronger coupling between absorbing and non-absorbing modes is needed.

Furthermore, losses resulting from scattering and re-absorption in the core can again be reduced by fibre bending which increases the coupling coefficient by generating mode mixing and in that way reducing the absorption length.

In another study on absorption characteristics of double clad fibres, the authors report on a two and three dimensional analysis for fibres with circular inner cladding and centred core, fibres with circular inner cladding with off-centred core and finally for fibres with rectangular inner cladding [12].

First of all, they consider the mentioned inner cladding shapes as the most common cladding shapes used for fibres lasers at present. In most cases, the radius (and area) ratio of inner cladding to core is of the order of 20-100. Thus, the absorption efficiency is lower than that of a laser diode using core pumping technique. The optimisation of fibre cross-sections and parameters is important in order to discuss how different absorption efficiency is for each shape. Figure 3.2 shows the typical structures of double clad fibres.

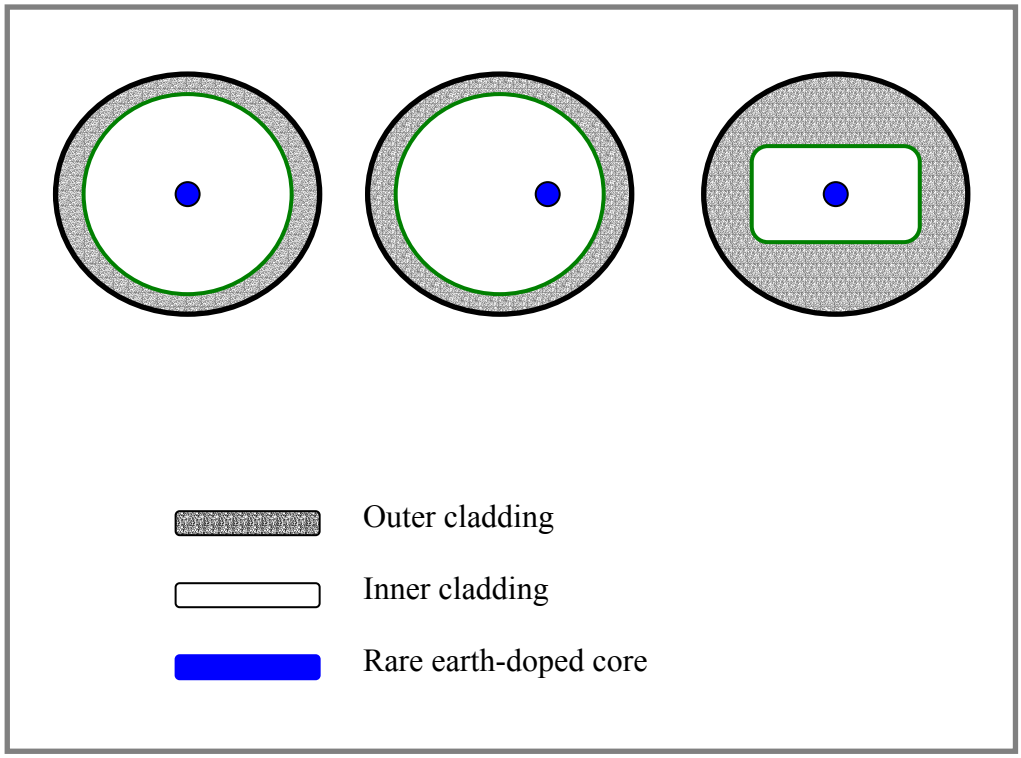

Fig. 3.4 Typical structures of cladding pumped fibre lasers

Initially, they analyse circular centred core fibres as shown in figure 3.4 (a) where a small surface element d*s* on the fibre, situated at Q with a position (r, θ) is pumped by different pumping modes with an intensity f(r, θ). The propagation region of a group of rays that have the same projection direction along the axis of the fibre is annular. The inner and outer radii are r(ϕ) and R, respectively. r(ϕ)= r sin ϕ, where R_0 is the radius of the first cladding d*s*=rd*r*dθ.

The total launched power at the fibre facet is [12]:

$$P_T = \int_0^{R_0} \int_0^{2\pi} f(r,\theta) r dr d\theta \qquad 3.4$$

For all pumping modes at Q and with a beam radius equal to R_0. The total absorbable power corresponding to the limit conditions may be determined by:

$$P_a = \iint f(r,\theta) r dr d\theta + \iint \frac{4}{2\pi} \sin^{-1}\left(\frac{r_0}{r}\right) f(r,\theta) r dr d\theta \qquad 3.5$$

For simplicity of last equation, it was assumed that the projections of launching rays on the entrance plane over d*s* have uniform distribution over 2π, and the coupling losses between the launching beam and fibre are neglected. A good description of the absorbable power could define the ratio of absorbable power to pump power as $\mu = P_a/P_T$, assuming that the pump power is completely absorbed by the appropriate fibre length. Now, for a diffuse source as the pump, with $f(\phi)$ and $f(r,\theta)$ constant, it is proposed that the absorbable power ratio can be determined as [12]:

$$\mu_1 = \frac{2}{\pi}\left[\frac{r_0}{R_0}\sqrt{1-\left(\frac{r_0}{R_0}\right)^2} + \sin^{-1}\left(\frac{r_0}{R_0}\right)\right] \qquad 3.6$$

$$\mu_2 = \frac{2}{\pi}\left[\frac{r_0 + p}{R_0}\sqrt{1-\left(\frac{r_0 + p}{R_0}\right)} + \sin^{-1}\left(\frac{r_0 + p}{R_0}\right)\right] \qquad 3.7$$

Where r_0 and R_0 are the radius of core and first cladding, respectively and p is the offset of which the core is situated from the fibre centre.

From modelling results in reference [12] they report that the absorbable power ratio is not proportional to the area ratio of core to cladding, and according to their results, the absorbable power ratio is very small and proportional to r_0/R_0, when the radius (and area) ratio of core to cladding is smaller than 0.4.

Equation 3.4 describes the absorbable power ratio for circular inner cladding with an off-centre core, and considering the offset distance p from the core to the axis of the inner cladding [12].

Comparing both cases, the increase of μ_2 caused by the offset distance p is the same as the increase of core of circular fibres. Thus, the larger the offset p, the higher the absorption is. Also, from results in reference [12] it can be noted that the variation of absorbable power ratio with respect to core radius is very small. In practise, considering fabrication technology the offset distance p must satisfy the relation $p+r_0+50\mu m < R_0$. In that case, μ_2 could be as high as ~0.9-0.95.

One of the most common inner cladding shapes used in our experiments is the rectangular shape. In rectangular double clad fibres (figure 3.4), the propagation path of the rays can be unfolded on the corresponding reflection planes if all of them are plane, which is normal. Those rays reflecting along the fibre obey the rule of plane mirror.

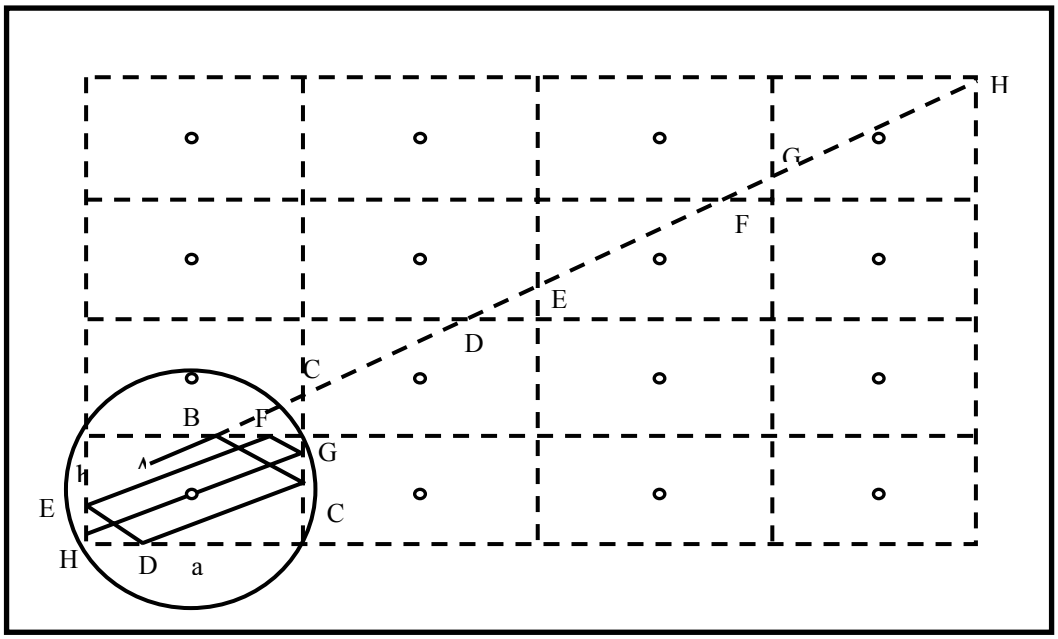

Figure 3.5 Unfolded propagation rays inside a double clad fibre

In this case, the ray paths inside the inner cladding scan the whole cross section of it and have the possibility of emerging anywhere after crossing the doped core. Therefore, the absorbable power ratio of rectangular double clad fibres is normally considered to be very close to unity. Furthermore, the ratio of a/b (see figure 3.4) does

not influence absorption efficiency. In practise, the cross section shape and dimensions of rectangular double clad fibres can be designed according to pump sources in order to obtain optimal launching efficiency.

3.4 Amplified spontaneous emission and gain calculations in cladding-pumped fibre lasers (CPFL)

Models developed for Erbium-doped systems are valid for Yb^{3+}-doped fibre lasers. The well-known three-level rate equations are used on which the population of the ground and excited state levels are taken into account. Other important variables are gain, pump saturation, absorption and emission cross-sections and amplified spontaneous emission (ASE).

Briefly, ASE can play a detrimental role in our systems due to the fact that all the excited ions can spontaneously relax from the excited state to the ground state by emitting a photon that is not related to signal photons. This photon can be amplified along the fibre and stimulate the emission of more photons from excited ytterbium ions reducing the total amount of gain because it can occur at any frequency of the fluorescence spectrum of the laser.

The noise power at a given point of the fibre can be expressed in terms of Planck's constant h=6.626 x 10^{-34} J·sec, frequency ν and bandwidth Δν as [13]:

$$P_{ASE}^{0} = 2h\nu\Delta\nu \qquad 3.8$$

The local stimulated emission at every point of the fibre will stimulate emission of photons from excited ions proportionally to $\sigma^{(e)}(\nu)\, N_2$. $\sigma^{(e)}$ is the stimulated emission cross-section at frequency ν, N_2 is the population of level 2. In any given direction, the equation describing propagation of the ASE power is [13]:

$$\frac{dP_{ASE}(\nu)}{dz} = \left(N_2\sigma^{(e)}(\nu) - N_1\sigma^{(a)}(\nu)\right)P_{ASE}(\nu) + P_{ASE}^{0}N_2\sigma^{(e)}(\nu) \qquad 3.9$$

Amplified spontaneous emission can actually propagate in both directions, either co-propagating or counter propagating with the pump. Backward ASE output at z=0 is higher than the forward ASE output at z=L, since the beginning section of the fibre, with a forward pump, is more inverted than the end section.

Although a mathematical study of how ASE affects laser operation is not the purpose of this work, one can state that ASE reduces the gain for the signal in saturation regime, as can be seen in figure 3.6.

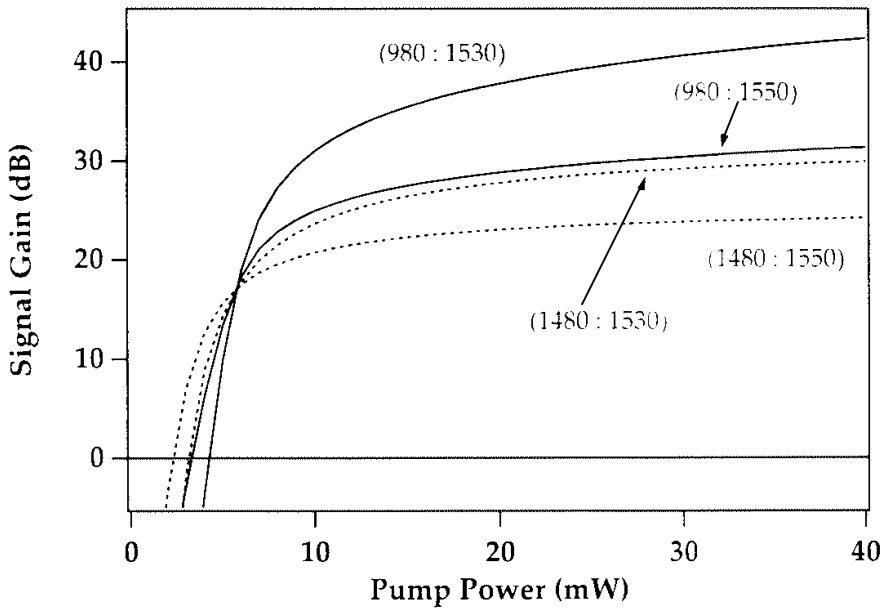

Figure 3.6 Typical signal gain as a function of pump power from numerical calculation of the pump and signal propagation equations [13]

Figure 3.6 shows how at low pump powers the amplifier is in the small signal gain regime; at higher powers when it is strongly inverted the gain is saturated. The first number in the parenthesis indicates the pump wavelength, and the second one the signal wavelength both in nm. Due to higher inversion from pumping at 980 nm, this wavelength yields higher gains than a 1480 nm pump at high powers. Moreover, due to the non zero emission cross section at 1480 nm, which drains population out of the upper state, there is incomplete inversion for this wavelength, even at high powers.

The gain at 1530nm is higher than that at 1550nm for higher powers due to its higher emission cross-section as well as the fact that the material is well inverted. Then, the gain factor is simply proportional to the emission cross section. The gain factor becomes strongly dependent on the exact distribution between the upper and lower states as well as to the ratio between the emission and absorption cross sections. When the populations are roughly equal, the small signal gain coefficient becomes proportional to the difference between the absorption and emission cross sections.

A lesser amount of pump power is needed to reach threshold for a 1550 nm signal than for a 1530 nm one because the absorption at 1530 nm is significantly higher than at 1550 nm. Finally, when the ASE starts growing as the pump power is increased, the higher inversion created at the beginning of the fibre by the 980 nm pump creates a better seed for the forward ASE than that created by the 1480 nm pump. This increases the transparency point for 980 pumping and robs gain from the signal when the fibre is long enough to allow the ASE to build up.

In general, the backward ASE benefits from travelling over a well-inverted piece of fibre, as compared to the forward ASE, and thus reaches a higher level. From the point of view of the backward ASE, any length of fibre acts as a source of spontaneous emission followed by a highly inverted piece of fibre. The forward ASE travels over a moderately inverted length of fibre and thus builds up more slowly than the backward ASE.

As an example, figure 3.7 shows the forward and backward ASE as a function of position, for 980 nm pumping slightly above threshold and well above threshold, using an Er^{3+} fibre laser with a length of 14 m.

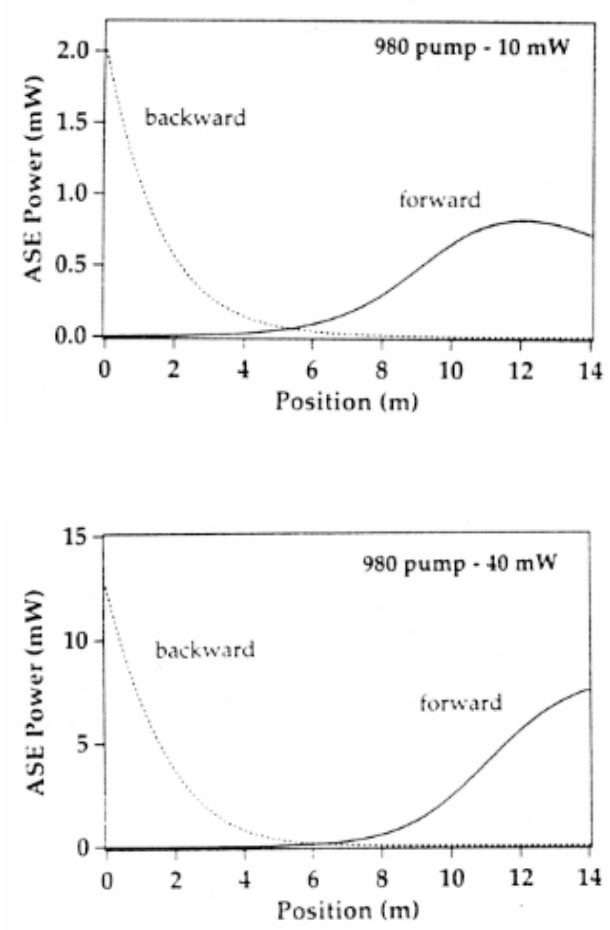

Figure 3.7 Typical evolution of forward and backward ASE in an erbium-doped fibre pumped at 980 nm

As it is shown in figure 3.7, ASE is directly proportional to gain and pump power thus, given that 980 nm pump power provides higher gains than 1480, the ASE is higher for a 980 nm pump than for a 1480 nm pump. The backward ASE is amplified along a well-inverted piece of fibre before exiting it, while the forward ASE travels along a piece of fibre that is progressively less inverted and thus has less gain per unit length than does the backward ASE. For 1480 nm, given that the population inversion is relatively flat across the fibre (for high enough powers), the backward and forward ASE is approximately equal.

In terms of the length of a fibre laser, the ASE build up depends on the ion concentration and level of pump power. In general, for a relatively "short" fibre, the pump power is able to almost completely invert the population of the fibre, since the ASE does not have enough fibre length to grow to a value where it is significantly depleting the population. When the fibre, according to its absorption value and length is a "long" fibre, the threshold for transparency at the wavelength of the signal moves significantly to higher powers, due to the fact that a longer fibre acts as a sequence of shorter fibre lengths.

Higher pump powers are then required at the input to invert the entire fibre, especially towards the end of the fibre itself. Such high pump powers generate a large amount of ASE, in particular backward ASE, which reduces the pump efficiency in producing signal gain and results in higher thresholds. A relatively short fibre is highly inverted, uniformly across its length. As a result, the forward and backward ASE at the ends of the fibre for a given wavelength and pump power, are essentially the same. A longer fibre could be so long that the backward ASE sees a much more propitious inversion than the forward ASE.

As for gain calculation, the following discussion assumes that the pump and laser intensity profiles are uniform over the area of the core, which is not normally the case for cladding-pumping techniques but it is to illustrate the way gain can be calculated.

Also, a uniform doping distribution is assumed which again is not always our case because some of our fibres were designed with doping distributions that help maintain good output beam quality. Steady state conditions of the fibre lasers are also assumed.

Moreover, the analysis below assumes that all the ions in the fibre are characterised by identical absorption and emission cross-sections, which means that we expect a homogeneous spectral broadening. Initially, the total population is [9]:

$$N = N_1 + N_2 \qquad 3.10$$

Where the total populations of level $2F_{7/2}$ and $2F_{5/2}$ are N_1 and N_2, respectively. In general, the gain achieved in a fibre length L is given by

$$\exp\left(\int_0^L g(z)dz\right) \qquad 3.11$$

Where

$$g(z) = N_2(z)\sigma_{el} - N_1(z)\sigma_{al} \qquad 3.12$$

$N_2(z)$ is determined from the pump power $P_p(z)$ at the location. σ_{el} and σ_{al} are the emission cross-section and the absorption cross-section for the laser wavelength, respectively. One can write

$$\frac{dP_p(z)}{dz} = -N_1\sigma_{ap}P_p(z) + N_2\sigma_{ep}P_p(z) \qquad 3.13$$

σ_{ap} is the absorption cross-section of the pump, σ_{ep} is the emission cross section of the pump. Equation 3.13 assumes no background losses as these losses are negligible for fibre lengths up to 100 m and we have been working with fibres much sorter than that, in the range of 5-30 m. Solving for $P_p(z)$ we use two previous equations and the following relation [9]:

$$\frac{dP_p(z)}{dz} = -\frac{Ah\nu_p}{\phi_p\tau}N_2(z) \qquad 3.14$$

A is the fibre area, τ is the upper level lifetime and ϕ_p is quantum efficiency for the pump, in our case $\phi_p \sim 1$.

The pump that reduces the absorption coefficient by a factor of 2 is an important value to know, it is calculated by

$$P_s = \frac{h\nu_p A}{\sigma_{ap}\tau\phi_p} \qquad 3.15$$

Thus the single pass gain exponent of equation 3.11 for a length l of fibre, can be expressed as:

$$\left(\sigma_{el} + \sigma al\right)\int_0^l N_2(z)dz - N\sigma_{al}l \qquad 3.16$$

It can also be expressed as

$$\frac{\phi_p\left(\sigma_{el} + \sigma_{al}\right)\tau P_a}{Ah\nu_p} - N\sigma_{al}l \qquad 3.17$$

The absorbed pump power P_a is: $P_a = P_p(0) - P_p(l)$.

Effectively, the procedure for calculating the gain reduces to calculating $P_p(l)$ from the following equation:

$$\ln\left(\frac{P_p(z)}{P_p(0)}\right) + \frac{P_p(z) - P_p(0)}{P_s} = -N\sigma_{ap}z \qquad 3.18$$

$P_p(0)$ is the input pump power.

So, the procedure for calculating the gain reduces to calculating $P_p(l)$ from 3.18, hence P_a then the gain exponent from 3.17, or by using the same equation expressed in dB [9]:

$$G_{dB} = 4.34\left[\frac{\phi_p\left(\sigma_{el} + \sigma_{al}\right)\tau P}{Ah\nu_p} - N\sigma_{al}l\right] \qquad 3.19$$

One must take into account a simplification condition for the previous equation that occurs when σ_{al} is negligible, that is for long wavelength operation such as 1140 nm.

For our case in which we work with cladding pumped fibre lasers, if the area of the inner cladding is x times the area of the core, then the equation for effective saturation intensity becomes x times greater than 3.15 and the right hand side of 3.17 becomes - $N\sigma_{ap}z/x$.

3.5 Device length and its implication on performance

In general, the length of a fibre laser initially depends on the total absorption of the pump power. As we mentioned earlier, there is a critical pump power level at which the gain coefficient is zero, i.e transparency for the signal is reached. This pump power level is given by [9]:

$$P_{cr} = \frac{Ah\nu_p}{\tau} \frac{1}{\frac{\sigma_{el}\sigma_{ap}}{\sigma_{al}} - \sigma_{ep}} \qquad (3.20)$$

Where A, h, ν_p and τ are the fibre core area, Planck's constant, pump frequency and upper level lifetime, respectively. σ_{el} and σ_{al} the emission and absorption cross-sections at the laser wavelength; σ_{ep} and σ_{ap} are the emission and absorption cross-sections at the pump wavelength. Note that P_{cr} is independent of concentration and that in the previous equation no background loss was assumed. In [9] it was theoretically demonstrated that the maximum gain shifts towards longer wavelengths for longer fibres as a result of re-absorption in the extra length of fibre. They compared two ytterbium-doped fibres of 1 and 20 m. Also, as pump power increases, the peak gain shifts to shorter wavelengths in both fibres.

For the same reason, selective oscillation can be introduced and suppression of lasing at 975 and/or 1040 nm can be reached by using longer fibres. Furthermore, under appropriate conditions strong amplified spontaneous emission (ASE) at 1040 and 975 nm could occur, and while travelling along the fibre could be re-absorbed, the ASE that emerges from the input end would result in lower pumping efficiency and higher thresholds.

In [9] it was determined both theoretically and experimentally an optimum fibre laser length for reaching laser threshold for various launched pump powers. The experiments were carried out using Yb^{3+}-doped germano-silicate fibres with NA~0.17, dopant concentration ~550 ppm and diameters of either 3 μm or 3.75 μm. The background loss was measured to be ~10 dB/Km.

The pump source was launched into the fibre using either an x10 or an x16 microscope objective from a Ti-sapphire laser, Nd:YLF or Nd:YAG laser. Typical launched efficiencies were ~50% for the Ti-shapphire and ~70% for the Nd:YLF laser. Feedback was provided either from the two bare, cleaved fibre ends or from a one cleaved end and a butted dielectric coated mirror at the other end.

In their results, it was shown that theoretical results are within 30% of the measured results, on which it was found a pump threshold of 40 mW for a minimum fibre length of 9 metres for both 974 nm and 1040 nm pump. With respect to wavelength, results showed that for fibre lengths in the range of 0.7 m to 6 m, the lasing wavelength was ~1040 nm, whereas for fibre lasers up to 100 m the lasing shifted to 1100 nm as a consequence of the tail in the Yb^{3+}-absorption spectrum. There is clearly an optimum length for reaching threshold at low values of launched pump powers.

Also, highly efficient laser performance has been demonstrated when pumping Yb-doped fibre lasers at 1064 and 1047 nm [14]. Due to the very weak pump absorption at these wavelengths which is ~0.1 dB/m for a ~550 ppm doping level, it is necessary to use long fibre lengths of ~100 m to obtain efficient pump absorption. However, very high slopes efficiencies can be reached due to the closeness between the pump and lasing wavelength.

In their experiments, they demonstrated a 90-m fibre laser with a threshold of 30 mW of lunched power. The device operated at 1102 nm and showed a slope efficiency of 90% with respect to launched pump power. It must be noted that when such long fibres are used, the laser wavelength of operation does not depend on pump wavelength from 840 to 1060 nm.

This work also represents an early attempt of power scaling from Yb^{3+}-doped fibre lasers. Output powers of 2W at 1090nm were obtained by using a continuous wave lamp-pumped laser at 1060 nm to pump a 90m fibre with two flat-cleaved ends. As expected, no damage to the fibre facets and rollover in the laser performance was observed at those power levels. Also, the paper illustrates that Yb^{3+}-doped fibre lasers are an option for very efficient conversion of high power Nd:YAG sources for carefully selecting longer wavelengths by using fibre gratings.

In theory, the fluorescence spectrum of a fibre laser corresponds to different homogeneous contributions determined by the Boltzmann distribution and in-homogeneous contributions due to site-to-site variation of the electric ligand field. At room temperature, only two of the four Stark levels of the Ytterbium electronic levels structure are resolved in fluorescence as shown in figure 3.8.

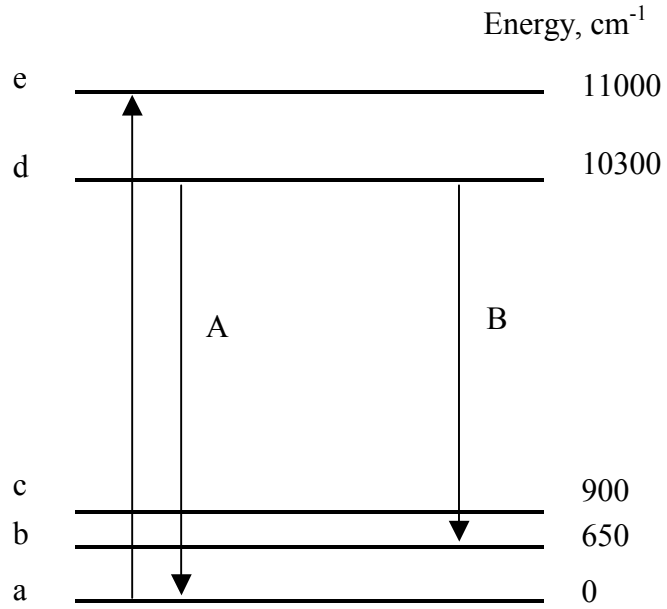

Figure 3.8 Electronic structure of Ytterbium ions

Below saturation of the laser transition, the ASE line narrowing is described by [15]:

$$\frac{\Delta\nu}{\Delta\nu_{inh}} = \frac{1}{\sqrt{g_0}} \qquad (3.21)$$

Where $\Delta\nu_{inh}$ is the inhomogeneous linewidth, measured from the absorption spectrum, $\Delta\lambda_{inh}=c\Delta\nu_{inh}/\nu^2=10$ nm. $\Delta\nu$ is the ASE-narrowed linewidth and g_0 is the unsaturated gain of the fibre laser, along its length L, at the centre of the gain profile $g(\lambda)$, which was derived in [16].

The peak stimulated emission cross section can be estimated using the modified Fuchtbauer-Ladenburgh equation from which it yields a value of 1.8×10^{-20} cm^2 at 976 nm.

As for fibre length optimisation, the laser transition in a three-level laser scheme suffers re-absorption losses from the ground state, while the laser transition operating in a four level presents a smaller re-absorption loss provided that only 4% of the total population is in the Stark level (b) of $^2F_{7/2}$ in figure 3.8 at room temperature.

Therefore, the gain of the three level scheme laser reaches a maximum at an optimal length, and the threshold of the fibre laser reaches a minimum at this same length. The fibre laser operates better in a three-level scheme for interaction lengths shorter than the optimal and in a four-level scheme the gain spectrum shifts towards longer λ's as the length increases beyond the optimal length owing to re-absorption from the ground state manifold. At the optimal length the local gain becomes zero and the pump power has a value defined by [17]:

$$P_p(L_{opt}) = \frac{\sigma_a(\lambda)}{\sigma_e(\lambda)} \frac{\eta_s}{F} P_{sat} \qquad (3.22)$$

Where $P_p(L_{opt})$ is the residual pump power at the optimal length. This length can be determined by solving the following equation of the pump mode evolution as reported in [16], where they used a Gaussian approximation for the fundamental guided mode,

$$\frac{dP_p(z)}{dz} = \alpha_p P_{sat} \ln\left(\frac{1 + \left[\frac{P_p(z)}{P_{sat}} \right] \left(1 - \eta_p\right)}{1 + \frac{P_p(z)}{P_{sat}}} \right) \qquad (3.23)$$

These two previous formulae are valid since the pump transition is mainly homogeneously broadened, with a pumping yield close to unity. Furthermore, site selective excitation is clearly seen because the homogeneous linewidth far exceeds its inhomogeneous counter-part at room temperature.

3.6 Conclusions

In this chapter, we briefly described power scaling in cladding-pumped fibre lasers. From a review of key results, the highest output power from a CW Yb-doped fibre device is found to be 110 W obtained by a company in the USA. We also analysed how inner cladding geometry affects total absorption of pump power in double clad fibres. Several inner cladding geometries have been proposed to increase the total amount of launched pump power into double clad fibres. From inner cladding geometries used in our experimental work, we can conclude that maximum mode mixing and pump absorption is obtained from rectangular inner cladding with appropriate NA. Finally, gain and ASE were discussed as important parameters that limit performance of rare-earth fibre lasers and amplifiers.

References to Chapter 3

3.1 Snitzer E., "Proposed fibre cavities for optical masers", Journal of Applied Optics, Vol. 32, No. 1, 36-39 (1961)

3.2 Po H., Tumminelli R., Zenteno L., Hakimi F., Cho N. M, Hau T., "Double-clad, high brightness Nd fibre lasers pumped by GaAlAs phased array", OFC Technical Digest, paper PD7, (1989)

3.3 Zellmer H., Willamowski U., Tunnermann A., Welling H., "High-power cw neodymium-doped fibre laser operating at 9.2W with high beam quality", Optics Letters, Vol.20 No. 6, (1995)

3.4 Wysocki P. F., "Accurate modelling of next generation rare-earth doped fibre devices", in OSA TOPS Vol. 16, Zervas M N., Willner A. Eds., Optical Society of America, (1997)

3.5 Muendel M. H., "High-power fibre laser studies at the Polaroid corporation", SPIE Conference on High Power Lasers Technical Digest, Vol. 3264, SPIE (1998)

3.6 Muendel M. H., "Optimal inner cladding shapes for double-clad fibre lasers", in Proc. Conference on Lasers and Electro-optics, paper CTuU2, USA (1996)

3.7 Muendel M. H., "35-Watt CW single mode Ytterbium fibre laser", Proc. CLEO 1997, Paper CPD30, Baltimore USA (1997)

3.8 Agrawal G.P., *Non-linear Fibre Optics*, Associated Press (1999)

3.9 Pask, H.M., Carman R.J., Hanna D.C., Tropper A.C., Mackechnie C.J., Barber P.R, Dawes J.M, "Ytterbium-doped silica fibre lasers: versatile sources for the 1-1.2 μm region", IEEE Journal of Selected Topics in Quantum Electronics, Vol. 1, No. 1, 2-13 (1995)

3.10 Minelly J.D., Barnes W.L., Morkel P.R., Townsend J.E., Grubb S.G. and Payne D.N., "High-power Er/Yb fibre laser pumped by a 962 nm diode array", Proceedings CLEO, Post-deadline paper CPD17, pp.33-34 (1992)

3.11 Bedo S., Luthy W. and weber H.P., "The effective absorption coefficient in double-clad fibres", Optics Communications, Vol.99, No.5-6, (1993)

3.12 Liu A., Ueda K., "The absorption characteristics of circular, offset, and rectangular double-clad fibers", Optics Communications 132, Elsevier Eds., pp. 511-518 (1996)

3.13 Becker P.C., Olson N.A., Simpson J.R., *Erbium-doped fibre amplifiers: fundamentals and technology*, Academic Press (1999)

3.14 Mackechnie C.J., Barnes W.L., Hanna D.C., Townsend J.E., "High-power Yb^{3+}-doped fibre laser operating in the 1-1.2 μm region", Electronics Letters, Vol. 29(1), pp.52-53, (1993)

3.15 Casperson L.W., Yariv A., "Spectral narrowing in high-gain lasers", IEEE J. Quantum Electron., Vol. 8, pp.80, (1972)

3.16 Digonnet M., "Rare-earth doped fibre lasers and amplifiers", Marcel-Dekker, USA (1993)

3.17 Weber M.J., *Laser Spectroscopy of solids,* Eds. Yen W.M., and Selzer P. M., Springer Ed., USA (1998)

Chapter 4

Conventional Cladding Pumped Fibre Lasers

4.1 Introduction

Optical gain is realized when the laser medium is pumped to achieve population inversion. Depending on the energy levels of the dopant, lasers and amplifiers can be classified as three- or four-level schemes. Three and four level leasers are shown figures 4.1 and 4.2, respectively. Since the host glass plays an important role and determines the operating characteristics of a fibre laser, considerable scientific work has been done to understand the interaction between the host glass and the dopant ions for both silica and non-silica fibres.

In this section we describe fibre lasers developed at the beginning of our research. When a new fibre was developed then the process of fibre characterization included determination for absorption and slope efficiency. The later was taken when a fibre laser was operation in free running mode. Depending upon fibre design we are able to study Q-switched regime of operation, single polarization generation, widely-tuneable operation. All this regimes will be described in the following sections.

4.2 Fibre characterization

Two most important characteristics of a laser are the efficiency with which the laser converts the pump power into laser power once it has reached threshold and threshold level itself.

Let us consider a round trip in a simple Fabry-Perot cavity formed by placing two mirrors of reflectivity R_1 and R_2 at the two ends of a fibre length L. The threshold condition can be written as:

$$G^2 R_1 R_2 e^{(-2\alpha_{int}L)} = 1 \qquad (4.1)$$

Where G is the single-pass gain and α_{int} is the internal loss of the cavity that includes coupling and other kinds of losses. Because of fibre laser nature it has a distributed local gain g (z) so that total gain G can be written as:

$$G = e^{\left(\int_0^z g(z)dz\right)} \qquad (4.2)$$

Where the local gain coefficient and the population inversion are related by:

$$g(z) = \sigma_s \left[N_2(z) - N_1(z)\right] \qquad (4.3)$$

Where σ_s is the transition cross-section; N_1 and N_2 are the ion densities for the lower and upper energy levels participating in the stimulated emission process. Thus the threshold condition becomes:

$$\frac{1}{L}\int_0^L g(z)dz = \alpha_{mir} + \alpha_{\text{int}} = \alpha_{cav} \qquad (4.4)$$

$\alpha_{mir}=\ln(R_1R_2)/2L$ is the effective mirror loss and α_{cav} is the total cavity loss.

Approximate analytic expressions can be found in [1] for many practical cases. One can use a simple model for the following analysis.

Lasers are commonly classified in two main categories: three-level and four-level lasers. A brief explanation of these systems follows:

In an idealised model, of a four level laser shown in figure 1.1, the characteristic feature is that the separation E_1 of the terminal laser level from the ground state is large enough that at the temperature T of operation, $E_1>>kT$. This guarantees that the thermal equilibrium population of level 1 can be neglected. If the lifetime t_1 of atoms in level 1 is short compared to t_2, we can neglect N_1, the average population of level 1 compared to N_2, the average population of level 2 [2] and the following condition:

$$N_t \equiv (N_2 - N_1)_t = \frac{8\pi n^3 \upsilon^2 t_{spon}}{c^3 t_c g(\upsilon)} \qquad (4.5)$$

Because $N_2 >> N_1$ one may conclude that

$$N_2 \cong N_t \qquad (4.6)$$

Where:

n is the refractive index

υ is the optical frequency

t_{spont} is the spontaneous lifetime of the transition $2 \rightarrow 1$

c is the speed of light

t_c is the exponential decay time constant (of the intensity in the cavity)

$1/g(\upsilon) \cong \Delta\upsilon$ is the width of the laser transition

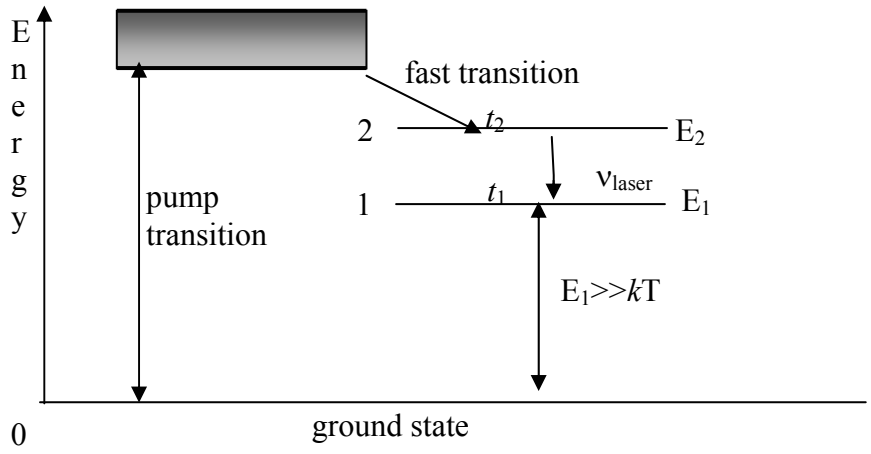

Fig 4.1. Energy level diagram of an ideal four-level laser

Therefore, the oscillation begins when the upper laser level acquires, by pumping, a population density equal to the threshold value N_t.

A three-level laser is one in which the lower laser level is a level whose separation E_1 from the ground state is small compared to kT. Therefore, at the condition of thermal equilibrium a substantial fraction of the total population occupies the ground level. At

a pumping level (figure 4.1) strong enough to create a population $N_2=N_1=N_0/2$ in the upper laser level, the optical gain γ is zero, since $\gamma \propto N_2-N_1 = 0$. To satisfy the oscillation condition the pumping rate has to be further increased until the following conditions are satisfied:

$$N_2 = \frac{N_0}{2} + \frac{N_t}{2} \tag{4.7}$$

And

$$N_1 = \frac{N_0}{2} - \frac{N_t}{2} \tag{4.8}$$

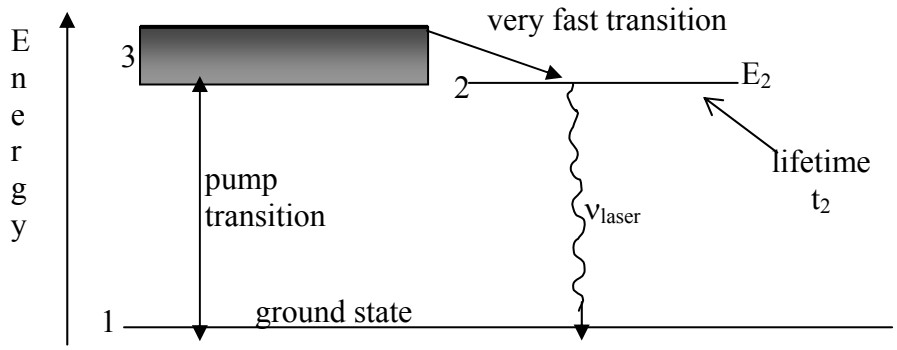

Figure 4.2 Energy level diagram of an ideal three-level laser

Since in most laser systems $N_0>>N_t$, we find that the pump rate at threshold in a three-level laser must exceed that of a four-level laser by

$$\frac{(N_2)_{3-\text{level}}}{(N_2)_{4-\text{level}}} \sim \frac{N_0}{2N_t} \tag{4.9}$$

or

$$(N_2)_{3-level} \cong \frac{N_0}{2N_t}(N_2)_{4-level} \tag{4.10}$$

The need to maintain about $N_0/2$ atoms in the upper level of a three-level system requires a minimum of pump power obtained by

$$(P_s)_{3-level} = \frac{N_0 h\upsilon V}{2t_2} \qquad (4.11)$$

And for a 4-level system

$$(P_s)_{4-level} = \frac{N_t h\upsilon V}{t_2} \qquad (4.12)$$

Where V is the volume. Multiplying the decay rate (in atoms per second) derives the last two expressions from the upper level at threshold by the energy per transition. If the decay rate per atom in t_2^{-1} from the upper level is due to the spontaneous emission only, we can replace t_2 by t_{spont}. P_s is equal to the power emitted through fluorescence by atoms within the mode volume V at threshold and is called critical fluorescence power. In the case of a four -level system we use equation (4.9) for N_t and obtain:

$$(P_s)_{4-level} = \frac{N_t h\upsilon V}{t_2} = \frac{8\pi n^3 h\Delta\upsilon V}{\lambda t_c}\frac{t_{sp}}{t} \qquad (4.13)$$

Where $\Delta\upsilon \cong 1/g\,(\upsilon_0)$ is the width of the laser transition line shape.

4.2.1 Absorption

For providing an expression for pump and signal absorption we should consider a number of atoms N_t per unit volume in an active material, from which we could calculate the transition rate. We first consider a particular case: homogeneous broadening. W_h is the transition rate for this case. It remains the same for every atom so a simple expression for it could be:

$$W_h(\nu - \nu_0) = W^{sa}(\nu - \nu_0) \qquad (4.14)$$

Let us now assume that all atoms remain in the ground state. Then, the power absorbed per unit volume dP_a/dV can be expressed as:

$$\left(\frac{dP_a}{dt}\right) = W_h N_t h\nu \qquad (4.15)$$

So, the photon flux F = I/hν since the W_h is considered proportional to the wave intensity. The absorption cross section, σ_h can be defined as:

$$\sigma_h = \frac{W_h}{F} \qquad (4.16)$$

But, from a more specific study [3], σ_h can be given by

$$\sigma_h = \frac{2\pi^2}{2n\varepsilon_0 ch}\left|\mu\right|^2 \nu g(\nu - \nu_0) \qquad (4.17)$$

So, the variation of the photon flux along the z direction could be expressed as:

$$dF = -\sigma N_t F dz \qquad (4.18)$$

In a more physical interpretation, let us think about each atom having an effective absorption cross section σ_a, such that if a photon enters this cross section, it will be absorbed by the atom. If S is the cross sectional area of the electromagnetic wave, then the number of atoms hitting (being absorbed or not) the material section dz would be N_tSdz, leading to the following expression for the average cross section:

$$\sigma_a N_t S dz \qquad (4.19)$$

In time variant domain, we can see that the fractional change of photon flux in the element dz is therefore:

$$\left(\frac{dF}{dF}\right) = -\left(\frac{\sigma_a N_t S dz}{S}\right) \qquad (4.20)$$

By comparison of the last two equations one can see that $\sigma_a=\sigma_h$ so that they define the effective absorption cross section, a very usual parameter for the total absorption present in a fibre.

Pump absorption of a double clad fibre depends on three main parameters: core/cladding ratio, fibre length and doping concentration. Pump light is launched into the inner cladding and is reflected by the interface between the first and second cladding, then is absorbed by the RE-doped core. In the first cladding, pump light is propagated as meridional and skew modes (high-order modes). In normal conditions, without fibre bending, skew modes have paths along the fibre that do not cross the doped-core. Thus, skew modes have a low probability of being absorbed.

Now, with the bending effect that can be applied onto a double clad fibre, the two classes of modes (skew and helical) can be converted into each other during propagation. Because of scattering irregular fibre shape, microbending, material non-uniformity, propagation aberrations and other reasons, intermode diffusion and mode mixing is unavoidable and in this case helpful to increase pump absorption since these effects lead to the conversion of un-absorbable skew rays into absorbable ones and also causes power coupling between skew and helical modes.

Modelling for propagation and mode mixing between these two types of modes is a complex problem and requires a fairly time consuming mathematical study, which is out of the scope of this work. Nevertheless, we can provide here a brief explanation of what are the fibre parameters involve in absorption when mode mixing is present. This simple explanation is based on the paper by: Bedo [4]. Assuming that:

$$P = P_a + P_n \qquad (4.21)$$

Represents the total pump power and P_a and P_n are the absorbable pump power and non-absorbable pump power, respectively. Both are described by a geometrical model in [5], using the absorption coefficient α. We then can assume that coupling between the two powers occurs with a power-coupling coefficient γ. After a mathematical procedure that uses the standard solution method (also described in [5]), solutions for

P_a and P_n in terms of fibre length z, absorption coefficient α and power coupling coefficient γ are also found to be an exponential function of two new parameters:

$$\sigma_1 = \frac{\alpha + 2\gamma - \sqrt{\alpha^2 + 4\gamma^2}}{2} \qquad (4.22)$$

and

$$\sigma_2 = \frac{\alpha + 2\gamma + \sqrt{\alpha^2 + 4\gamma^2}}{2} \qquad (4.23)$$

Considering that in normal conditions (with no mode mixing) the absorbable pump is considered to have higher possibilities of passing through the core than the un-absorbable pump, then the absorption coefficient α is larger than γ. Then $\gamma/\alpha \ll 1$ and the two previous equations can be simplified as:

$$\sigma_1 = \gamma\left(1 - \frac{\gamma}{\alpha}\right) \qquad (4.24)$$

and

$$\sigma_2 = \gamma\left(1 + \frac{\gamma}{\alpha}\right) + \alpha \qquad (4.25)$$

So, both σ_1 and σ_2 are determined by γ and α and reflect the absorption characteristics of P_a and P_n. Now the total absorption efficiency can be defined as [5]:

$$\eta = 1 - \frac{P_a(z) + P_n(z)}{P(0)} \qquad (4.26)$$

And by using the absorbable power ratio $\mu = P_a/P_T$; where P_T is the total pump power, and after several substitutions, the equation for total absorption efficiency can be written as [5]:

$$\eta = 1 - \left(1 + \frac{\gamma}{\alpha}e^{(-\sigma_1 z)} + \frac{\gamma}{\alpha}e^{(-\sigma_2 z)} + \mu\left[e^{(-\sigma_1 z)} - e^{(-\sigma_2 z)}\right]\right) \qquad (4.27)$$

Which describes the absorption characteristics of bend circular double clad fibres, where the total absorption efficiency depends on the absorption coefficient α, power

coupling coefficient γ and absorbable power ratio μ. For that reason, the total absorption efficiency of this type of fibres can be improved via mode mixing.

In practical fibres, a 30% increase of pump absorption is observed after bending the fibre into figure of eight or kidney shapes. Figure 4.3 shows spectral absorption of an Er/Yb-doped fibre which was used in our experiments described in chapter 7. The fibre was fabricated in house using the MCVD method. It has a high silica content, a low index polymer constitutes the outer cladding with an NA=0.41, an inner cladding diameter of 127 μm, a core NA=0.17 with a diameter of 14 μm, a calculated mode area of 110 μm^2 approximately and a measured pump absorption of 13dB/m at 975 nm.

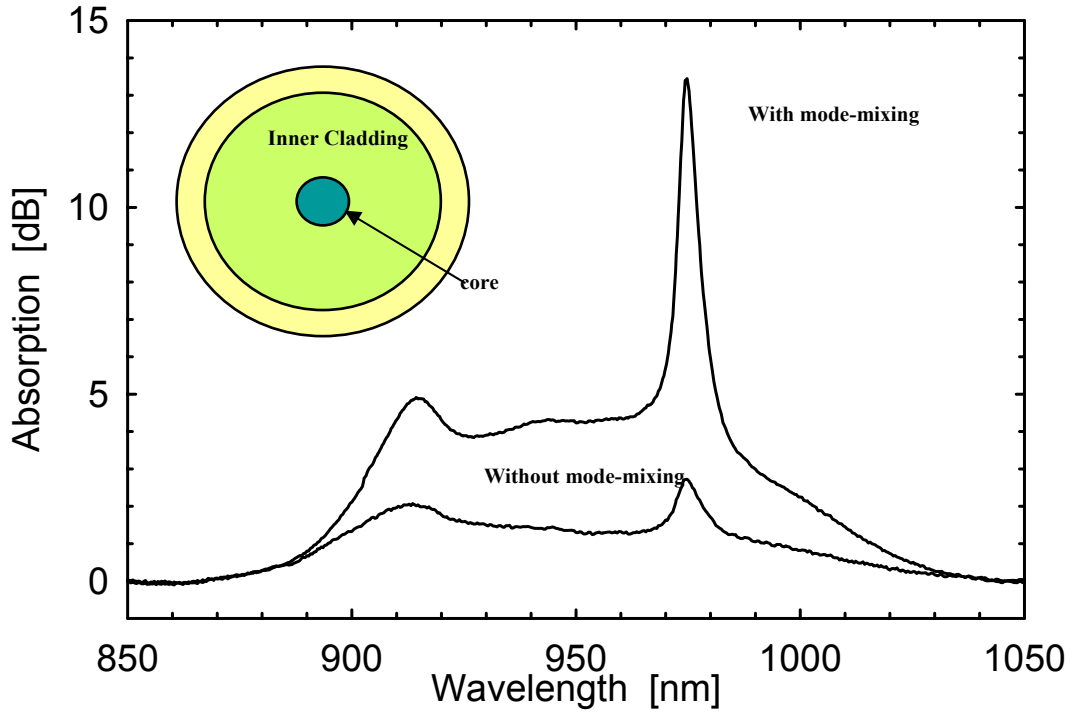

Figure 4.3 Absorption spectra and cross section of an Yb^{3+}-doped fibre with and without mode mixing

It must be noted that fibre length is 1 meter, pump absorption is rather high and it increases by around 10 dB/m after bending it the appropriate radius (mode mixing). Experimental results from this fibre are to be discussed in chapter 7.

4.2.2 Cut-back technique for optimal laser cavity

The absorption spectrum will give absorption rates over the wavelength range of interest. The length of fibre required for absorbing the pump power available, will be given by the absorption value at pump wavelength. The absorption spectrum can be measured by the cut-back technique, using a white light source. A curve relating the pump power that goes through the fibre against the fibre length, also represents the absorption rate.

One must take into account that fibre length should be short enough to avoid saturation absorption.

4.2.3 Slope efficiency and threshold power

The slope efficiency of a fibre can be experimentally determined. Initially, absorption spectrum is required so that we can estimate the appropriate length of the fibre, which will normally be so that ~10 dB of total absorption is obtained from the doped fibre. The laser power and pump through from the fibre is also measured for each value of pump power, which can be changed by changing the applied current to the pump laser.

4.3 Launching techniques

In order to improve absorption efficiency, the cladding pumping technique is used with several cladding/core fibre geometries to launch more power into the doped core. Due to the small area ratio $A_{core}/A_{cladding}$, the coupling of the pump radiation from the inner cladding to the core is relatively weak. Achieving high laser efficiency depends on optimising this coupling, which in turn depends on the cross-sectional shape of the inner cladding.

Fibres with the centered core (within a circular inner cladding) perform poorly because, as it was discussed earlier, the skew rays miss the core and only meridional rays are absorbed, i.e., they are depleted during propagation along the fibre so the intensity in the core falls and the overall absorption coefficient drops.

Several core/cladding geometries have been used. Among these, we can mention the D-Shape fibre, on which one side of the outer cladding is a plane, which gives some flexibility to be fabricated. Figure 4.4 shows some of these geometries, some of which were initially proposed by Muendel [6].

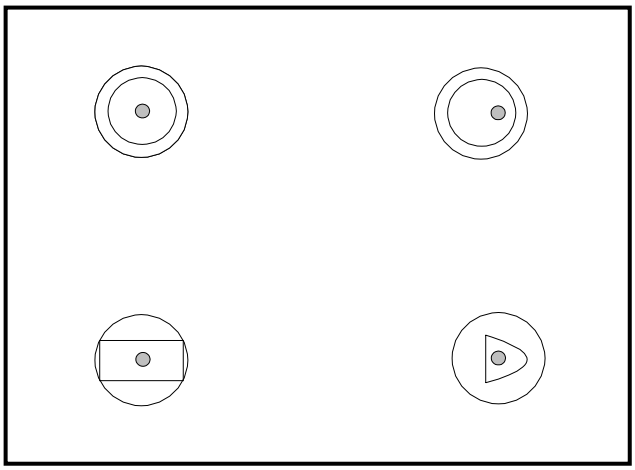

Figure 4.4 Core-cladding geometries of Yb^{3+} fibres

The rectangular inner cladding fibre, along which more rays can cross the doped core, leads to an increasing laser efficiency in respect to launched power (note that laser efficiency in respect to absorbed power remains the same) . Finally, certain fibres can be fabricated with an offset between the inner cladding and the doped core, which gives the possibility to use the cladding pumping technique, as the inner cladding is several times larger than the core.

Cladding-pumping technique allows the major part of the incident pump power to be launched into and guided by the outer core (inner cladding). All of this power is eventually absorbed into the doped inner core, provided the fibre is sufficiently long, thus giving rise to a more efficient laser action. Slope efficiency as high as 85% has been achieved using this technique. Besides increasing laser efficiency, the cladding-

pumping scheme allows lower tolerances on launch alignment and beam quality of the pump sources, important benefits for practical purposes. It has also been shown that this double clad fibre design is compatible with direct fabrication of photo-refractive gratings into the doped core, so that high efficiency should be achieved.

4.4 Continuous wave 21 W fibre laser

Our first CW fibre laser was developed with the intention of taking advantage of the high power diode bars that had been set-up in our facilities at the ORC. The diode bars and beam shaper technique used to equalise the beam in orthogonal planes will be described in following chapters.

4.4.1 Fibre characteristics

The double clad fibre employed in this experiment had a circular inner cladding. The core diameter was 200 μm and it was coated with silicone rubber. The absorption of pump at 915 nm was measured to be 1 dB/m. The length of the laser cavity was 12 m. This fibre was pumped from both ends and Fresnel reflection from both flat-cleaved ends was enough to generate lasing at the ~1080 nm wavelength of operation. The laser was only studied in continuous wave (CW) regime.

4.4.2 Experimental set-up

The experimental set-up is shown in figure 4.5. We pumped the fibre from both flat cleaved ends. The launching efficiency was 65% from both diode bars.

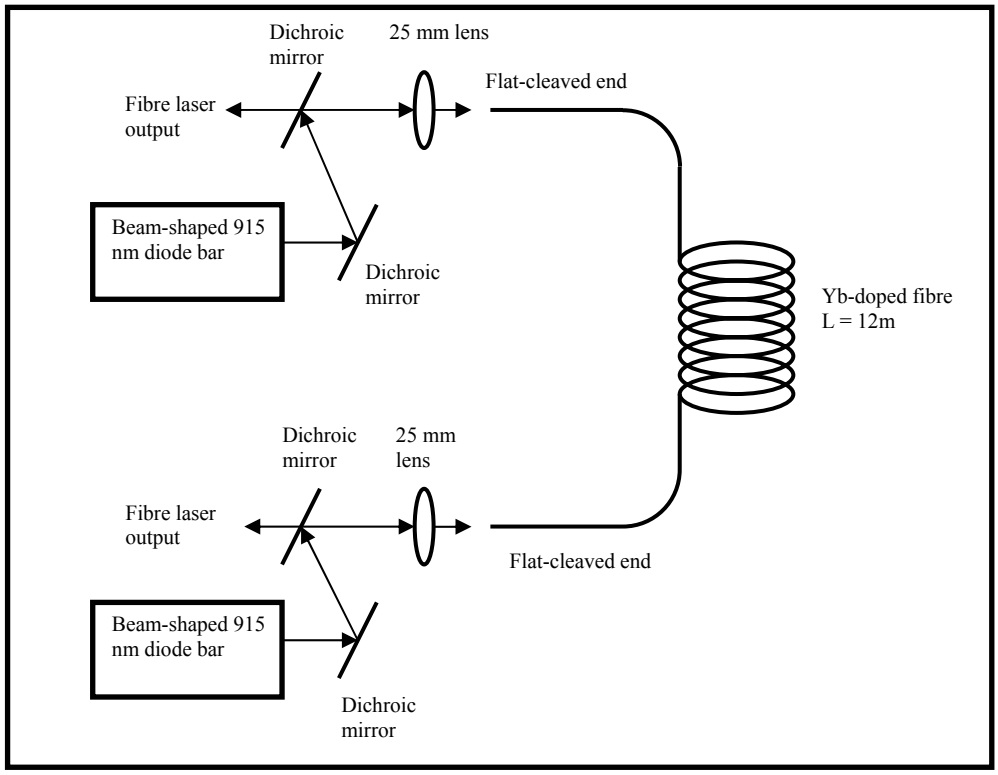

Figure 4.5 Experimental set-up of a CW fibre laser

4.4.3 Results on maximum power and slope efficiency

As can bee seen in figure 4.6, the maximum output power at 1080 nm was ~21W from the HD550-01 Ytterbium-doped fibre. As mentioned, the cavity length was 12 m. The maximum launched power (at 915 nm) was 46W (~23 W from each end of the fibre). The slope efficiency is 53% with respect to launched power and the fibre laser showed no signal degradation.

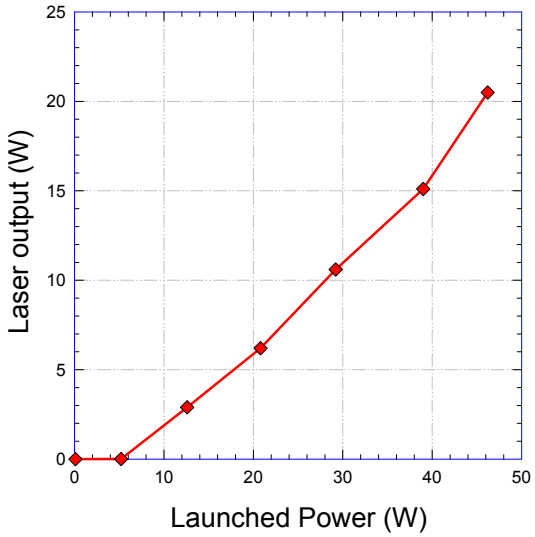

Figure 4.6 Maximum power and slope efficiency from the HD550-01 fibre laser

The maximum pump power that came through the ends of the fibre (without being absorbed) was ~ 2 W. The threshold was reached at nearly 6 W of launched pump power. In all the experiments we made sure that fibre ends had the same reflection from the facet so that the laser was balanced, i.e. same laser power was extracted from both ends.

4.5 Yb^{3+}-doped fibre laser with tapered region

In many applications of fibre lasers a diffraction-limited output is required and this dictates the use of single mode rare earth-doped fibres. However, because of the small diameter in a single mode core, the inner cladding to core area ratio is large in single-mode cladding-pumped fibre lasers. Very large cladding-to core ratio results in low pump absorption which in turn leads to device lengths too long for certain applications.

Single-mode operation following selective excitation of the fundamental mode of large-core multimode fibre amplifiers was recently demonstrated in short fibres [7]. A ring-doping technique has also been proposed to allow high pump absorption and slope efficiency by locating the gain medium in a ring around a single mode core [8]. The use of large mode area fibres on which the refractive index profile was carefully designed to create preferential gain for low-order modes has recently been proposed [9, 10].

4.5.1 Description of the taper

The tapering applied to the fibre had the main objective of improving output beam quality of the laser. Basic idea is that when light enters the tapered section, it transforms the local fundamental core mode of the un-tapered fibre to a mode that also travels along the cladding of the taper waist.

The fibre taper is schematically shown in Fig. 4.7. It should satisfy two conditions: (i) low insertion loss for the fundamental mode LP_{01}, and (ii) high insertion loss for higher order modes. The first condition, described by equation 4.28, is easily met by making the taper angle Ω small compared to the numerical aperture of the core [11].

$$\Omega(z) << \frac{NAW^2}{4\pi V} \approx 0.2NA \qquad (4.28)$$

Where NA is the numerical aperture of the core, $W = \rho(\beta^2-k^2n_2)^{1/2}$ is the cladding parameter, ρ is the radius of the core, β is the propagation constant, $k=2\pi/\lambda$ is the wave number, n_2 is the refractive index of the cladding, n_1 is the refractive index of the core and $V = k\rho(n_1^2-n_2)^{1/2}$ is the normalized frequency, which determines the number of LP modes propagated along the fibre.

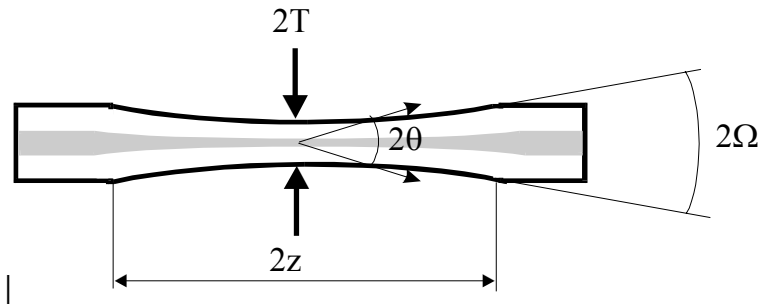

Fig.4.7 Schematic drawing of fibre taper used in experiments.
2T: taper waist
2z: taper length

The second requirement is more difficult: Higher-order modes, especially LP_{11}, can propagate through the taper as leaky modes even below cut-off [2]. A numerical solution indicates that in order to suppress LP_{11}-mode the V-parameter of the taper should be as low as ~1.5, which may be hard to reach in practice.

For the characterization of the beam quality from the conventional and tapered laser we used the beam quality factor known as the M^2 parameter. In a physical interpretation, this factor is a measure of the near field times far field space-beamwidth product of the real beam normalized to the space beamwidth product for an ideal Gaussian beam.

The spatial beam quality is a critical parameter since it determines optic requirements for focusing the beam of any laser system and how it will spread as the beam propagates along the optical axis. It is also related to the launching efficiency η obtainable when launching into a single mode fibre. The relation between the two parameters is $\eta \approx 1/\sqrt{M^2}$ [2].

4.5.2 Conditions for efficient taper structures: mode coupling and adiabaticity

Multimode doped core fibres allow for a larger mode volume compared to single-mode doped cores. Some of the problems associated with tapers are mode mixing and coupling of leaky modes. As the fibre taper increases its radius, higher order modes can couple back into the fibre. Smooth tapering in both directions would help avoiding this situation.

Reducing the core to a normalised frequency V value of 2.4 is not enough because at that point higher order modes are no longer guided by the core but could be guided in the cladding as leaky modes and radiated only when using a very long section of fibre with low V value. Very low V values (~1.5) will be required for the taper lengths and radius achievable with double clad fibres. Such a low V value could result in a fragile taper section, unsuitable for practical experiments in high power.

Furthermore, too short or thick tapers will not allow us to radiate higher order modes and as it become thicker at the end, these modes could be guided again.

A minimum taper length, directly proportional to the difference between the initial core radius and the final radius after tapering process divided by the taper angle [2], must be kept. This will ensure that all modes reflecting from the interface of the taper are bound modes. It will also keep low losses for the fundamental mode. In practice, short devices are more robust and stable for high powers.

To maintain diffraction limited output, no mode coupling to LP_{11} or higher order modes is required, although taper structure itself (either linear or parabolic) could lead to mode coupling at the taper-up region, where higher order modes are likely to be coupled back for long fibres.

On the other hand, as light propagates down the fibre, a too sharp transition will mean that the beam is unable to change its transversal distribution rapidly enough to maintain propagation characteristics ideal for fundamental mode. This situation leads us to an important characteristic for tapers: adiabaticity. In general, a sufficiently

gradual tapering section will allow transmitted light to remain in the LP_{01} mode with low losses; i.e. the taper section is adiabatic.

4.5.3 Tapers fabrication technique

Tapers fabrication technique is very simple. It can be fabricated using a technique called fused-biconical tapering. This technique is easy to implement simply by stretching the fibre in a flame or an electric arc. This fairly simple technique results in that tapers and taper-based devices are now popular and arguably not expensive, although a complex fabrication set-up allows for deep control of taper diameter and length, stretching time and strength. Figure 4.8 schematically shows the fabrication set-up.

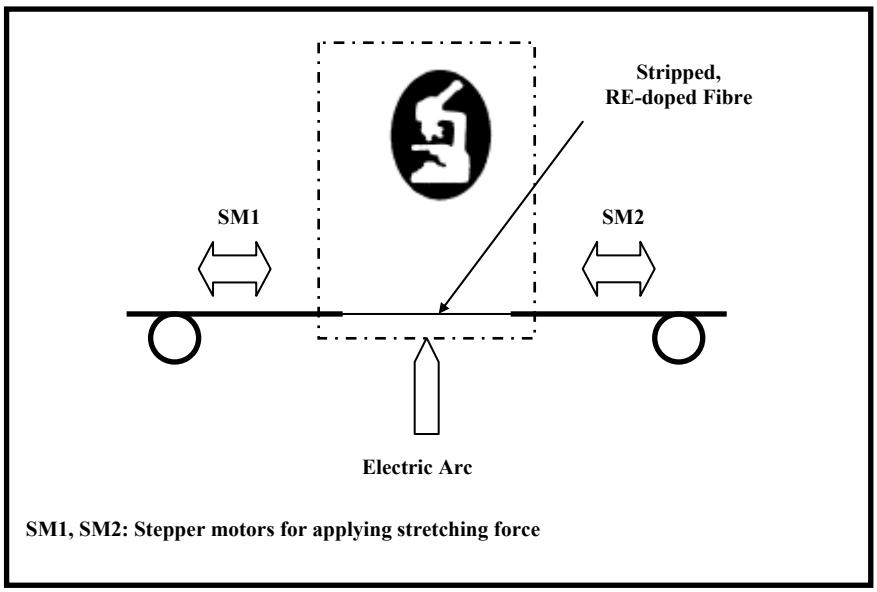

Figure 4.8 Fabrication set-up for tapers

It must be taken into account that our fabrication machine and procedure is not too complicated so there is room for improvement. This simple fabrication process can be describe in the following steps:

1) Selection of the appropriate fibre. In our case, double clad, rare earth-doped fibre of outer diameter of 200-350 μm is used. The core size is normally 10-30μm

2) Stripping of ~10 cm of fibre using a mix of dichloro-methane and acetone, then cleaning the stripped section of fibre with methanol

3) Placing and fixing the fibre ends on the stretching device, which in our case is a stepper motor

4) Setting the desired strength and current level in the stretching device

5) Applying the current and stretching into the fibre, while monitoring the length and the taper size

6) Stop the stretching and the current into tapered section. Measuring final outer dimensions

7) Splice the taper with un-tapered rare earth-doped fibre or use it directly as a fibre laser

Laser performance in CW and Q-switched was evaluated and compared with an equivalent cavity only without taper section. Insertion losses were also measured in both operation regimes.

Some of the taper-based devices are commercially available: single and multimode fibre couplers, which have a controllable splitting ratio, low excess loss and good thermal stability.

Wavelength division multiplexers are basically a fused coupler which multiplex and de-multiplex different information channels with different carrier wavelengths, as long as the coupling region is such that no net power transfer occurs at one wavelength while complete power transfer occurs at the other.

Polarization beam-splitter is another taper-based device, whose principle is based that in a fused tapered coupler the coupling coefficients for *x* and *y* polarizations are usually slightly different. It is therefore possible, by pulling a long coupler, to split a randomly polarized input into its orthogonal components.

Filters can also be made from tapered fibre devices by exploiting the wavelength dependent transmission of non-adiabatic tapers. A wavelength dependent loss is required for optical filtering. That behavior (normally detrimental in tapers) is present when using depressed clad fibres due to the difficulty in tapering them down, which mode coupling and ultimately a wavelength-dependent loss.

4.6 Experimental set-up of an Yb^{3+}-doped fibre laser with tapered region

The experimental set-up is illustrated in Fig. 4.9. A beam-shaped 915-nm diode bar [12] pumped the double-clad, Yb-doped fibre with measured launch efficiency ~60%. A set of antireflection-coated dichroic mirrors was used to steer the diode beam and to separate the signal from the pump. A lens with a 25-mm focal length was used to focus the input beam into the fibre. The total output power was taken from both ends. The first fibre we used had a 200 μm cladding diameter and a 15 μm core diameter. The core NA was 0.15. Hence, the V parameter was 6.7. Thus, this core supports seven LP modes at a lasing wavelength of 1080 nm. The second fibre has a 33 μm core diameter and also a 200 μm cladding diameter. For this fibre the core NA was 0.13 thus the V parameter was 12.5. This core supports thirteen LP modes.

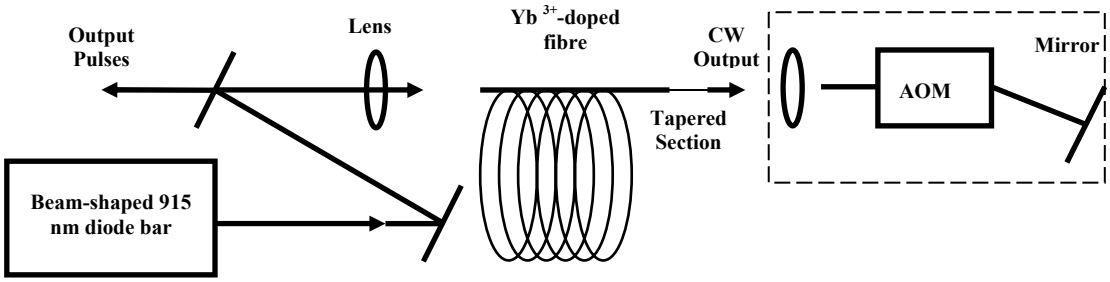

Fig. 4.9 Experimental configuration of cladding pumped fibre laser. Inset: layout for Q-switched regime

4.6.1 Yb^{3+}-doped fibre and fibre taper characterization

The fibre characterization process is general for any type of fibre or dopant. After receiving the fibres made in-house we take the following steps to characterize them:

1. Measurement of spectral absorption:

   - Striping and cleaving both ends of 1m of RE-doped fibre
   - Launching light from a white light source into one end of the RE-doped fibre
   - Take readings of absorption initially for a wide range (750 – 1750 nm) using an Optical Spectrum Analyser (OSA)
   - Increase the resolution of OSA and reduce the range for measuring absorption at peaks: 915 nm, 975 nm and 1060 nm for Yb-doped fibres and 980 nm and 1480 nm for Er^{3+}-doped fibres

2. According to the peak absorption obtained from 1, take the required length of fibre for absorbing the total pump power from the source. Note that depending on the inner cladding shape, the absorption increases when adopting a figure of 8 or a kidney shape arrangement of the fibre [13]. Note that 3 dB absorption is equivalent to 50% of pump power absorbed and that 9 dB ~90% of the pump being absorbed.

3. Characterisation as free-running laser:

- With the appropriate length of fibre determined by the peak absorption at pump wavelength (at 975 nm in typical absorption spectra of Yb^{3+} shown figure 4.12) the following set-up in figure 4.14 is used to implement a fibre laser.

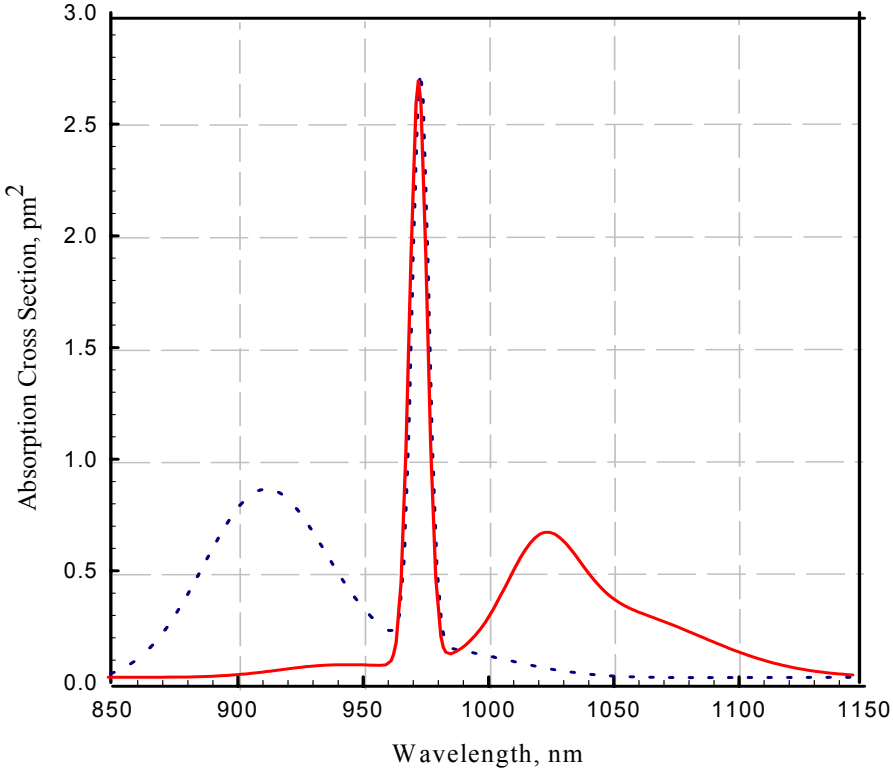

Figure 4.12 Typical absorption (dotted line) and emission (solid line) spectra of an Yb^{3+}-doped fibre

- Initially, light from pump source described below is focused into the inner cladding of RE-doped fibre using DM1, DM2 and L1. In our case, DM1 has high reflection (>99%) at the pump wavelength ~915 nm. DM2 has high reflection (>99&) at 915 nm and high transmission (>99%) at 1060 nm. The position of DM2, prevents pump reflection from the input end of the fibre to damage the laser diode bar

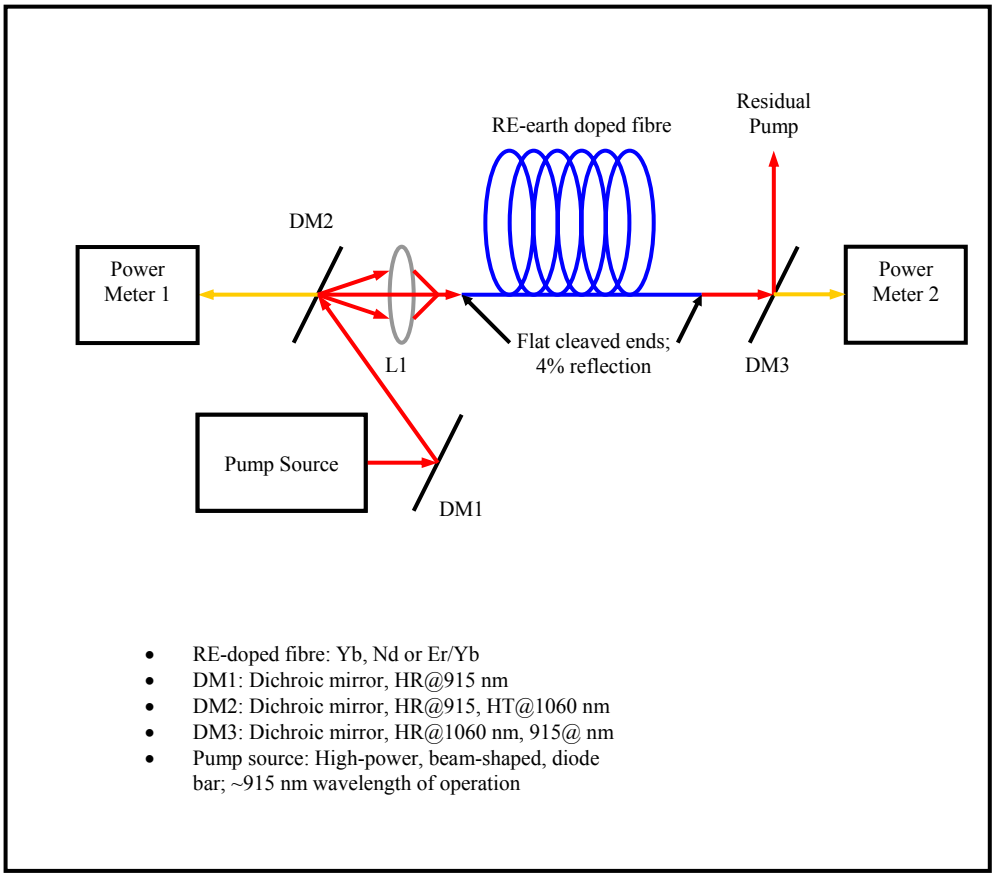

4.13 RE-doped fibre as free-running laser

- L1 is normally a 1-inch, 25-mm focal length, antireflection coated lens that focuses down power from the beam-shaped diode bar into inner cladding of RE-doped fibre. Typical launching efficiency after DM1, DM2 and L1 is 60%

- 4% Fresnel reflection from bare, flat-cleaved ends is enough to create gain inside the laser cavity

- Pump power is gradually increased until threshold is reached and fibre starts lasing at the wavelength of maximum gain. After threshold, signal power is measured with power meters 1 and 2

- Non-absorbed pump power and signal emerge from the far end of the fibre; this amount of power is also measured. After that, DM3 (high reflection, >99% at 915nm, high transmission, >99% at 1060nm) separates signal from pump, which enables us to measure residual pump. A curve that relates total signal power from both ends with launched (or absorbed) pump power is obtained. See figure 4.6.

The process described above was performed with every fibre included in this thesis. After obtaining curves on total signal and residual pump vs. absorbed pump, the process of fibre characterisation in continuous wave regime is completed. Next, experimental results on a fibre laser with tapered section inserted in the cavity are presented.

4.7 Experimental results

We experimented with several tapers. Results for maximum power, M^2 value and power penalty with and without tapers are presented.

4.7.1 Efficiency, M^2 square value and maximum power with and without taper

In CW regime, we first measured the output power of the laser without any tapered section. As can be seen from Fig. 4.14, the maximum output power from the cladding pumped multimode fibre laser is 11 W and the slope efficiency is 85% with respect to absorbed power.

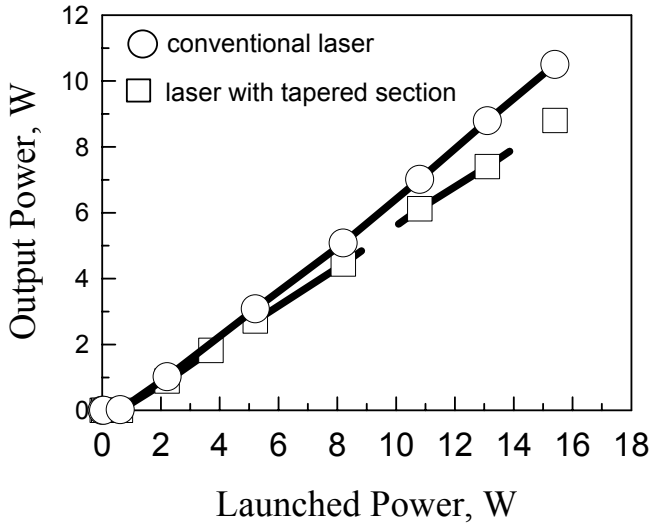

Fig. 4.14 CW output power vs. launched pump power in cladding pumped fibre lasers

Then, we investigated fibre lasers with tapered sections. Several tapers with different lengths and widths were fabricated. We obtained the best results with a 3 cm long taper with a waist diameter 2T of outer cladding of 70 μm. Maximum output power from the laser was now 9 W and the slope efficiency was 67%. Measurements of the M^2-parameter give the value of 2.6 for the conventional laser and 1.4 for the tapered-fibre laser. Thus, the tapered section inside the laser cavity increased the brightness by a factor of ~ 3.5 with a power penalty of 1 dB or ~20%.

4.8 Conclusion

In this chapter we have given fundamentals of cladding pumped fibre lasers and presented results on CW fibre lasers both with and without a tapered section inside the cavity. A 21-W Yb^{3+}-doped fibre laser (without taper) has been developed. It showed a slope efficiency of 85% and good temporal stability, although no relative intensity noise (RIN) measurements were performed.

We have also studied a high power cladding pumped Yb^{3+}-doped fibre laser with a tapered section for selection of transverse modes. We have shown that such a fibre taper results in significant increase of the laser brightness with a close-to diffraction-limited output beam, while the power penalty is small. We have also demonstrated that tapered fibre lasers result in shorter device lengths, are easy to make and reproducible. More importantly, that they are compatible with other techniques for improving beam quality while obtaining high energy pulses, such as large mode area fibres as we could obtain high-energy pulses. The main problems were identified being fibre facet damage and mode conversion after propagation along the un-tapered fibre.

References to Chapter 4

4.1 Digonnet M., "Rare-earth doped fibre lasers and amplifiers", Marcel-Dekker, USA (1993)

4.2 Snyder A.W., Love J.D., *"Optical waveguide theory"*, Chapman and Hall, 1983

4.3 Svelto O., *"Principles of Lasers"*, Chapter 2, (1998)

4.4 Bedo S., Luthy W. and Weber H.P., "The effective absorption coefficient in double-clad fibres", Optics Communications, Vol.99, No.5-6, (1993)

4.5 Liu A., Ueda K., "The absorption characteristics of circular, offset, and rectangular double-clad fibers", Optics Communications 132, Elsevier Eds., pp. 511-518 (1996)

4.6 Muendel M. H., "Optimal inner cladding shapes for double-clad fibre lasers", in Proc. Conference on Lasers and Electro-optics, paper CTuU2, USA (1996)

4.7 Fermann M.E., "Single-mode excitation of multimode fibres with ultra-short pulses", Opt. Lett. 23(1), 52-54 (1998)

4.8 Nilsson J., Minelly J.D., Paschotta R., Tropper A.C. and Hanna D.C., "Ring-doped cladding-pumped single-mode three-level fibre laser", Opt. Lett. 22, 1092, (1997)

4.9 Richardson D.J., Offerhaus H.L., Broderick N.G.R., "Large Mode Area Fibre Lasers and Their Applications", ASSL 2000, Davos Zwitzerland, 13-16 Feb. Invited Paper, (2000)

4.10 Offerhaus H.L., Broderick N.G.R., Sammut R.S., Dong L., Caplen J.E. Richardson D.J., "High-energy single-transverse-mode Q-switched fibre laser based on a multimode large-mode-area erbium-doped fibre", Opt. Lett. 23, 1683-1685 (1998)

4.11 Farwell S. G., "Fused tapered fibre optic devices", PhD. Thesis, University of Southampton (1997)

4.12 Clarkson W.A. and Hanna D.C., "Two-mirror beam-shaping technique for 2 high-power diode bars", Opt. Lett. **21**, 375-377 (1996)

4.13 Chen, Z.J., "Double clad fibre devices", PhD Thesis, University of Southampton, (1998)

Chapter 5

Single Polarisation Ytterbium Doped Fibre Laser

5.1 Introduction

In previous chapters we described some basic concepts of fibre lasers in terms of launching efficiency, doping material, maximum output power, and included basic rate equations although without having solved them yet for our particular fibre lasers.

In this chapter we will we describe an experiment made with the objective of developing a reliable high-power Yb^{3+}-doped fibre source, with output power in the region of several watts that can be used in conjunction with optical parametric oscillators (OPO) and amplifiers (OPA) to frequency convert to a broad band of wavelengths.

Among other important characteristics that a high-power fibre laser could have for certain applications are single mode, single-polarisation, narrow linewidth output, and broad tunability. The several tens of watts of diffraction-limited power available from cladding-pumped ytterbium-doped fibre lasers operating in the region of 1 – 1.1 μm [1] makes them attractive for non-linear frequency conversion via frequency doubling and via pumping of OPOs and OPAs [2]. In addition to high brightness, ideally these sources should have a linearly polarized output beam and narrow linewidth.

5.2 Fibre characterisation

The fibre used in the experiment was made in-house with the standard modified chemical vapour deposition (MCVD) technique. It had a pure-silica circular inner cladding with a diameter of 220 μm and a silicone outer cladding. The NA of the inner cladding was 0.4. The alumino-silicate core was placed 30% off-centre and had

a diameter of 7.6 μm, an NA of 0.11 and its cut-off wavelength was measured to be 1.0 μm. The ytterbium concentration (molar) was 0.3%, which gives an estimated small-signal absorption of 0.3 dB/m for the 915 nm. The corresponding measured absorption peak at 975 nm was 0.7-dB/m. Representative absorption and emission spectra are shown in chapter one.

5.3 Optical passive elements for polarisation control

Although a detailed study of polarization characteristics of fibre lasers is out of the scope of this work, it should be mentioned that for any laser source, output polarisation is one of the most important characteristics given the fact that laser light is the result of several processes: excitation of the activators, relaxation to meta-stable state, spontaneous emission from upper to lower level, and amplification of stimulated emission.

It is known that in theory an ideally round, straight, strain-free, single mode optical fibre has two degenerate modes of propagation and conserves the state of polarization of light guided in the core. In a real fibre, various imperfections such as asymmetric cross-section, thermal stress, variable core to clad area ratio, micro bends, etc. introduce birefringence [3].

On the other hand, even when the state of polarization of pump light is linear (for example), that fact does not imply an understanding of the polarization state of the laser light. It is known that lasing transitions are determined by the energy level structure as well as the pump wavelength. Another important fact to mention is that the phase and polarization of the pump light which plays a principal role in the polarisation evolution in an un-doped fibre, is totally lost during the electronic transition.

The state of polarisation (SOP) of the signal in a fibre laser in some cases follows the SOP of the pump. In real situations however, even small perturbations inside and outside the fibre result in alterations of the state of polarisation. For that reason it is

not possible to predict any polarisation characteristics of a fibre laser. And that is why polarisation maintaining fibres are required.

5.4 Polarisation effects in single mode fibres

Polarisation effects, in ordinary single mode fibres have created difficulties and problems in applications where a stable state of polarization is necessary, such as polarimetric fibre optic sensors, polarisation transformers, polarizers, de-polarizers and optical filters. In some of our experiments we are going to use external polarization controlling devices to manipulate the polarization of the output beam. Polarization is an important characteristic of a high-power fibre lasers for certain applications along with narrow linewidth, and broad tunability.

Below we describe experiments and discuss the results of developing a reliable high-power Yb^{3+}-doped fibre source, with output power in the region of several Watts that can be used in conjunction with optical parametric oscillators (OPO) and amplifiers (OPA) to frequency convert to a broad band of wavelengths.

It should be mentioned that single mode optical fibres do not normally preserve the polarisation state of the light propagating along the fibre. This could be of little consequence in many applications as the devices detecting the transmitted light are not sensitive to its polarisation state. However, recent applications such as the ones mentioned above and others, for instance, fibre optic interferometric sensors and coherent communications systems, do rely in some way on the polarisation state of propagating light, both along the fibre and at its output. These applications would benefit from optical fibres that can support a single polarisation state along their length.

Research effort has concentrated on identifying the various birefringence mechanisms that can exist or be induced in a fibre and thus affect the polarisation state of the guided light. In many cases, these birefringences are disturbing as it is their combined action, together with their extreme environmental sensitivity, that causes the unstable polarisation state at the output.

5.4.1 Polarisation eigenmodes

The transverse electric field of the lowest order mode that an optical fibre supports can arbitrarily be chosen to be polarised predominantly along the x direction as it is shown in figure 5.1.

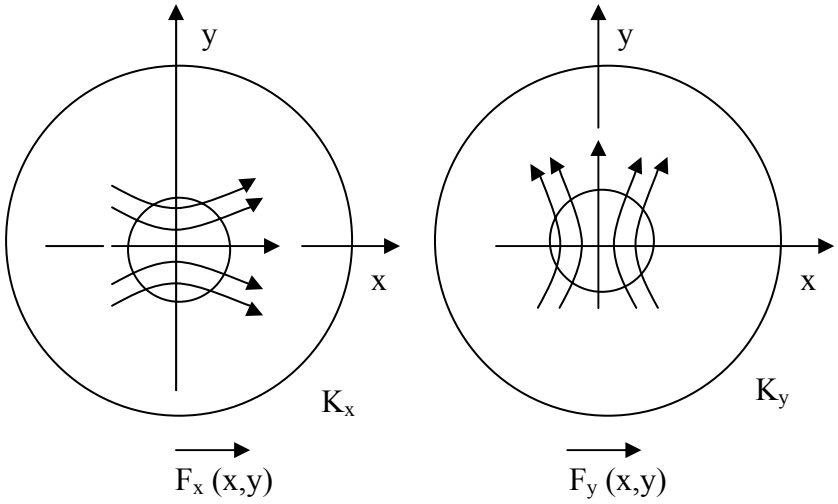

Fig. 5.1 The two polarisations of the fundamental HE_{11} mode of a fibre [4]

The orthogonal polarisation is an independent mode. These two modes constitute the two polarisation modes of a single-spatial-mode fibre, in this case linear polarisation is intuitively appealing although any two orthogonally-polarised modes could be chosen as the polarisation modes.

The linear superposition of the two orthogonal modes describes the electric field vector of any wave propagating along the z direction, according to [4]:

$$E(x,y,z) = \left[C_x F_x(x,y) + C_y F_y(x,y)\right] e^{-i\omega t} \qquad (5.1)$$

Where monochromatic propagation is assumed and $C_j = c_j e^{ikjz}$; $k_j = (2\pi/\lambda_0)n_j$ are the propagation constants of the polarisation modes, λ_0 is the free space wavelength, and n_j are the effective indexes of the modes. $C_{x,y}$ factors are complex coefficients which describe the amplitudes and phases of the modes. $F_{x,y}$ describe the spatial variation of

the electric fields. The state of polarisation of the modes is described by the average direction of its electric field vector, in this case linear along the x- and y- directions.

In ideal fibres of perfect rotational symmetry, the two modes are degenerate with $k_x=k_y$ and any polarisation state injected into the fibre would propagate unchanged. In practical fibres, any imperfections such as asymmetrical lateral stress, non-circular core, etc., break the circular symmetry of the ideal fibre and lift the degeneracy of the two modes. They propagate with different phase velocities and this difference between their effective refractive indexes is the fibre birefringence $B_f=n_y - n_x$ or equivalently, $\beta=k_0(n_y - n_x)$. Here, the x-mode is taken to be the fast mode. If light is injected into the fibre so that both modes are excited, one will slip in phase relative to the other while they propagate. When this phase difference is an integral number of 2π , the two modes will beat, and at this point, the input polarisation state will be reproduced.

The effect of a uniform birefringence is to cause a general polarisation state to evolve through a periodic sequence of states as it propagates. An important parameter is the length over which this beating occurs, known as the fibre beat length $L_p= 2\pi/\beta$.

Beat lengths of available single-mode fibres are in the range of 10 cm $< L_p <$ 2m, corresponding to $10^{-7} < n_y-n_x <10^{-5}$; a much smaller difference than the index difference between the core and cladding regions. We must note that in some cases, available single mode fibres have beat lengths of even several kilometres.

5.4.2 Birefringence mechanisms

There are several mechanisms which introduce birefringence whenever the circular symmetry of the ideal fibre is broken, thus producing an anisotropy refractive-index distribution in the core region. These mechanisms are shown in figure 5.2.

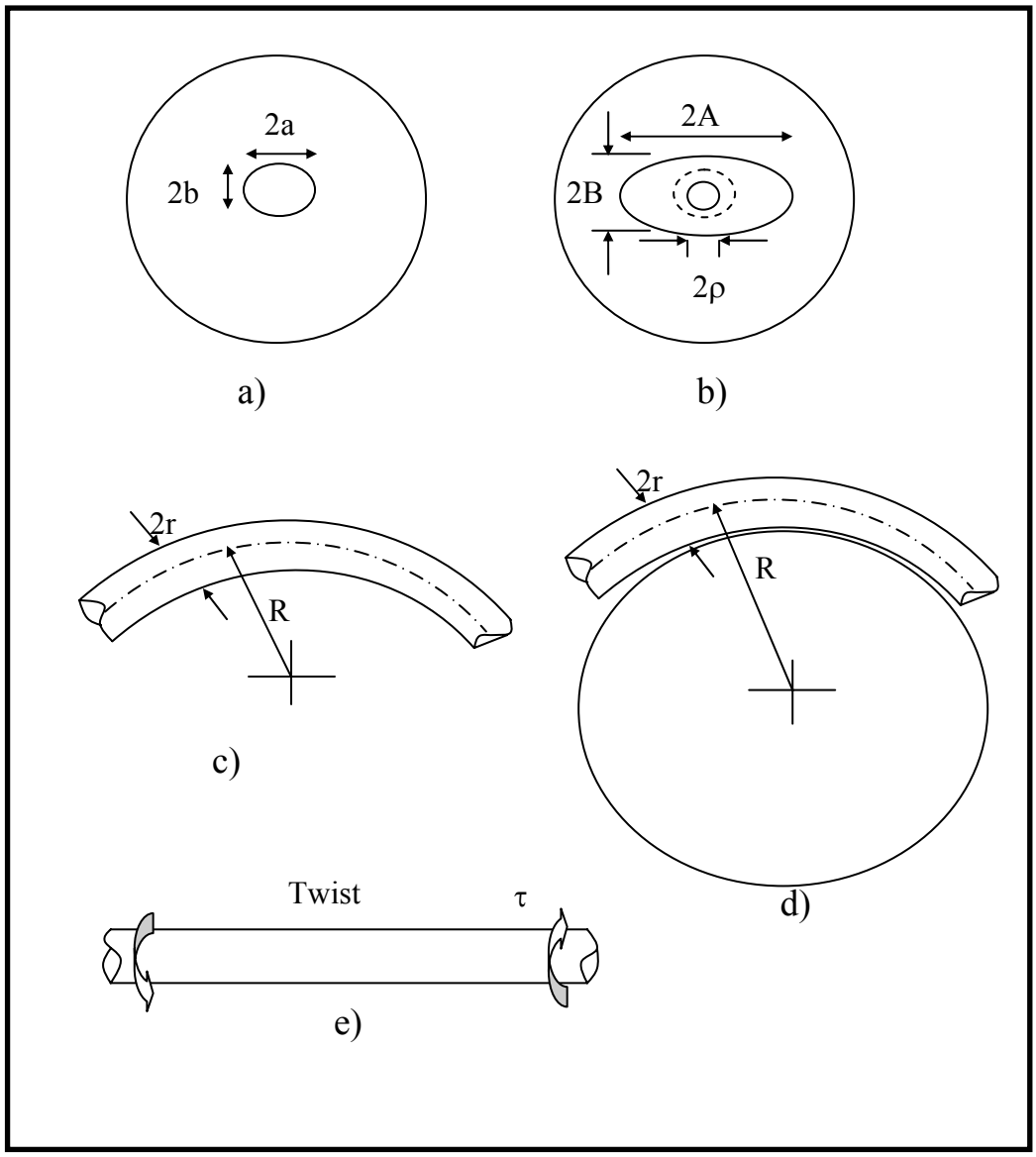

Figure 5.2 Birefringence mechanisms introduced due to some internal deformation or external action [4]

a) The geometrical anisotropy of a noncircular core introduces a linear birefringence in the fibre. Light travels fastest when polarised along the direction of the minimum polarisability; i.e. the smallest transverse dimension of the core.

This is the fast axis for the birefringence. This birefringence depends strongly on the frequency, or V-value, at which the fibre is being operated. If only frequencies near the higher mode cut-off are considered (V=2.4 for step index fibres), the birefringence for fibres with small core ellipticity , $(a/b - 1) \ll 1$, can be approximated by:

$$\beta_c \approx 0.2k_0\left(\frac{a}{b}-1\right)\left(\Delta n^2\right) \qquad (5.2)$$

For fibres with ellipticity in the region $2<(a/b-1)<6$, the birefringence near the higher mode cut-off is simply $\beta_c \cong 0.25k_0(\Delta n)^2$, which is also the maximum birefringence that can be introduced in an elliptical core while still operating in the single-mode regime. From equation 5.2 in order to fabricate a relatively low birefringence fibre L_p = 50 m at λ= 0.85 nm, the value of the typical index difference $\Delta n = 5 \times 10^{-3}$, or an ellipticity of less than 0.3%.

b) Any asymmetrical transverse stress introduces a linear birefringence via elasto-optic index changes. During fabrication of the fibres and as the result of different thermal contraction between differently doped non-circularly symmetric regions of the fibre (Figure 5.2 b), the stress zone can be generated. The usually more heavily doped noncircular cladding is constrained by the outer fibre jacket producing the stress asymmetry. The birefringence in this case can be calculated using $C_s=0.5k_0n_0^3(p_{11}-p_{12})(1+\nu_p)$ within the equation [4]:

$$\beta_s = \frac{C_s}{(1-\nu_p)}\Delta\alpha\Delta T\frac{A-B}{A+B} \qquad (5.3)$$

A and B are dimensions indicated in figure 5.2. $\Delta\alpha$ is the difference between the expansion coefficients of the cladding and the substrate tube materials. p_{11} and p_{12} are the components of the strain optical tensor of the fibre material, ν_p is Poisson's ratio and ΔT is the difference between the room temperature and the softening temperature of the more heavily doped material. This stress birefringence is constant everywhere within the elliptical cladding and provided B>>p (the core radius), the mode field is confined within the elliptical cladding; thus β_s is independent of the V-value.

Using some practical values for the parameters involved, we can estimate the strength of this birefringence. If n=1.46, p_{11}=0.12, p_{12}=0.27, and ν_p=0.17 for fused silica yields $C_s=2.02 \times 10^6$ m^{-1} at 850 nm. Assuming a boron-doping level of q≈4 mole% in the cladding to result in a $\Delta n=2.1 \times 10^{-3}$ and thus, $\Delta\alpha=3.8 \times 10^{-7}$ $^oC^{-1}$ and $\Delta T=800^o$ results

in a cladding ellipticity (A-B)/(A+B)<1.7 x10^{-4} to achieve a L_p=50 m. That is, the fibre structure must be circularly symmetric to a very high degree unless the fibre is fabricated to make two of the birefringences approximately cancel β_c-$\beta_s \approx 0$.

c) Freely bending of a fibre places the outer portion of the fibre cross section in tension, which presses laterally on the inner portion which is in compression. This second-order birefringence is described as [4]:

$$\beta_b = 0.5 C_s \frac{r^2}{R^2} \qquad (5.4)$$

Where R is the radius of the arc that describes the bending fibre. The fast axis of this birefringence is perpendicular to the bending axis. For large diameter coils, this birefringence is small $\beta_b \approx 0.01$ rad/m yielding a L_p=622μm for 2r = 100μm, 2R =1m, and λ= 850 nm. However, for small diameter coils, it can be large $\beta_b \approx 100$ rad/m, L_p= 6.2μm when 2R= 1cm.

d) Bending a fibre under tension F around a drum induces linear birefringence which adds to the bending birefringence. It results from the lateral force exerted by the drum on the fibre in reaction to the tensile force F. It is described by [4]:

$$\beta_{tc} = C_s \frac{2 - 3\nu_p}{1 - \nu_p} \frac{r}{R} \in \qquad (5.5)$$

R is the radius of the drum along which the fibre is bent. ν_p is Poisson's ratio, ν_p=1.7 for fused silica. In the equation $\in$ is the mean axial strain in the fibre, thus $\in \approx F/(\pi r^2 E)$. E is Young's modulus of the fibre material. For 2R =1m, and a moderately large $\in$=0.5 percent, β_{tc} and β_b are comparable, as β_{tc}= 180 rad/m for a L_p= 3.5cm.

d) The resulting shear stress induced by a twisting force applied into fibre, couples the longitudinal electric field of one mode with the transverse field of the orthogonal mode. Because these field components are π/2 out of phase, a circular birefringence

α_τ which is proportional to the twist rate τ results: $\alpha_\tau = g\tau$; where $g=-0.5n_o^2(p_{11} - p_{12})=$ 0.146 for silica. The modes of this birefringence are the left and right circular polarisations. Because g is small, the circular birefringence that can be introduced in this way is small unless the twist rate is very large. A twist rate of 137 turns/m is necessary to achieve a beat length L_p= 5 cm (α_τ =126 rad/m).

In any fibre the different birefringences are present in unknown numbers, strengths, and distributions along the fibre. This causes the polarisation state, both along the fibre and at the output to be unpredictable and unstable. The combined effect of several birefringences on the polarisation can be described by the Poincaré sphere in which any general elliptical polarisation state can be represented.

5.5 Results on slope efficiency, tuning range and output power

The resulting system described here is a polarised, wavelength-tunable, cladding pumped Yb^{3+}-doped single-mode fibre laser.

5.5.1 Experimental Set-Up

Figure 5.3 shows the experimental set-up of the single polarisation fibre laser. In the case of free-running laser operation, two beam shapers [5] transformed the highly elliptical output from two high-power 915 nm diode bars into pump beams with nearly equal M^2 values in orthogonal planes and approximately similar divergence.

The output beam from the beam shapers were launched using dichroic mirrors and anti-reflection-coated gradient-index lenses with a focal length of 25 mm, into both ends of a Yb^{3+}-doped double-clad fibre. After the 25-mm focal length lenses, an incident beam with a numerical aperture of 0.25 was obtained.

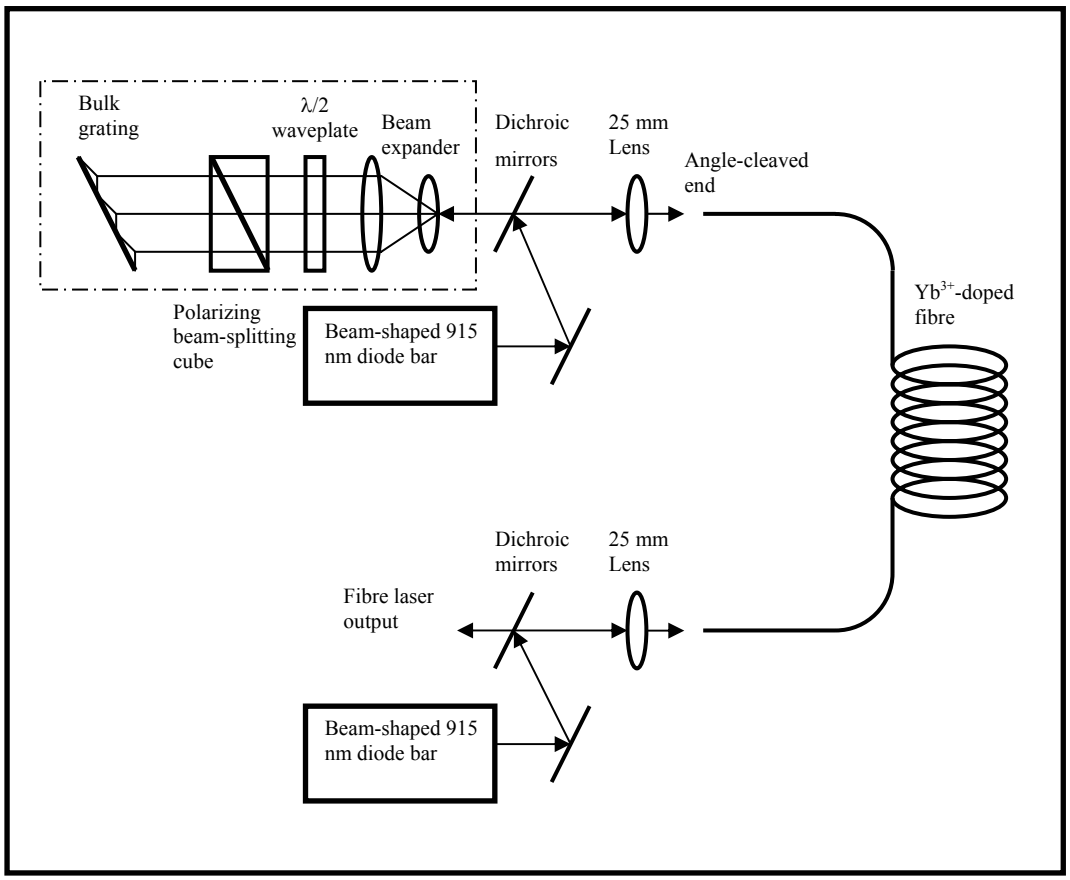

Figure 5.3 Single polarisation, narrow-linewidth, Yb-doped fibre laser
Inset: arrangement for tunable fibre laser

The flat-cleaved fibre ends formed the cavity with the 3.5% Fresnel reflection. Next, we built a single-polarisation tuneable fibre laser using the set-up shown in figure 5.3 with the included arrangement drawn in the inset. One fibre end was angle-cleaved to suppress the 3.5% broadband feedback. In its place, an external blazed bulk grating with 600 lines/mm mounted on a rotation stage was used to obtain a wavelength selective tuneable feedback. A polarising beam-splitter and a zero order λ/2 waveplate were also inserted in the feedback path.

5.5.2 Results on single mode, single polarisation operation

For the free running laser, the fibre used was 30 m in length with a lasing threshold of 1.8 W. A slope efficiency of 72% was measured with respect to launched pump power. The lasing wavelength was 1090 nm and the maximum output power taken from both ends was 18 W.

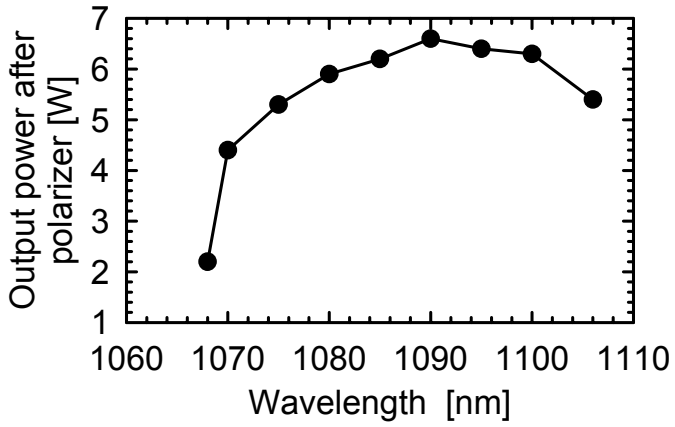

Figure 5.4 Tuning range for single polarisation fibre laser

In the case of the single-polarisation tuneable fibre laser, the output power from the laser using this new set-up was now 7.5 W, from which at least 90% was in a single linear polarisation. The threshold and slope efficiency were measured to be 1.6 W and 24% respectively, both with respect to launched power.

The laser showed a tuning range from 1070 to 1106 nm, shown in figure 5.4, with a laser linewidth consistently below 0.2 nm.

Power fluctuations from the laser were investigated using a fast detector. We observed that at high pump powers close to the maximum power available, the output was truly continuous wave with small fluctuations, although it sometimes drifted over minute-long scales. On the other hand, at low powers the laser emitted irregular pulses, with an average repetition frequency in the range of 100-200 kHz. In this case,

the λ/2 waveplate orientates the polarisation angle of the already linearly polarised light relative to the birefringence axis of the fibre, which helped to increase the stability of the laser. This indicates that the fibre was sufficiently birefringent to partly suppress coupling between the two polarisation modes.
The fibre used had an offset core which is likely to induce some stress during manufacture. Besides, it is well known that rare-earth doped fibres are often significantly more bi-refringent than standard fibres. Nevertheless, we believe a higher birefringence would make the laser more stable.

The reason for the lower power in the case of the tuneable laser could be that we operated the diode bars at slightly less power, corresponding to 15 W of output from the free running laser of figure 5.3. Although in fact, the output power did not decrease significantly when we inserted the polarizer into the cavity, polarisation losses could be another reason for reduced output power. As a matter of fact, coupling losses when launching the beam back into the core and diffraction losses were more important source of loss. We obtained typical coupling efficiencies of 30%, while the overall feedback becomes approximately 20% as the measured diffraction efficiency into the back-scattered beam was measured to be of 65%.

In order to calculate powers P_1 and P_2 that are delivered at different ends of the fibre depend on the feedback R_1 and R_2 as:

$$\frac{P_1}{P_2} = \left[\frac{(1-R_1)}{(1-R_2)}\right]\left[\frac{R_2}{R_1}\right]^{1/2} \qquad (5.6)$$

Equation 5.6 is correct for a fibre laser with a high small-signal gain and for lasers working in saturation, so the total power delivered by the fibre is largely independent of the amount of feedback over a wide range of values.

In our case, with the 20% feedback at one end and 3.5% at the other out-coupling end, we calculate that the fraction coupled out becomes 74% of the net power emitted from the fibre, with the other 26% lost in the grating end. If we start estimation with the original 15 W of output power from the free running laser, this means that 11 W of

output are obtained from the polarised laser, i.e. considerably more than what we actually measured.

Although the precise value of the angle-cleaved end is not very critical, during this experiment we noticed that it was difficult to obtain a predetermined reflectivity by means of angle-cleaving one fibre end. Up to some degree, we found that the angle cleave significantly impacts the launching efficiency of the pump power. This was reflected by the fact that the launched power dropped by 30% in the angle-cleaved end. The combined output power was measured from both ends of the fibre laser without any feedback, which resulted to be of only 10.8 W.

For future experiments, the fibre ends can be coated for low reflectivity. Coated fibre ends could lead to a higher launching efficiency of the pump power with the advantage that the anti-reflection coating would extend to the pump wavelength.

5.5 Conclusions

In this chapter we presented the experimental study of a single polarisation, wavelength tuneable, cladding-pumped, Yb-doped fibre laser with more than 6.5 W of output. The laser was tuneable over approx. 40 nm from 1070 to 1107 nm, and with a linewidth of less than 0.2 nm over the whole range. Further significant improvements in terms of improving the feedback in the grating end can be done by improving the launching efficiency. Improving the output power by reducing the feedback in the out-coupling end is also feasible. The required single-pass gain of the fibre laser is 17 dB using the reflectivity of the type of cavities used in this work. Thus, even with a smaller feedback, which could lead to a lower output power and a reduced tuning range, the fibre laser would remain strongly saturated. At the same time it would imply that the power conversion efficiency as well as the tuning range would be almost the same.

References to Chapter 5

5.1 Mundial M., Engstrom B., Kea D., Laliberte B.M., Mins R.A., Robinson R.F., Rockney B.H., Zhang Y.H., Collins R., Gravilovic P., and Rowley A., "35 watt single-mode ytterbium fibre laser", Proc. Conference on Lasers and Electro-Optics, Baltimore, May 1997, Post-deadline paper CPD30-2

5.2 Britton P.E., Offerhaus H.L., Richardson D.J, Smith P.G.R., Ross G.W., Hanna D.C., "A parametric oscillator directly pumped by a 1.55μm erbium fibre laser", Opt. Lett., **24**, No. 14, 975-977, (1999)

5.3 Lin T.J., "Polarisation effects in fibre lasers", Ph.D Thesis, University of Southampton, 1990.

5.4 Rashleigh S.C., "Origins and control of polarisation effects in single-mode fibres", J. Light. Tech., Vol. LT-1, No. 2, (1983)

5.5 Clarkson W.A. and Hanna D.C., "Two-mirror beam-shaping technique for high-power diode bars", Opt. Lett. 21, 375-377 (1996)

Chapter 6

Experiments on Pulse Generation in Cladding Pumped Fibre Lasers

6.1 Introduction

There are two main techniques for the generation of short optical pulses, which are known as Q-switching [1,2] and mode-locking [3,4], which is a practical means of short pulse generation compatible with telecommunication and sensor systems. In this chapter we consider Q-switched operation only since this techniques allows us to increase peak power by several orders of magnitude compared with continuous wave fibre lasers.

6.2 Description of Q-switched operation of fibre lasers

The operation of a Q-switched laser can be described as follows: the Q (quality factor) of an optical cavity is defined as the ratio of energy stored in the cavity to that lost per round trip. Initially the losses of the cavity are set at a very high value, reducing the Q value of the cavity, and the gain medium is excited. As the losses are high the laser is normally unable to reach threshold.

This causes the population inversion to build up to a value that is well in excess of the value that would be achieved under normal conditions, i.e. in a regime of a free running laser. At a certain point, the losses are abruptly reduced to their normal values, then the small signal gain is much larger than the losses and it results in rapid building up of laser output power, which quickly saturates the maximum gain.

Gain saturation obtained at that point is so strong that drives the inverted population well below the threshold population level, thus inhibiting laser action again. The pulsed regime is then a result of this rapid rise and fall of the intra-cavity flux.

Q-switching operation can be obtained using mechanical, acousto-optic, electro-optic methods, or by the use of a saturable absorber, all of them are compatible with fibre lasers. Rapid modulation of the cavity can be achieved by using an acousto-optic modulator (AOM) which commonly offers high switching speeds in the range of 50 to 150 ns and fast repetition rates up to the mega Hertz (MHz) level. However, it suffers from a low extinction ratio, typically in the region of 50 to 70%.

Some of the important characteristics of transversally single-mode fibre lasers such as: good spatial mode and high average power, at the same time represent a limit in average power for these devices, when operated in Q-switched regime.

6.3 Equations to describe pulse generation and energy

From equations 6.1 and 6.2 [5] it can be seen that the population n_i at the opening time of the q-switched cavity determine both the pulse duration and energy per pulse. So, the difference between n_i and n_f should be large in order to obtain a high-energy pulse from the system. It has been demonstrated that the energy of the pulses could be considerable [6], given the fact that they are directly related to the intrinsic losses of the cavity, which are relatively small so, it should be feasible to produce high-energy pulses from Q-switched fibre lasers.

$$E = \frac{Vh\upsilon\left(n_i - n_f\right)}{\frac{\sigma_a}{\sigma_e}} \frac{\ln\left(\frac{1}{R}\right)}{\ln\left(\frac{1}{R}\right) + \alpha} \tag{6.1}$$

$$t_p = t_c \left\{ \frac{n_i - n_f}{n_i - n_t \left[1 + \ln\left(\frac{n_i}{n_t}\right) \right]} \right\} \tag{6.2}$$

Where:

E is the energy,

t_p is the duration of the Q-switched pulse

n_i is the inverted population before the opening of the cavity

n_t is the threshold population

n_f is the inverted population after opening the cavity and the q-switched pulse has formed

R is the reflectivity of the output coupler of the laser

α represents the intrinsic losses of the fibre

V is the mode volume of the gain medium

υ is the wavelength of the laser transition

h is the Planck's constant

t_c is the photon lifetime in the cavity

γ is σ_a/σ_e

The optical fibre length governs the photon lifetime in the cavity t_c which in turn determines the pulse duration.

Several publications [7, 8, 9] have been focused on Q-switched, cladding-pumped fibre lasers on which the design of the doped-core is a key aspect. In this work, we explore the possibilities of increasing high-intensity, high-energy short pulses using a relatively complex fibre structure. A maximum energy level of 2.3 mJ was reported [10] using a large mode area (LMA) fibre for a high brightness beam and an M^2=3.

6.4 Q-switched fibre laser with tapered region

For the first of the two Q-switching experiments described in this chapter, we implemented the experimental configuration shown in figure 6.1. The same beam shaped-diode bar that was used for CW fibres lasers pumped the pulsed fibre laser. It has a nominal output power of 60 watts before the beam shapers. Incident power into fibre is approximately 35 watts. Beam steering dichroic mirrors and 25-mm lenses were used for focusing the beam.

The output end was angled-cleaved to suppress feedback and light from this end was collimated and directed to the acousto-optic modulator (AOM) that was used to Q-switch the fibre laser. A high reflectivity mirror was used to reflect first-order diffracted light from the AOM back into the fibre end, while a perpendicular fibre facet closed the cavity at the input.

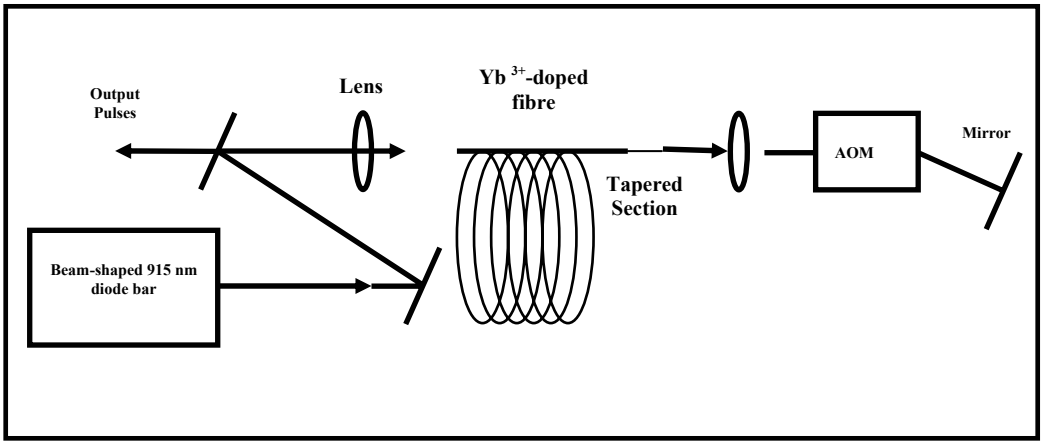

Fig. 6.1. Experimental set-up for the Q-switched fibre laser with tapered fibre

In order to measure the output pulses we used both a fast and a slow detector. The slow detector integrated the pulse energy and was used to determine the energy in the pulse in the presence of amplified spontaneous emission (ASE), while the pulse shapes of pulses were obtained with the fast detector.

The slow detector was calibrated by measuring the output energy at high repetition rates where there is no significant ASE (verified using a spectrum analyser).

6.4.1 Results of Q-switched fibre laser with tapered region

The obtained pulse energy dependence on repetition rate is shown in figure 6.2

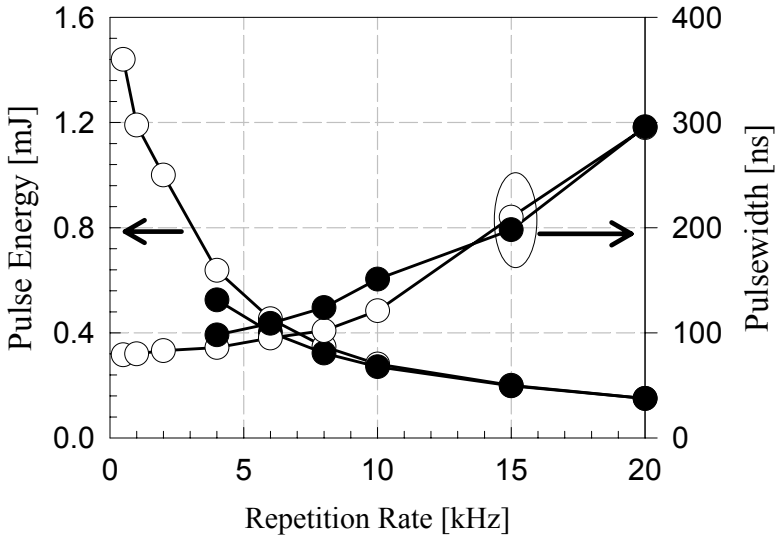

Fig. 6.2 Experimental results on pulse energy and average power as a function of repetition rate for the Q-switched, tapered fibre laser

The Gaussian-type pulses obtained reached pulse energies of 0.6 mJ at 4 kHz using a tapered fibre laser and 1.3 mJ at 500 Hz using un-tapered laser, corresponding to average powers of 2.1W for the tapered laser and 0.8 watts for the conventional laser. The pulse duration ranged from 100 ns to 280 ns and from 130 to 310 ns, for the tapered and conventional laser, respectively, which decreased with increased pulse energy.

However, at high pulse energies, we estimate that the peak intensity would exceed the damage threshold for the front facet and therefore limit the pulse energy to 0.6 mJ. The output beam was of good spatial quality, multimode in the case of conventional fibre, with an M^2=7.5 and quasi mono-mode in the tapered case, with an M^2=1.8.

6.5 Q-switched large mode area (LMA) fibre laser

6.5.1 Introduction and fibre design

The main performance advantages of a large mode area (LMA) fibre laser relative to conventional bulk solid state lasers arise from the combination of beam confinement and the excellent heat dissipation due to the large surface area to gain volume ratio of doped fibre. High efficiencies and high gains are readily achieved and the problems of thermal loading and beam distortion can essentially be eliminated. Moreover, extremely compact and robust sources can be constructed. Continuous wave powers in excess of 100 W have now been achieved using the cladding pump technique [11].

Whilst the comparison with bulk lasers is favourable in relation to CW operation the situation is quite different for pulsed (e.g. Q-switched) performance. In this instance, the rapid build up of amplified spontaneous emission (ASE), and ultimately the onset of lasing due to the high-gains achievable within conventional single-mode fibre, limits the energy storage to a few tens of μJoules. This is to be compared to the milli joules that are routinely obtained from bulk laser systems in which the mode sizes are much larger and less constrained.

One route to increasing the pulse energies in fibre is to increase the mode area, although this clearly cannot be increased indefinitely without compromising the modal-quality of the output. In a sense the problem of improving the pulsed performance, reduces to one of making a fibre laser as much like a bulk laser as possible whilst retaining the desirable features of the fibre approach.

Previously, experiments with core-pumped erbium doped fibre lasers showed that lowering the numerical aperture (NA) of the fibre could increase the mode size within a purely single mode (SM) fibre. A factor of ten increase in mode area (and pulse energy) relative to conventional designs for a purely SM core was obtained [12]. Further

increases in mode area are limited by bend-loss and fabrication tolerances using this simple approach.

High energy, single mode (SM) output can be obtained from fibre lasers and amplifiers based on fibres which are pulled to multi-mode dimensions. Complex strategic distribution of the dopant along the transverse axis of the fibre is performed in those cases to give maximum overlap, and hence preferential gain, to the fundamental mode [13,14].

Mode-quality degradation is an issue, however it has been shown that using a low NA core design (similar to the one described herein), and an appropriately large outer cladding to reduce mode-coupling [15], significant further increases in SM mode-area are possible [16]. In this work, we refer to such fibres as large mode area (LMA) fibres.

Most importantly, the concept of the LMA fibre has been extended to encompass both the cladding pump technique, and ytterbium doping for the first time. Cladding pumping allows the use of high-power broad stripe diode and diode bars [17,18], making for a practical system and far higher average powers than previously demonstrated. In addition, we investigate a new cavity design that recycles ASE that would ordinarily be lost from the system.

The fibre was designed by scaling the previous erbium-doped LMA fibre core design reported in [13] to a dimension appropriate for Yb^{3+}, and adding a high NA inner cladding for cladding pumping. A cross-section of the refractive index profile of the fibre is shown in Figure 6.3. The fibre preform was fabricated in-house using the conventional modified chemical vapour deposition (MCVD) technique. This preform was then milled to produce the rectangular shape for the inner cladding.

The outer cladding was applied at the fibre pulling stage and consists of a silicone rubber coating. The coating-glass interface defines an inner cladding NA of 0.4. The rectangular, inner cladding measures 175×350 μm. The rectangular shape was chosen to eliminate

helical trajectories for the pump radiation so as to obtain efficient pump absorption, as previously suggested in [19].

Pump absorption for this fibre was ~3dB/m at 915nm. The alumino-silicate LMA-core was centred in the inner cladding. It had a NA of 0.075, a diameter of 44 μm (diameter of the inner ring) and was doped with 0.3% Yb^{3+} by weight. The radial doping distribution creates preferential gain for the fundamental mode due to a higher overlap of that mode with the doped region. The large mode area of approximately 1500 μm^2 provides a saturation energy of the order 0.5 mJ at 1090 nm, whereas a more standard fibre with a core diameter of ~9 μm offers a saturation energy of only ~25 μJ.

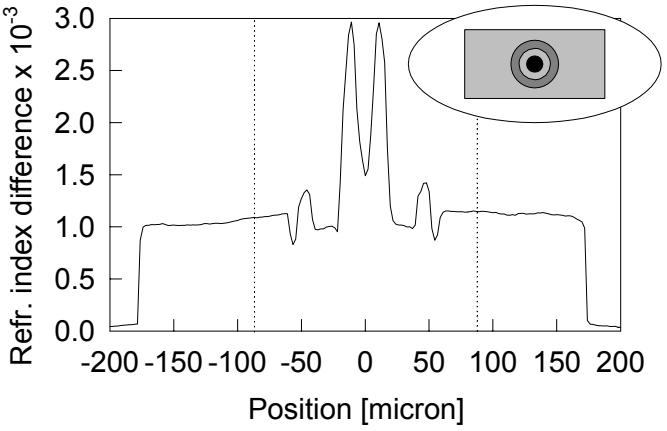

Fig. 6.3 Core index profile, as evaluated in the preform and scaled to the fibre dimension (350 μm). The dashed lines indicate the width of the outer cladding in the milled (175 μm) direction. The squared-shape inner cladding increases absorption of the pump

6.5.2 Set-up for the large mode area Q-switched fibre laser

Figure 6.4 depicts our laser set-up. The Yb^{3+}-doped fibre was 36m long. It was end-pumped by a 915-nm beam-shaped diode bar [20] that produced up to 35W in a circular beam. We measured a launch efficiency of approximately 60%. A set of anti reflection-

coated dichroic mirrors was used to steer the diode beam and to separate the pump from the signal. A lens with a 25-mm focal length was used to focus the light into the fibre.

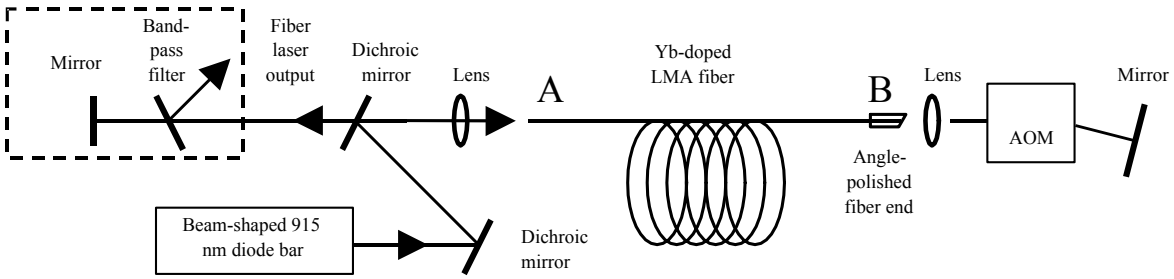

Fig. 6.4 Experimental Set-up of the LMA fibre laser

The output end B was angled-polished to suppress feedback and light from this end was collimated and directed to the acousto-optic modulator (AOM) that was used to Q-switch the laser.

A high reflectivity mirror was used to reflect first-order diffracted light from the AOM back into fibre end B. Initially, a perpendicular fibre facet closed the cavity at end A. The end was polished because it proved difficult to cleave the rectangular fibre with sufficient precision. The laser performance at low repetition rate was critically dependent on the quality of this facet. Due to the low NA of the fibre, a maximum bend radius of 25cm was kept during experiments to avoid bending losses.

6.5.3 Results on maximum pulse energy and discussion

The output pulses were measured with both a fast and a slow detector. The pulse shapes were detected with the fast detector. The slow detector (response time 10 μs) effectively integrated the pulse energy and was used to determine the energy in the pulse in the presence of ASE. The slow detector was calibrated by measuring the output energy at high repetition rates where there is no significant ASE (this was verified using a spectrum analyser).

Figure 6.5 shows the pulse energy dependence on repetition rate and pump power. We reached pulse energies of 1.6mJ at 1kHz and 1mJ at 5 kHz, corresponding to an average power of 5 Watts. The pulse duration ranged from 0.1 to several microseconds (decreasing with increased pulse energy), and exhibited peaks separated by the cavity round-trip time (0.36 μs). At high energies, a single peak shorter than 0.1 μs dominated the pulse. It is to be noted that by using a shorter length of fibre (<10m), the pulse structure can be eliminated, so that a smooth short single pulse is obtained.

However, for this particular fibre the pulse energy was somewhat compromised in this limit. Damage to fibres operating at these pulse energies and powers is a key issue. Operation of our laser at pulse energies above 1.5 mJ could only be maintained for relatively short periods of time before damage to the output facet would take place. However, various beam expanding and facet-preparation techniques exist which should allow solving this problem.

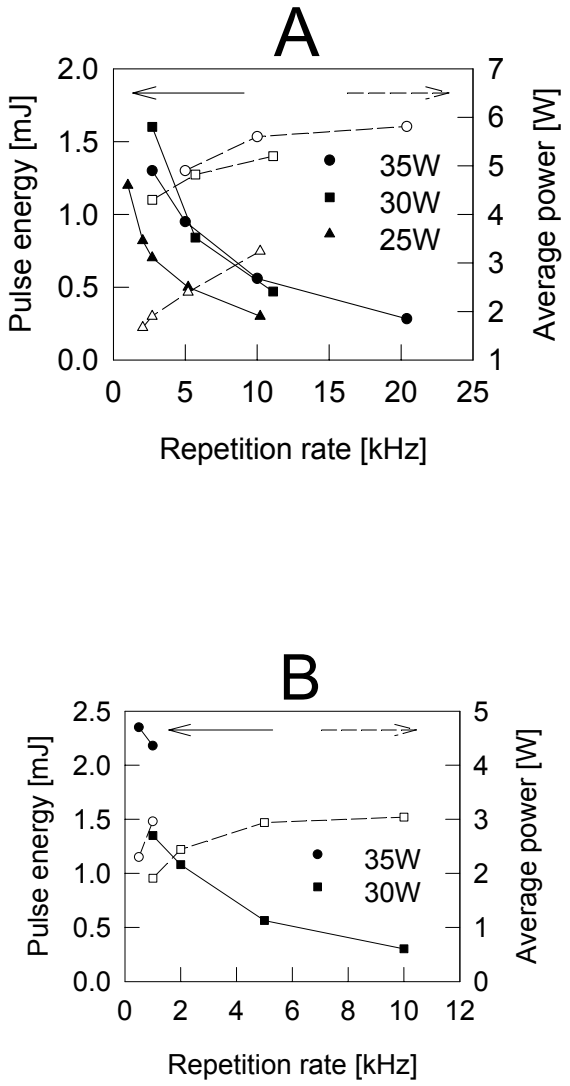

Fig. 6.5 Pulse energy and average power as a function of repetition frequency (for several incident powers)(A) Without ASE feedback, (B) with ASE feedback

The low NA LMA-design reduces the number of guided core-modes, which further improves the energy storage relative to a higher NA design. Even so, the core supports ~20 modes at the operating wavelength of 1090 nm. The M^2 value of the output beam was ~3, as measured with a commercial beam scope system from Merchant Ltd.

Using a similar fibre with a 20 μm diameter core, we measured an M^2-value of less than 1.3. Note that for the larger diameter fibre the shape of the lowest-order mode follows the ring-shaped index profile and has a somewhat donut-like character in the near field. This in itself goes a long way to accounting for the increased M^2.

In the initial 36m-cavity design ASE build up between pulses reduced the pulse energy when we operated the laser at repetition rates below 2 kHz. In this instance most of the ASE was emitted from the cavity at end B since it is seeded by the ~4% Fresnel reflection at end A.

Note that due to the long cavity length, and signal re-absorption, the peak of the ASE emission was centred at 1090 nm. However, by eliminating the reflection from end A we could ensure that most of the ASE was emitted at end A, and at a shorter wavelength of 1035 nm [21].

By now adopting the more complex out-coupling design shown in Fig. 6.4 we could separate the ASE from the laser output with a narrow band filter and reflect it back into the cavity, whilst keeping feedback around 1090 nm low. The ASE is thus recycled and used to help pump longer signal wavelengths (in particular towards end B of the fiber by which point most of 915 nm pump radiation has been absorbed). This lowered the ASE losses by approximately 2.5W or 65%. A similar scheme has previously been used in erbium-doped fiber amplifiers [22].

The ASE output at end A was now negligible, even at low repetition rates. At 500 Hz repetition rate, we reached intra-cavity pulse energy of 2.3 mJ, of which 1.8 mJ was output from the band-pass filter. Given that the filter reflected only ~78% a better band-pass filter would allow us to retrieve most of the 2.3 mJ of output pulse energy available after the dichroic mirror.

6.6 Conclusions

We have explored two approaches for Q-switching fibre lasers which proved to be compatible. Firstly, The experiment using an LMA fibre gave us interesting results. A novel Q-switch fibre laser cavity design that recycles ASE emitted between pulses was demonstrated, we obtained 2.3 mJ pulse energies from a fibre laser system. In addition, we demonstrate average powers in excess of 5W (1 mJ-pulse energies) under Q-switch operation.

We view that realistic improvements in fibre design should allow for further increases in pulse energy, improved power handling and even better beam quality. This part of our work represents a different approach to develop a robust, high power, single-mode, cladding-pumped Yb-doped fibre laser that is one of our major objectives.

Secondly, we saw that both approaches are compatible with other techniques for improving beam quality while obtaining high-energy pulses as we could obtain similar (in level) high-energy pulses. Again, for the approach with tapered fibre, the main problems were identified being fibre facet damage and mode conversion after propagation along the un-tapered fibre.

References to Chapter 6

6.1 Mears R.J., Reekie L., Poole S.B., Payne D.N., "Low-threshold, tuneable, CW and Q-switched fibre laser operating at 1.55 μm", Elect. Lett. Vol. 23, No. 3, pp. 159, (1986)

6.2 Reekie L., Jauncey I.M., Poole S.B., Payne D.N., "Diode laser-pumped operation of an erbium-doped single-mode fibre laser", Elect. Lett. Vol. 23, No. 20, pp. 1076, (1987)

6.3 Alcock I.P., Tropper A.C., Ferguson A.I., Hanna D.C., "Q-switching, mode locking and tuneable operation around 0.9 μm of a neodymium-doped monomode fibre laser, "IEEE proceedings, Vol. 134-J (3), pp. 183, (1987)

6.4 Duling I.N., Goldberg L., Weler J.F, "High-power, mode-locked neodymium fibre laser by an injection-locked diode array", Elect. Lett. Vol. 24, No. 21, pp. 1333, (1988)

6.5 Koeckner W., *Solid State Laser Engineering*, Chap. 8 Springer Verlag, Berlin, (1988)

6.6 Hanna D.C., Smart R.G., Suni P.J., Ferguson A.I., Phillips M.W., "Measurements of fibre laser losses via relaxation oscillations", Opt. Commun., Vol. 68, No. 2, pp. 128, (1988)

6.7 Chernikov S.V., Zhu Y., Taylor J. R., Platonov N.S., Samartsev I.E., Gapontsev V.P., "1.08 – 2.2 μm supercontinuum generation from Yb^{3+}-doped fibre laser", Technical Digest CLEO, p. 210, (1996)

6.8 Gapontsev V.P., Fomin V.V., Samartsev I.E., Unt A., "25kW peak power, wide-tuneable repetitio-rate and pulse ruration eye-safe MOPFA laser", Technical Digest CLEO, pp. 209-210, (1996)

6.9 Nilsson J., Jaskorzynska B., "Modelling and optimisation of low-repetition-rate high-energy pulse amplification in cw-pumped erbium-doped fibre amplifiers", Optics Letters, Vol. 18, pp2099-2101(1993)

6.10 Offerhaus H.L., Alvarez-Chavez J.A, Nilsson J., Turner P.W., Clarkson W.A., and Richardson D.J., "Multi-mJ, multi-Watt Q-switched fibre laser", in *Proc. Conference of Lasers and Electro-Optics*, Baltimore Ma. USA, Post-deadline paper CPD10-1, (1999)

6.11 Dominic V., MacCormack S., Waarts R., Stevens S., Bicknese S., Dohle R., Wolak E., Yeh P.S., Zucker E., "110W fibre laser", Post-deadline paper CPD11 in *Proc. Conference on Lasers and Electro Optics*, Baltimore (1999)

6.12 Taverner D., Richardson D.J., Dong L. and Caplen J.E., "158μJ pulses from a single transverse mode, large mode-area EDFA", Opt. Lett. 22(6), pp. 378-380 (1997)

6.13 H.L. Offerhaus, N.G.R. Broderick, R.S. Sammut, L. Dong, J.E. Caplen D.J. Richardson, "High-energy single-transverse-mode Q-switched fibre laser based on a multimode large-mode-area erbium-doped fibre", Opt. Lett. 23, 1683-1685 (1998)

6.14 Sousa J.M., Okhotnikov O.G., "Multimode Er-doped fiber for single-transverse-mode amplification", Appl. Phys. Lett. 74(11), 1528-1530 (1999)

6.15 Fermann M.E., "Single-mode excitation of multimode fibres with ultra-short pulses", Opt. Lett. 23(1), 52-54 (1998)

6.16 Broderick N.G.R., Offerhaus H.L., Richardson D.J, Sammut R.A., Caplen J., Dong L., "Large mode area fibres for high power applications", Optical Fibre Technology 5, 185-196 (1999)

6.16 Nilsson J., Alvarez-Chavez J.A., Turner P.W., Clarkson W.A., Renaud C.C., Grudinin A.B., "Widely tuneable high-power diode-pumped double-clad Yb^{3+}-doped fiber laser", Paper WA2 In *Proc. Advanced Solid State Lasers*, Boston (1999)

6.17 Goldberg L., Koplow V, Kliner D.A.V., "Highly efficient 4W Yb-doped fibre amplifier pumped by a broad-stripe laser diode", Opt. Lett. 24 (10), 673-675 (1999)

6.18 Muendel M., "Optimal Inner cladding shapes for double clad fibre lasers", in *Proc. Conference of Lasers and Electro-Optics*, Anaheim Ca. USA Technical digest series, paper CTuU2, Vol. 9, 209 (1996)

6.19 Clarkson W.A. and Hanna D.C., "Two-mirror beam-shaping technique for high-power diode bars", Opt. Lett. 21, 375-377 (1996)

6.20 Paschotta R., Nilsson J., Tropper A.C., and Hanna D.C., "Ytterbium-doped fibre amplifiers", IEEE J. Quant. Electron. 33, 1049-1056 (1997)

6.21 Nilsson J., Yun S.Y., Hwang S.T., Kim J.M., and Kim S.J., "Long-wavelength erbium-doped fibre amplifier gain-enhanced by ASE end-reflectors", IEEE Photonics Technol. Lett. 10, 1551-1553, (1998)

Chapter 7

Experiments with Er^{3+}-Yb^{3+} Co-Doped Fibre Lasers

7.1 Introduction

In previous chapters we have already discussed cladding pumped Yb^{3+}-doped fibre lasers as the main part of our work. In the present chapter, we discuss experiments carried out using the Er^{3+}/Yb^{3+} approach, which increases the choice of pump wavelengths for the erbium-doped fibre lasers as they still are the most widely applied in telecommunications and several other fields.

Erbium-doped glasses sensitized by Ytterbium have been investigated for the last 30 years [1-5].

Although Yb^{3+}-doped fibre lasers are attractive due to their efficiency, laser emission in other wavelengths requires other dopants. Er^{3+}/Yb^{3+}-doped fibres directly amplify signals within the third telecommunications window, at ~1550 nm. Some of the applications of Er^{3+}/Yb^{3+}–doped fibre amplifiers are found in the distribution of common antenna television (CATV), free-space communications, long-wavelength L-band amplifiers and super-fluorescent sources.

Power level requirements for optical communications are in the region of a few Watts, where Erbium/Ytterbium-doped fibre lasers (EYDFLs) and amplifiers (EYDFAs) are already available. However, Er^{3+}/Yb^{3+}-doped devices can actually deliver even higher power, making them useful for applications like LIDAR and in medicine that benefit from the eye-safe nature of 1550 nm light. Lower efficiency of EYDFs leads to lower

available output powers, compared to those from Ytterbium-doped fibre lasers (YDF's) [6].

7.2 Er^{3+}/Yb^{3+} co-doping scheme

For cladding pumping, the absorption of Erbium is impractically low. Therefore, Ytterbium is added to absorb the pump energy. The Er^{3+}/Yb^{3+} co-doping technique allows pumping of Yb^{3+} ions using broad-stripe high-power pump sources to reach much higher output power levels [10].

Yb^{3+} ions exhibit strong absorption centered at 980 nm and can be pumped over a wavelength range extending from 800-1100 nm. Yb^{3+} excited ions then transfer their energy to Er^{3+} ions as shown in figure 7.1 [9]. The $^2F_{7/2}$ level of the Yb^{3+}, exciting it into the $^2F_{5/2}$ level, absorbs pump photons. From there, a cooperative energy transfer process between the excited state Yb^{3+} and the ground state Er^{3+} in the $^4I_{15/2}$ level excites the Er^{3+} to the $^4I_{11/2}$ level while dropping the Yb^{3+} back to its ground state.

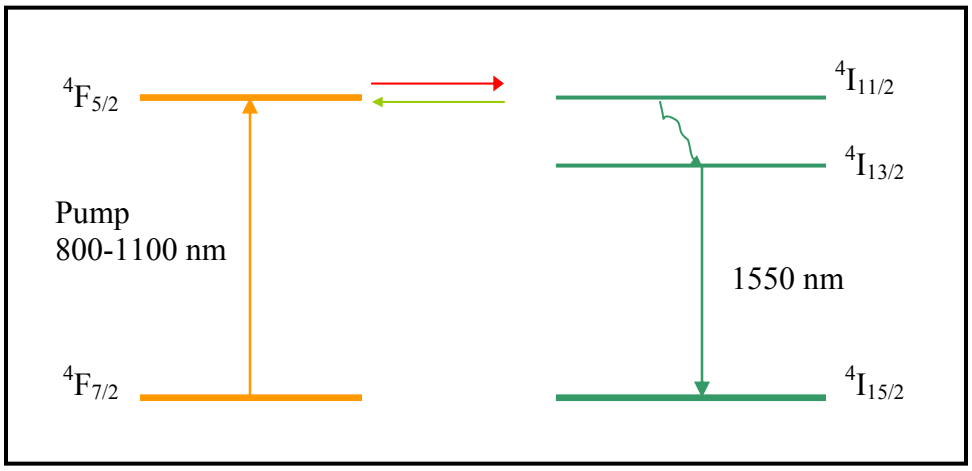

Figure 7.1 Energy transfer from Yb^{3+} to Er^{3+} ions

This co-doping technique offers a broader absorption with a particular high peak at 976 nm, which is reinforced by the fact that high absorption can be maintained even when the Yb^{3+} concentration is low if the Yb^{3+} to Er^{3+} concentration ratio is high. This is particularly advantageous because concentration quenching is much less pronounced in Yb^{3+} than in Er^{3+} [11, 12].

Also, it has been reported that several loss mechanisms deplete the population of the $^4I_{13/2}$ excited state of Er^{3+} such as spontaneous radiative decay, up-conversion and stimulated emission of the signal and the ASE [15, 16, 17]. Some of the Er^{3+} ions are thought to exist in clusters leading to rapid de-excitation of the upper level. This effect seems to depend on glass preparation.

Clustering of Yb^{3+} also occurs and arguably leads to a distributed loss at the pump wavelength. This loss is proportional to the Yb^{3+} absorption spectrum, but is not able to pump the Er^{3+}. Ultimately, this decreases the pump conversion efficiency.

7.3 Novel pumping schemes

One of the main challenges since the first development of fibre lasers back in the 1960's was the approach for launching pump power. Er^{3+}/Yb^{3+}-doped fibre lasers are no exception. While the first Er^{3+}/Yb^{3+} fibres were core pumped with a wavelength of 1060 nm, just recently, cladding pumping in the 920–980 nm band of Ytterbium ions has been used.

Briefly, some of the pumping schemes that have been used in the development of Yb^{3+}-doped and Er^{3+}/Yb^{3+}-doped fibre lasers will be described.

Side pumping: Goldberg and colleagues [18] developed a super fluorescent source with a side-pumped Yb^{3+}-doped double cladding fibre as power amplifier. The side pumping approach is shown in Figure 7.2.

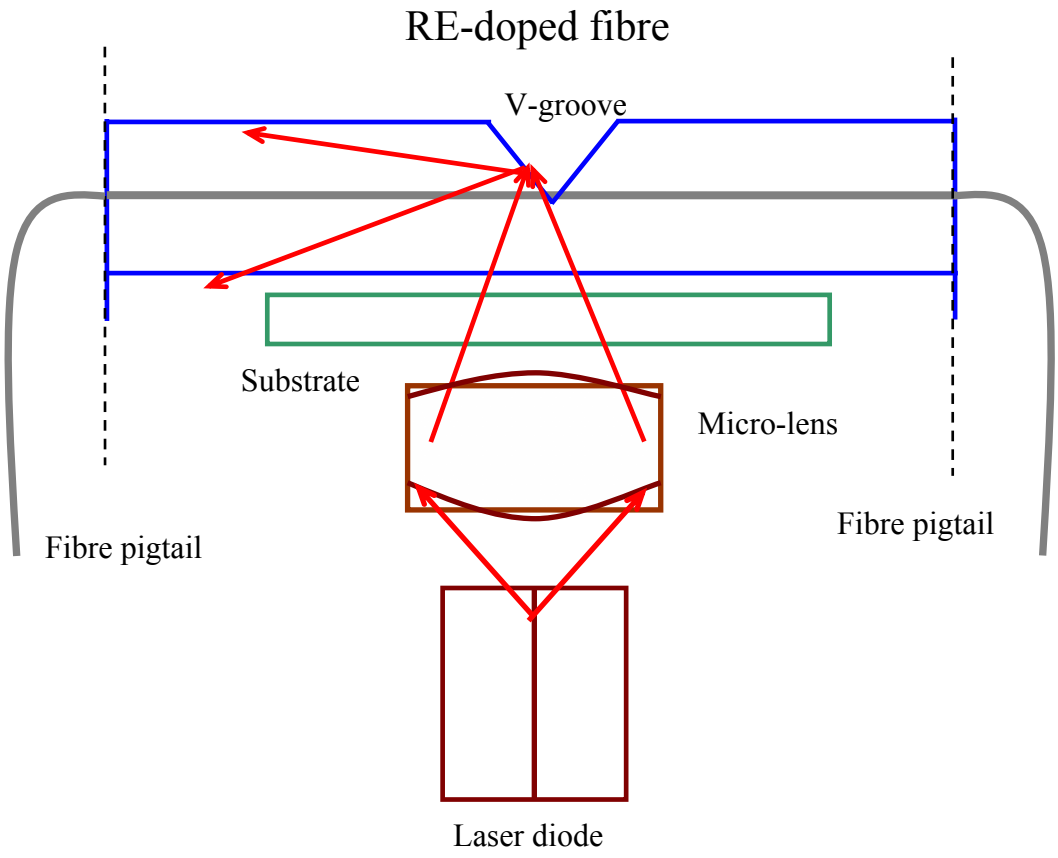

Figure 7.2 Arrangement for V-grove coupling of a broad stripe into the inner cladding of a DCF from [18]

The authors report on a compact, packaged super fluorescent source (SFS) based on an Yb^{3+}-doped double clad fibre (DCF) and a V-grove side-pumping scheme. A maximum of 485mW of amplified spontaneous emission was generated, with a full width half maximum (FWHM) spectral width of 41 nm and a –130 dB/Hz relative intensity noise (RIN).

A diode to fibre pump coupling efficiency of 65% was measured with V-groves made in short pieces of DCF. The main advantage of the V-groove pump-side pumping technique consists in that it leaves the fibre ends free for splicing to other fibres and introduces zero losses to the fibre core. Bonding the DCF to a 250-μm thick, antireflection-coated glass

substrate and then fabricating a 40-μm deep V-grove into the fibre sidewall near one end of the fibre implemented the technique.

Cladding pumping by fibre bundles: Light is coupled from a plurality of semiconductor emitters to a cladding-pumped fibre via tapered fibre bundles fusion spliced to the cladding-pumped fibre. The individual fibre can be bundled together in a close-packed formation, heated to melting temperature, drawn into a taper and then fusion spliced to the cladding-pumped fibre [19].

The taper is then over coated with cladding material such as low-index polymer. A fibre containing a single mode core can be included for the purpose of coupling light into or out of the single mode core of the cladding pumped fibre. Figure 7.3 shows the tapered bundle of MM for pumping a fibre laser.

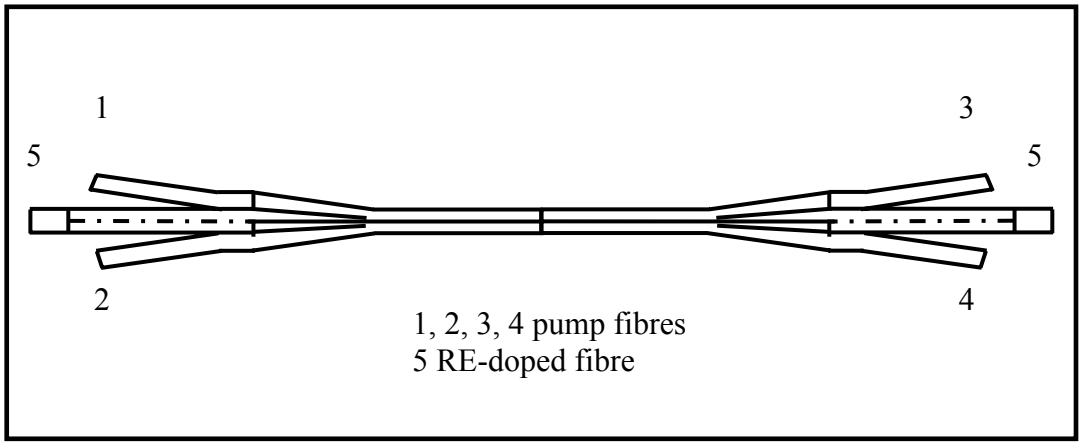

Figure 7.3 Cladding pumping by fibre bundles: Tapered multimode fibres used for pumping a double clad fibre laser from [19]

This approach intends to overcome some of the difficulties that prevent the full exploitation of cladding pumped fibre lasers. Coupling a sufficient number of low brightness sources into the inner cladding of DCFs efficiently is one of them.

One of the disadvantages of the approach is that it requires a number of fine interfaces with associated problems of matching and alignment. Polishing, antireflection coatings and maintenance of precise alignment are also required. Another problem is the coupling of multimode pump light into the inner cladding while simultaneously coupling single mode light into or out of the normally singe mode core.

Once this problem is overcome, one could construct bi-directionally pumped cladding-pumped fibre lasers. Pump energy could be coupled into the inner cladding of both ends of the DCF while single mode fibre laser could be extracted from the core.

Cladding pumping by single clad coiled optical fibres: This technique was implemented by Grudinin et.al. [20] from Southampton Photonics Ltd. in the UK. By combining a highly efficient Yb^{3+}-doped fibre and a glass-air wave-guide for multipoint pump injection, the device length can be reduced to less than 3 m. The single clad-coiled optical fibre-pumping scheme is shown in figure 7.4

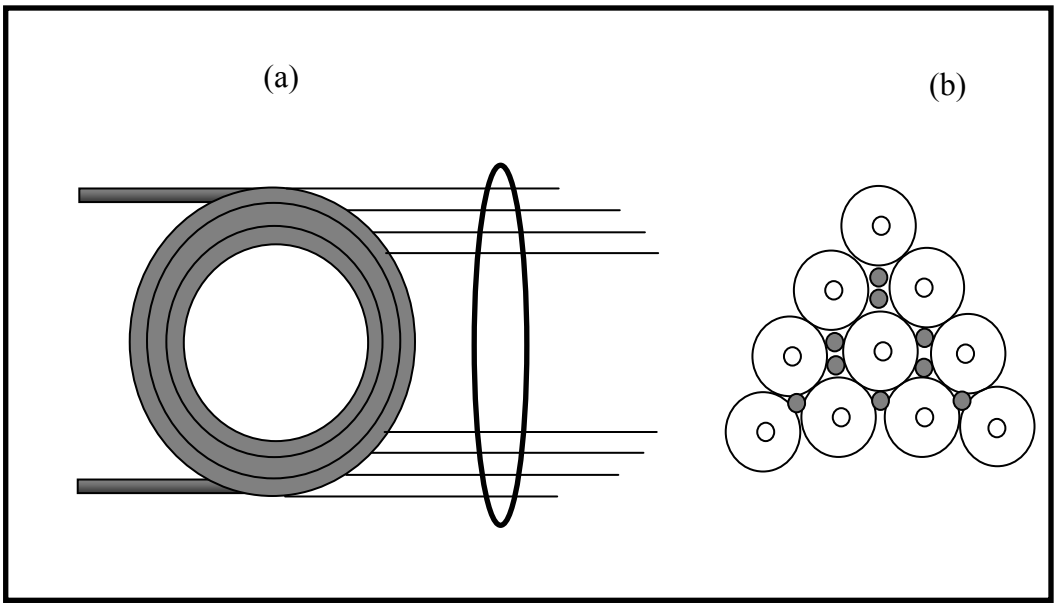

Figure 7.4 Schematic of the single-clad coiled optical fibre pumping scheme from [20]

In this scheme, the pump delivery fibre and doped fibre interact over a relatively long length, which is comparable to the pump absorption length of a normal doped fibre. The fibre design consists of a length of single clad silica fibre with a ~10 μm, ~0.08 NA Yb3+-doped core centered within a ~120 μm cladding.

The fibre surface is coiled into a tightly bounded ring (~5 cm diameter) in such a way that adjacent turns are in close optical contact. Two silica rods of adequate diameter can be implemented for delivering pump power inside the laser coil.

The use of air-glass wave-guide results in a very high NA for pump, which allows great flexibility in choice of pump source as the pump spot size of the beam at the focus can be of about 200-250 μm with NA = 0.3.

7.5 Er^{3+}/Yb^{3+}-doped fibre laser: preliminary results

The double clad fibre used in this preliminary experiment was a 3-m long, double-clad Er^{3+}/Yb^{3+}-doped, multimode fibre with a ~13 μm core and an NA of 0.17. The fibre showed a threshold of 160 mW and a slope efficiency of 49% with respect to absorbed pump power. The maximum output power was 6.2 watts at 1535 nm and a linewidth of 1 nm (FWHM).

7.5.1 Experimental set-up for CW regime

A beam shaper transformed the elliptical output from a high power 915 nm diode bar into a pump beam with nearly equal M^2 value in orthogonal planes and similar divergence. The output was launched into the fibre using dichroic mirrors and anti-reflection coated gradient-index lenses of 25 mm focal length. An incident beam with an NA=0.25 was obtained.

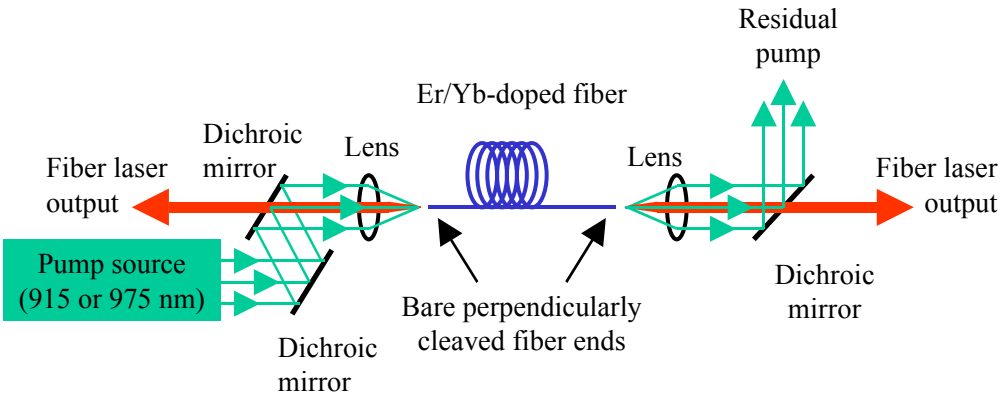

Figure 7.5 Experimental set-up for the CW Er^{3+}/Yb^{3+}-doped fibre laser

7.5.2 Results from a CW Er^{3+}/Yb^{3+}-doped fibre laser

The maximum output power and slope efficiency characteristics obtained from the Er^{3+}/Yb^{3+} fibre are shown in figure 7.6

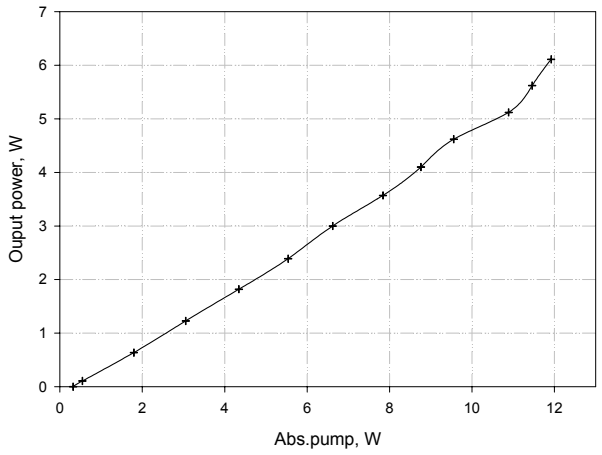

Figure 7.6 Output power and slope efficiency of dual fibre as free-running laser

In this experiment we aimed at efficient absorption of pump light from a broad stripe diode bar. For the continuous wave fibre laser, the cavity consisted of a 3-m long, double-clad Er^{3+}/Yb^{3+}-doped, multimode fibre with a ~13 μm core and an NA of 0.17.

7.5.3 Results from Q-switched Er^{3+}/Yb^{3+}-doped fibre laser

For this first Q-switched fibre laser experiment, we employed the experimental set-up shown in figure 7.7

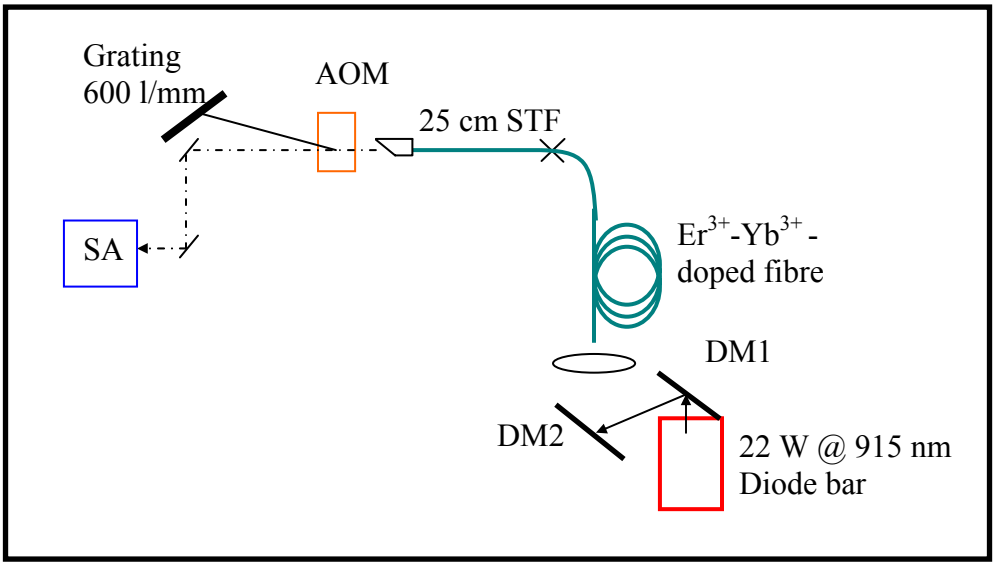

Figure 7.7 Er/Yb Q-switched dual fibre laser experimental set-up

The same beam-shaped 915 nm diode bar was used as a pump source together with two dichroic mirrors to launch power into the Er^{3+}/Yb^{3+} -doped fibre. The fibre length in this case was 3.2 m. The fibre cavity was opened by angle polishing the far end in order to suppress the 4% feedback from the facet.

We then spliced 25 cm of standard telecommunications fibre, which is single mode at 1550 nm in order to avoid pulsing in several modes due to the fact that during preliminary experiments lower energy pulses and higher ASE levels were obtained from the fibre laser.

An acousto-optic modulator (AOM) was used to Q-switch the laser. An external bulk grating with 6600 lines/mm that was mounted on a rotation stage providing the feedback at the desired wavelength and tunability.

The non-diffracted beam from the AOM was also used to extract the spectrum from this end of the cavity, by using an optical spectrum analyzer. The repetition rate for this case ranged from 47 to 136 kHz with measured average powers from 1.98 to 4.23 watts and pulse energy from 31 μJ to a maximum pulse energy of 47 μJ at 73 kHz. Pulse duration ranged from 47 ns to 120 ns. Figure 7.8 shows the results output pulse energy vs. repetition rate.

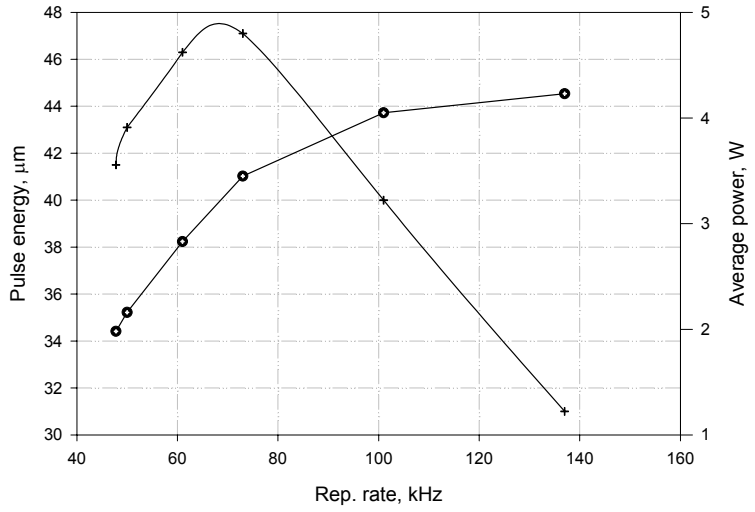

Figure 7.8 Pulse energy and average power as a function of repetition rate

As shown in previous figure, the maximum average power was 4.2 watts for nearly 140 kHz repetition rate. The maximum pulse energy corresponds to an average power of 3.45 W at a repetition rate of 73 kHz. It was observed that for repetition rates lower than 43

kHz amplified spontaneous emission started to build-up and from that point dominating the pulse shape which otherwise was Gaussian-type.

7.5.4. Tuning range

We then investigated the tuning range at a repetition rate of 28 kHz using the same experimental set-up by gradually rotating the bulk grating. The results are shown in figure 7.9

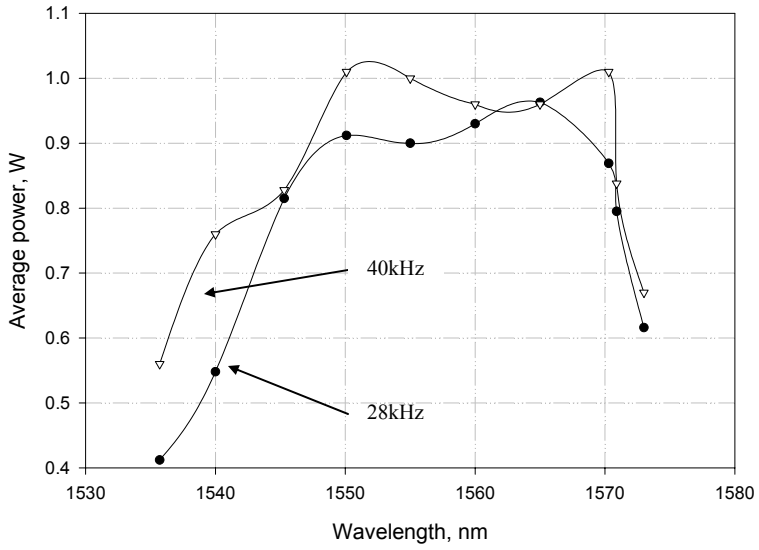

Figure 7.9 Tuning range of Er^{3+}/Yb^{3+} Q-switched fibre laser at 40 kHz. The curve on triangles corresponds to 40 kHz and in circles to 28 kHz.

A tuning range of >35 nm was obtained. Output wavelength ranged from 1540 to 1573 nm with a laser linewidth in the range of 0.1 nm up to 2 nm. It is worth mentioning that

this tuning range was obtained at only 35% of the full pump power available from the diode bar (22 W maximum), i.e. at 8 watts of pump power.

We then repeated the readings for tuning range at the higher repetition range of 40 kHz. The new results show that a broad tuning range can be obtained from this type of Er^{3+}/Yb^{3+} fibre laser.

As can be seen in figure 7.9, the tuning range obtained from the Q-switched fibre laser did not depend strongly on repetition rate, although the output power level changed into higher levels, but the tuning range remained at around 35 nm. For higher repetition rates the tuning range was slightly broader and the pulse width ranged between 88 and 425 ns.

We then investigated Q-switched operation for a particular wavelength of interest. That is 1553 nm suitable for many applications in telecommunications in wavelength division multiplexing (WDM) systems. For instance, we selected 1553 nm as the wavelength of operation of the laser again, by fixing the grating at the right position. We repeated the procedure of varying the repetition rate and measuring average power and pulse width.

For this part of the experiment, we operated with the maximum pump power, ~22 W, from which we were able to launch ~13 W into the 125-μm inner cladding of the fibre. Thus, a 60% launching efficiency was obtained for the experiments described.

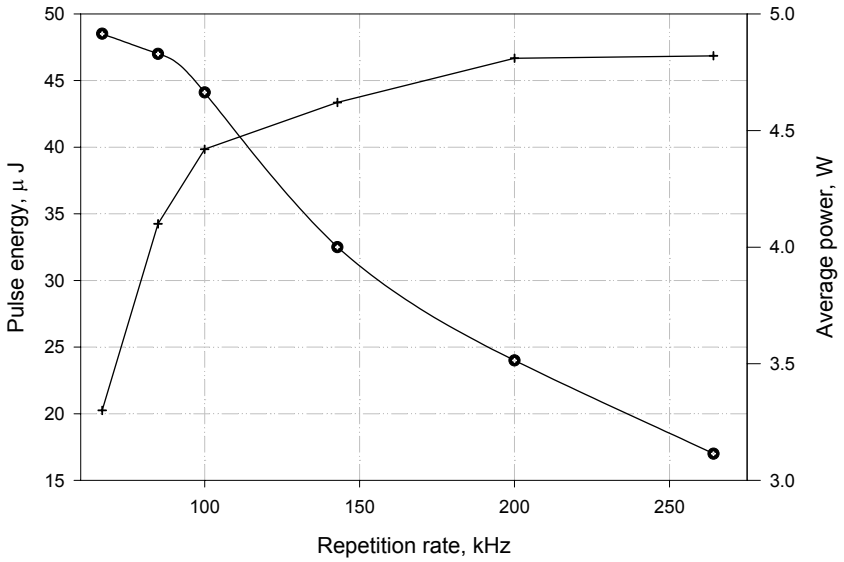

Fig. 7.10 Pulse energy and average power as a function of repetition rate

At this point, the maximum average power was 4.82 watts for a repetition rate of 264 kHz. The maximum pulse energy was 48.5 μJ that corresponded to an average power of 3.3 watts at a repetition rate of 67 kHz. It is clear that there is no obvious difference between pulse energies and average power from figure 7.8 to those of figure 7.10. The main differences are slightly higher pulse energy and average power for also higher repetition rates.

The average output power of the laser, for both cases, increases for high repetition rates because the time-averaged excited state population reduces. Thus this decreases the energy lost due to spontaneous emission, which clearly allows more energy to be generated in the laser modes so the average power up to almost the same level of power obtained for the case of CW operation.

7.5.5 Peak power

In the case of pulse peak power, figure 7.11 shows three different curves for different repetition rates and pulse energies.

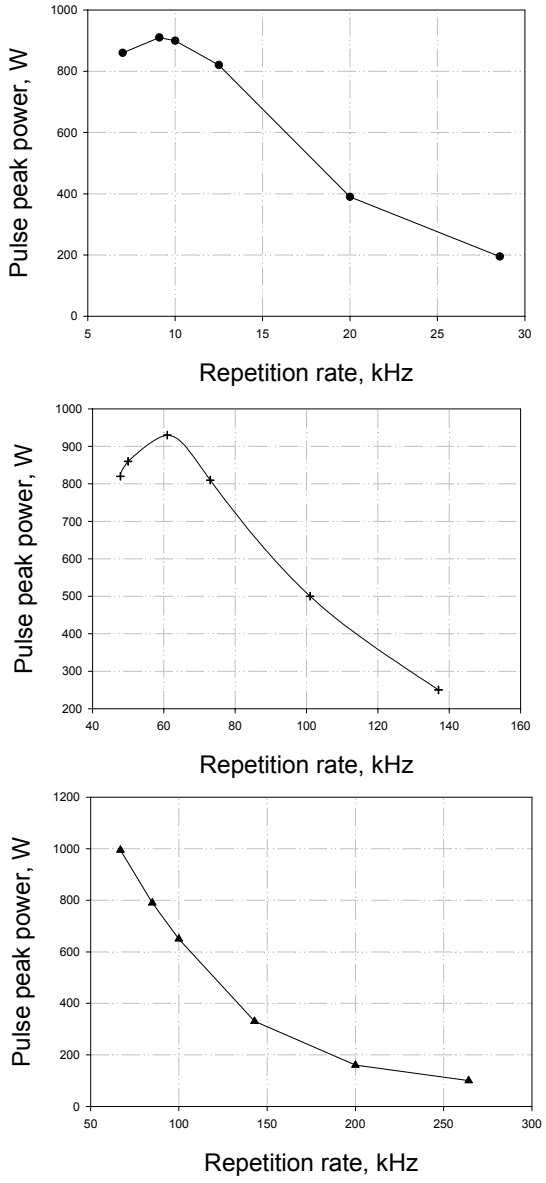

Fig. 7.11 Pulse peak power as a function of 3 ranges of repetition rates

It can be seen from figure 7.11 that the maximum peak power obtained from this fibre laser was 1kW, which is relatively low compared to the ~10kW obtained in the

experiment on which we used the special LMA fibre, designed specifically for high pulse energies, which also lead to very high peak powers.

The same tendency is observed for the three different ranges of repetition rates, i.e., the pulse peak power is high at the beginning of the range and gets lower as the repetition rates increases. The peak power for the maximum repetition frequency of 265 kHz is ~100 W.

7.6 Er^{3+}/Yb^{3+}-doped fibre lasers for higher output powers

In this experiment, the influence of fibre length and pump wavelength in cladding pumped Er/Yb-doped fibre lasers was studied. A number of fibres were fabricated in house for the experiment described in this section. From that set of fibres a conventional DCF with a 12μm in diameter and 0.18 NA core made of phospho-silicate glass, was centered in a circular inner cladding. This core dimensions result in a cut-off wavelength of 2.7μm and five guided modes at 1550 nm.

7.6.1 Fibre characterization

The fibre cavity consisted of two flat cleaved ends of a conventional DCF made in house using the standard MCVD technique. This large core diameter fibre increased the pump absorption and helped reducing the effect of fibre non-linearities such as SRS and SBS. The inner cladding was coated with a low-index UV-curable polymer outer cladding that provided a nominal NA of 0.48.

Short fibres reduce the effect of various non-linear effects such as stimulated Brillouin scattering (SBS). The high absorption of our fibres allowed for a good efficiency and cavity lengths as short as 1.4 – 2 metres. The fibre absorption at 975nm and 915nm was measured to be 2.7 and 2.0 dB/m, respectively.

The absorption of pump modes that have poor overlap over the core is improved by scrambling the inner cladding modes via bending the fibre into a figure of eight or even via setting up the fibre in a "kidney shape" [21]. The resulting absorption spectra of the fibre is shown in figure 7.12

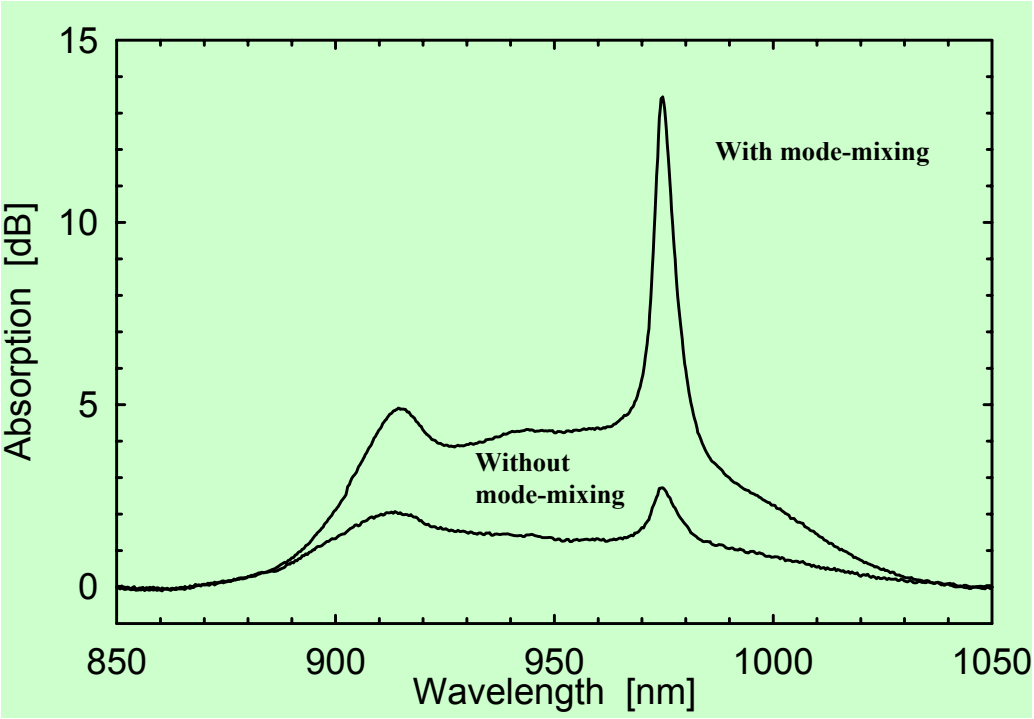

Figure 7.12 Absorption spectra of a 1 m long Er^{3+}/Yb^{3+}-doped fibre

The small signal absorption of the 1-m fibre was increased to 4.9 dB/m at 915 nm and to 13.4 dB/m at 975 nm, by bending it into a figure of eight. The peak absorption at 975 nm is still 5 times larger than the value of same parameter at 915 nm. Most of the transmitted power propagates in those modes with poor overlap with the core, thus these modes are poorly absorbed; although in a fibre with centered core (in a circular inner cladding) some of the lower order modes largely overlap are absorbed over 1 meter.

As mentioned earlier in this work, several fibre geometries help reducing the number of modes with poor overlap with the RE-doped core [22, 23], especially those with non-circular shape.

7.6.2 Experimental Set-Up

The experimental set-up is shown in Fig. 7.13. Slightly different configurations were used, with single-ended pumping at 980 nm or 915 nm (Fig. 7.13a) and double-ended pumping at 915 nm (Fig. 7.13b). For 915 nm pumping, we used beam shaped diode bar while for 980 nm pumping, a Polychrome laser system (Polaroid), combining eight broad-stripe diodes was used.

It is to be noted here that the centre wavelength of the Polaroid diode (980 nm source) shifts from 973 nm at threshold to 981 nm at maximum current. This shift exceeds the linewidth of the 975 nm absorption peak, affecting the total pump absorption. Pump beams were launched into the EYDF via dichroic mirrors and gradient-index lenses. The 4% reflecting bare fibre facets provided feedback for the laser.

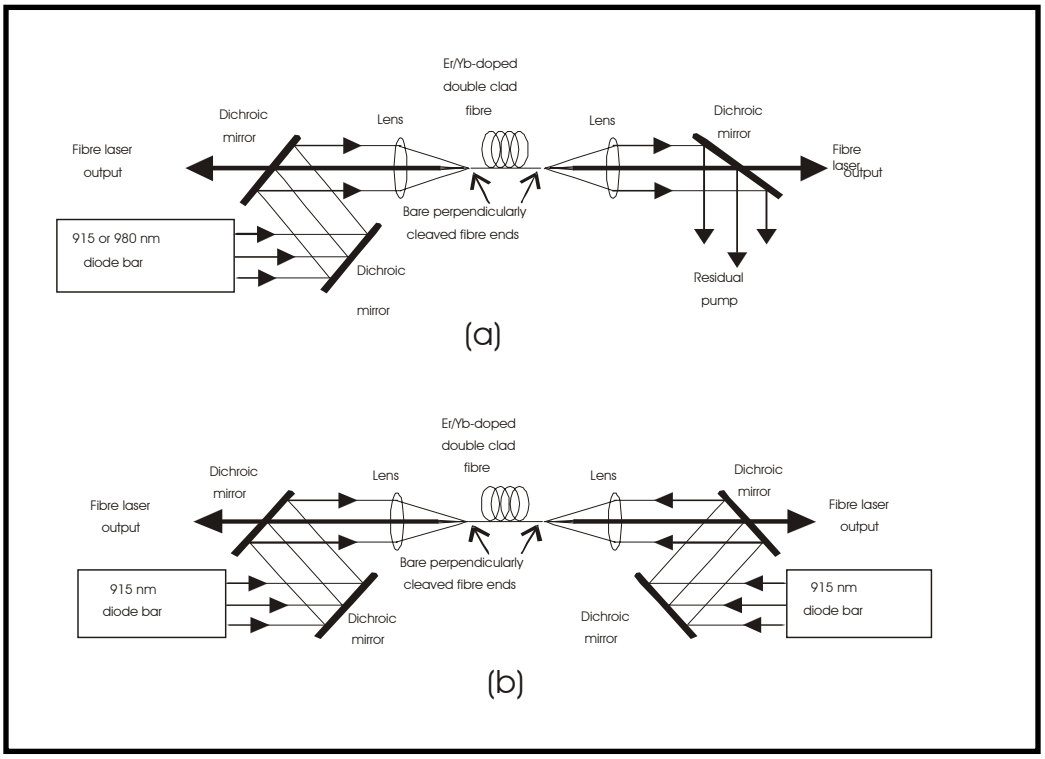

Figure 7.13 (a) Free running laser pumped by single 915 or 980 nm diode bar; (b) Free running laser pumped in opposite ends by two beam-shaped 915 nm diode bars

The output from the fibre laser was thus double-sided. This configuration, which has been used for all the experiments in CW regime described in this work, is suitable for characterization of fibre lasers. For a more practical laser with a single-sided output, we could use a high-reflecting element in one end (e.g., a butted dichroic mirror or a fibre grating).

Alternatively, a 4% reflecting end can be used together with a low-reflecting (e.g., angle-cleaved) fibre end to generate predominantly uni-directional output. The dichroic mirrors at the input and output ends separated the laser output from the pump beams (figure 7.14).

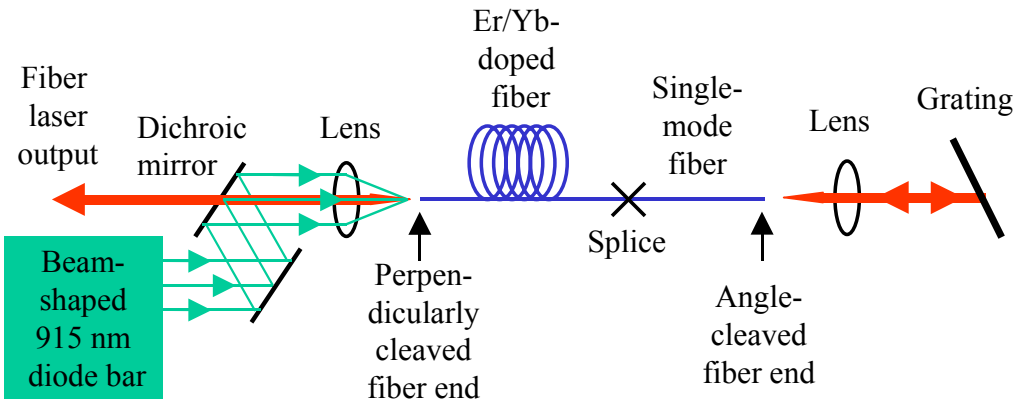

Figure 7.14 Tuneable laser pumped by single beam-shaped diode bar at 915 nm

For the tunable laser regime, single ended-pumping was used. A piece of standard single mode fibre with an 8-μm core was spliced to the far end of the Er^{3+}/Yb^{3+}-doped fibre in order to prevent signal light from being fed back into cladding modes. The losses of this splice were measured to be of less than 1 dB.

An external diffraction grating with 600 lines/mm (blazed for 1550 nm) provided the wavelength selective tunable feedback via an aspheric lens with a 14 mm focal length, from the angle-cleaved end of the SM fibre. The experimental set-up for tunable operation of the Er^{3+}/Yb^{3+} laser is shown in figure 7.14

We consider that a good splice between the EYDF and the single mode one can preserve a single mode operation and finally improve output beam quality. This effect was also studied in [24, 25]. The single-side output was taken from the pump launch and through a dichroic mirror. Furthermore, the usage of single mode fibre splice to the EYDF one protected the gratin from possible damage from high non-absorbed pump power.

7.6.3 Results and discussion

The total CW double-ended laser output power vs. launched single-ended pump power from different lengths between 1.5 and 4 metres with pump power at 915 nm is shown in figure 7.15 (a). In the same figure, the same output power for a 1.4 m fibre with pump power at 980 nm is also shown.

The slope efficiency of the 1.5 metres laser pumped at 915 nm was lower than that of longer fibres because of likely lower or incomplete pump absorption. The slope efficiency then increased before it gradually decreased again for longer fibres. The highest output power 6.0 W, which was reached with both 2 and 2.5 m long fibres. This decrease is attributed to the fact that excess losses start to surpass the benefits of increased pump absorption.

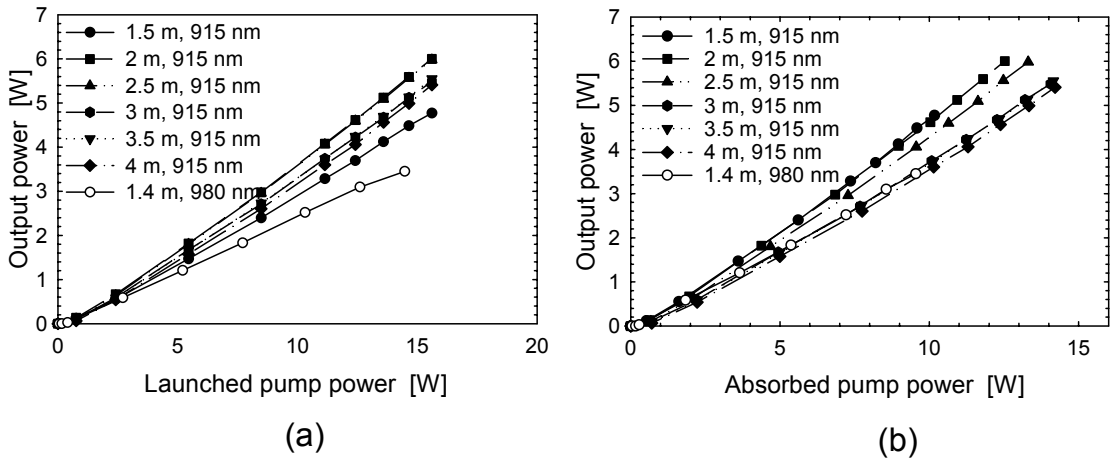

Figure 7.15 (a) Double-ended output power vs. launched pump power; (b) double-ended laser output power vs. absorbed pump power. Both curves were obtained with single-ended pumping at 980 and 915 nm

It must be noted that the 1.5 m fibre laser emitted at 1542 nm and 1536 nm simultaneously. The wavelength of operation for longer fibre shifted to the range between 1550 and 1560nm, which was attributed to increased Er^{3+} re-absorption. The lasers

showed better performance with a 915 nm pump than with pump at 980 nm. At the latter pump wavelength, the maximum output power was 3.5 W for a simultaneous wavelength of operation at 1536 nm and 1542 nm.

Figure 7.15 (b) plots the double-ended laser output power vs. absorbed pump power. The shortest fibres now have the highest slope efficiency with 915 nm pump power. This is due to the fact that excess propagations losses would be smaller in a shorter fibre.

It is worth mentioning that the normal cut-back technique that has been used in all our previous experiment to directly measure the launched pump power, proved to be impractical in this case due to the high absorption of EYDF of this experiment. For that reason the launched pump power on an un-doped, identical fibre with a length of ~1 metre was measured. The reflection loss at the fibre facet was compensated for the measurements.

The measurement of launched pump power in a ~1m long fibre is arbitrary due to the fact that pump power decreases over 1 metre even for un-doped fibres. Furthermore, pump modes near cut-off have a large loss over 1 metre of EYDF fibres. Thus, the different loss of different pump modes needs to be taken into account in a more precise characterization of these fibres.

The slope efficiency with respect to launched pump power peaked for fibre lengths of 2 and 2.5 m, with 40% being the maximum value. For 1.2 – 2 m long fibre laser cavities, the slope efficiency with respect to absorbed pump power reached a maximum value of 50%. Then, it decreased down to 41% for a longer 4-metres fibre. The slope efficiency with respect to absorbed pump power for the 1.4 metres fibre and the 980 nm pump source described previously was 38%.

It is also worth to note that we would normally expect higher efficiencies for 980 nm pump than with 915nm. In our case we must say that we do not have an explanation of why the lasers pumped with 980 nm sources were less efficient than those pumped with

energy at 915 nm. Nevertheless, the 980 nm pump energy interacts more strongly with the gain medium than the 915 nm pump energy. Non-linear loss mechanisms such as cumulative transfer could be expected to have an in impact with 980 nm pumping [26].

Tuning characteristics of EYDF laser using the same fibre were then investigated. For that, 25W of pump power from a single beam-shaped 915 nm diode bar were launched into a 3.3-m long EYDF. A variation in output power of less than 3 dB over a wide range of the Erbium gain band was obtained. This tuning range, of ~67 nm, was observed from 1533 to 1600 nm.

A much narrower linewidth was obtained with the tunable fibre laser than that with the free-running laser. It was always of less than 0.25 nm and constant over the whole tuning range.

The maximum output power was 6.7 W at 1550 nm with a pump to signal conversion efficiency of 27%. A reduction of conversion efficiency is attributed to losses at the diffraction grating and to fibre back coupling losses in comparison to the conversion efficiency of the CW laser.

A comparatively longer fibre is required to absorb higher pump powers. As a consequence, in our experiment, the wavelength of operation shifted from the intrinsic peak at 1535nm up to 1550 nm.

Although, typical tuning curves presented in previous chapters for fibre lasers tend to be relatively flat and drop at the edges of the tuning range, the tunable fibre laser presented in this section differed from that. Its tuning curve shown in figure 7.16 shows how the power drops for wavelengths larger than 1560nm.

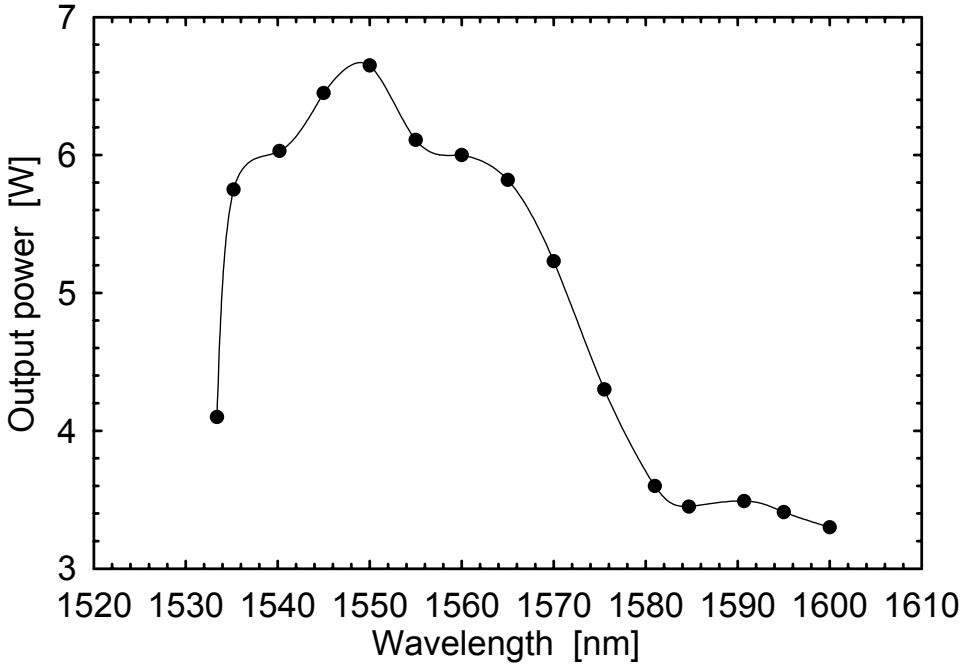

Figure 7.15 Tuning characteristics of a multi-moded, 3.3m EYDF laser: 67 nm tuning range (3 dB), maximum output power of 6.7 W

With respect to temporal behavior of the laser studied in this chapter, it was monitored using a fast InGaAs photodiode. Power fluctuations of less than 10% were observed leading to an acceptable temporal stability throughout the whole tuning range.

7. 7 Conclusions

In this chapter we presented results on Er/Yb-doped fibre laser capable of generating ~6 W of average power when operated in CW regime. The same fibre laser is capable of generating high-energy pulses close to 50 μJ per pulse at a repetition rate of ~65 kHz. The pulse energy is lower than that reported in Chapter 7. However, considering the much simpler design of the Er/Yb-doped fibre and tenability of such a source between 1535 and 1553 nm, and the fact that a tuning range of 35 nm was obtained, it represents

an interesting option for several applications in the telecommunications area. In addition, we demonstrated average powers close to 5 W (50 (J pulse energy) under Q-switched, single mode operation by splicing a25 cm length of standard telecommunications fibre.

In the second part of the investigation of Er^{3+}/Yb^{3+}-doped fibre lasers we have developed and described cladding-pumped fibre devices with slope efficiencies of up to 50% with pump power at 915 nm and 38% with pump power at 980 nm, both with respect to absorbed pump power. An output power of 16.8 W was obtained when pumping the laser from both ends with two 915-nm beam-shaped diode bars. High non-linear thresholds for short devices lengths were obtained due to the high pump absorption showed by our cladding-pumping lasers. Non-linear degradation can be suppressed by developing fibre lasers with characteristics mentioned previously, especially convenient with high-power cladding-pumped fibre amplifiers.

References to Chapter 7

7.1.1 Snitzer E. and Woodcock R., "Yb^{3+}- Er^{3+} glass laser", Appl. Phys. Lett., Vol.6, pp. 45-46, (1965)

7.1.2 Gapontsev V.P., Matitsin S.M., Isineev A.A., Kravchenko V.B., "Erbium glass lasers and their applications", Opt. Laser Technology, Vol. 14, pp. 189-196, (1982)

7.1.3 Tacheo S., Sorbello G., Longhi S., Laporta P., "Measurement of the energy transfer and up-conversion constants in Er^{3+}/Yb^{3+}-doped phosphate glass", Opt. Quantum Electronics, Vol. 31, pp. 249-162, (1999)

7.1.4 Hwang B.C., Jiang S., Luo T., Watson J., Sorbello G., Pyghambarian N., Cooperative up-conversion and energy transfer of new high Er^{3+}- and Yb^{3+}- Er^{3+}-doped phosphate glasses", J. Opt. Soc. Am. B, Vol. 17, pp. 833-839, (2000)

7.1.5 Francini R., Giovenale F., Grassano U.M., Laporta P., Tacheo S., "Spectroscopy of Er^{3+} and Er^{3+}/Yb^{3+}-doped phosphate glasses", Opt. Mater., Vol.13, pp. 417-425, (2000)

7.1.6 Dominic V., MacComarck S., Waarts R., Sanders S., Bicknese S., Dohle R., Wolak E., Yeh P.S., Zucker E., "110-W fibre laser", Electronics Letters, Vol. 35 No. 14, 1158-1160, (1999)

7.1.7 Vienne G.G., Caplen J., Liang D., Minelly J.D., Nilsson J. and Payne D.N., "Fabrication and Characterization of Yb^{3+}:Er^{3+} phosphosilicate fibres for lasers", J. Lightwave Technology, Vol. 16, No. 11, pp. 1990-2001 (1998)

7.1.8 Townsend J.E., Poole S.B. and Payne D.N., "Solution doping technique for fabrication of rare earth-doped optical fibres", Electron. Lett. Vol. 23, pp. 329-331, (1987)

7.1.9 Vienne G., "Fabrication and characterisation of ytterbium:erbium co-doped phosphosilicate fibres for optical amplifiers and lasers", PhD dissertation, University of Southampton (1996)

7.1.10 J.D. Minelly, W.L. Barnes, R.I. Laming, P.R. Morkel, J.E. Townsend, S.G. Grubb, D.N. Payne, "Diode-array pumping of Er/Yb co-doped fibre lasers and amplifiers", IEEE Phot. Tech. Lett., Vol. 5, No.3, (1993)

7.1.11 Paschotta R., Nilsson J., Barber P.R., Caplen J.E., Tropper A.C., Hanna D.C., Opt. Comm., Vol.136 (5-6) pp.375-78, *(*1997)

7.1.12 P.M. Meters, D.L. Veasey, D.S. Funk, N.A. Sanford, S.N. Houde-Walter, J.S. Hayden, "Ion-exchanged Er/Yb glass waveguide lasers in silicate glasses", Advanced Solid State Lasers - Technical Digest OSA, pp. 160-162, (1999)

7.1.13 Galant E.I., Kalinin V.N., Lunter S.G., Mak A.A., Przhevuskii A.K., Prilezhaev D.S., Tolstoi M.N., Fromzel V.A., "Stimulated emission from laser-pumped ytterbium- and erbium-activated glasses", Kvant. Elektron. (Moscow), Vol.3 pp. 2187-2196 (1976), [Sov. J. Quantum Electron., Vol. 6, pp. 1190-1195, (1976)]

7.1.14 Mursin A.G., Fromzel V.A., "Maximum gains of laser-pumped glasses activated with Yb^{3+} and Er^{3+} ions", Kvant. Elektron. (Moscow), Vol.8, pp. 495-503 (1981), [Sov. J. Quantum Electron., Vol. 11, pp. 304-308, (1981)]

7.1.15 Karasek M., Kanka J., "Numerical analysis of Yb^{3+}-sensitised, Er^{3+}-doped, fibre-ring laser", IEE Proc. Optoelectron. Vol. 145, pp. 133-137, (1998)

7.1.16 Becker P.C., Olsson N.A., Simpson J.R., *Erbium-doped fibre amplifiers, fundamentals and technology*, Academic Press, USA (1999)

7.1.17 Maurice E., Monnom G., Dussardier B., Ostrowsky D.B., "Clustering effects on double energy in heavily ytterbium:erbium-codoped silica fibres", J. Opt. Soc. Am. B, Vol. 13, pp. 693 (1996)

7.1.18 Goldberg L., Koplow J.P., Moeller R.P., "High-power superfluorescent side-pumped Yb^{3+}-doped double-cladding fibre", Optics Letters, Vol. 23, No. 13, pp.1037-1039, (1998)

7.1.19 DiGiovanni D., "Tapered fibre bundles for coupling light into and out of cladding-pumped fibre devices", US patent number 5864644, January (1999)

7.1.20 Grudinin A.B., Turner P.W., Nilsson J., Payne D.N., "Air-clad coiled fibre lasers and amplifiers", submitted for patent (pending), (2001)

7.1.21 Chen Z.J., Minelly J.D., Dong L., Vienne G.G., Payne D.N., "Efficient cladding-pumped Er^{3+}/Yb^{3+}-doped fibre amplifier and bending effect in cladding pumping scheme", CLEO Europe'96, paper CThL3, (1996)

7.1.22 Zellmer H., Tünnermann, Welling H., Reichel V., "Double clad fibre laser with 30 W output power", in Optical Fibres and Their Applications, OSA Trends in

Optics and Photonics, Vol. 16, Zervas M.N., Willner A.E. and Sasaki S. eds., pp. 199-202, Optical Society of America (1996)

7.1.23 Muendel M., "Optimal inner cladding shapes for double-clad fibre lasers", in Proc. Conference on Lasers and Electro-optics, paper CTuU2, USA (1996)

7.1.24 Fermann M.E., "Single mode excitation of multimode fibres with ultra-short pulses", Opt. Lett. Vol. 23, pp. 52-54, (1998)

7.1.25 Alvarez-Chavez J.A., Grudinin A.B., Nilsson J., Turner P.W., Clarkson A., "Mode selection in high power cladding pumped fibre lasers with tapered section", in CLEO Technical Digest, pp.247-248 (1999)

Digonnet M., "Rare-earth doped fibre lasers and amplifiers", Marcel-Dekker, USA (1993)

Chapter 8

Conclusions and Future Work

Rare earth-doped glass and crystal fibre lasers were first investigated experimentally as earlier as the 1960's, then in the 70's and in the early 80's. They have, since recent years, received considerable attention due to their numerous applications in sensing, medicine, optical communications, material processing, imaging, and laser ranging, just to mention a few.

The basic principle behind these devices is the use of a double clad structure, which consists of the active core of the fibre being surrounded by the normally not circular and relatively large cladding. The already available pump power from diode bars and broad stripe laser diodes can then be launched into the cladding and absorbed by the core, which normally is a few microns in diameter.

This pumping scheme has allowed fibre lasers to reach the mature technology and commercial status they have today. Up to 272 Watts of continuous power at 1060 have been reported [1] for an Ytterbium-doped fibre laser developed at the University of Southampton and 203W of CW output power has been demonstrated at 1565nm within the same group in collaboration with Southampton Photonics Inc. [2]. As for Q-switched fibre lasers, for instance in this work an Yb^{3+}-fibre delivered up to 2.3 mJ energy per pulse at around 500 Hz [3] and 7.7mJ of pulsed energy were obtained from a larger mode area Yb^{3+}-doped fibre [4]. With this level of average powers and energies, fibre lasers are now considered a mature technology.

In this chapter, key results, advantages and disadvantages of double clad fibre lasers, the cladding pumping technique, basic characteristics and important factors that affect double-clad fibre lasers and their operation are described. A summary and conclusions of the work carried out for the development of high-power, cladding-pumped, rare earth-doped fibre lasers and amplifiers are also provided.

Some ideas about further work that could be done in the High-Power Fibre Lasers Group of the Optoelectronics Research Centre at the University of Southampton are described.

8.1 Summary and key results

Main results obtained during my PhD study can be summarized as follows:

1) Both continuous and pulsed regimes of operation of Yb^{3+}-doped fibre lasers have been studied with different double clad fibres.

2) An Yb^{3+}-doped, 6.8-W polarised output fibre laser was experimentally studied. The laser was tuneable within the range of 1070-1106 nm. These results are very important for future experiments on which we should aim to obtain laser power at 633 and 540 nm.

3) A high power laser with tapered section was investigated. The taper was fabricated in the Yb^{3+}-doped fibre itself to improve brightness of the source. The device presented low losses and improved beam quality. A three times increase of intensity was obtained with a power penalty of 1 dB.

4) In Q-switched regime, energy levels obtained from tapered fibre lasers were comparable with results from large core area fibres. Maximum energy extracted from an LMA fibre reached 7.3 milli Joules at <500 Hz with pulse durations of ~100 ns. We think this is another interesting result for this thesis.

5) High energy, high average power pulses from Er^{3+}/Yb^{3+}-doped fibre lasers were obtained. Among these, pulsed fibre lasers with ~5W average power (for relatively low pulse energies of 50 μJ) at both 52 and 64 kHz repetition rate were developed. The peak power level obtained was ~1000W from different experiments.

6) In later results on Er^{3+}/Yb^{3+}-doped fibre lasers, a maximum output power of 16.8W CW was obtained. The laser was pumped using two 915nm diode bars.

No rollover of the laser output power was observed, which suggests higher output power possible. The laser showed a slope efficiency of 50% with respect to absorbed pump power. We consider this experiment an illustration of power capabilities of our co-doped lasers. The maximum output power obtained represents the highest reported so far for these types of devices. A tuning range of >60 nm was also obtained with this fibre. It ranged from 1530nm to ~1600nm. The linewidth of the output was 0.3 nm over the whole tuning range.

8.2 Future prospects

Our future work should probably be directed into the application of new pumping schemes such as pumping via fibre bundles, proposed by A.B. Grudinin [1]. It demonstrated to provide efficient pump coupling from pump fibre into the RE-doped ones. One should be able to demonstrate higher output powers in CW regime than our latest result of 21W if we pump an efficient Yb^{3+}-doped (HD465) fibre, using the referred scheme.

In terms of tapers, we should investigate into the effect of bending our tapers. That could out-couple higher order modes from the cavity and provide a higher beam quality.

The single polarization Yb^{3+}-doped fibre laser should be employed in frequency doubling experiment. It demonstrated to have ~6 W of single polarization and temporal stability, which should be enough as an input for a non-linear crystal and generated light in the visible.

Finally, pumping a dispersion compensated and/or dispersion shifted fibre with our 22W Yb^{3+}-doped fibre laser should represent an interesting experiment for efficient generation of Stokes waves at a broad range of wavelengths.

References

8.1 Jeong Y., Sahu J.K., Williams R. B., Richardson D.J., K. Furusawa K. and Nilsson J., "Ytterbium-doped large-core fibre laser with 272W of output power", Electronics Letters, accepted.

8.2 Sahu J.K., Jeong Y., Richardson D.J. and Nilsson J., "A 103 W erbium/etterbium co-doped large-core fibre laser", Optics Communications, submitted.

8.3 J.A. Alvarez-Chavez, H.L. Offerhaus, J. Nilsson, P.W. Turner, W.A. Clarkson, and D.J. Richardson, "High energy, high power Ytterbium-doped Q-switched fiber laser", Optics Letters, Vol. 52, No. 1, pp. 37-39, January (2000)

8.4 Renaud C. C., Alvarez-Chavez J. A., Sahu J. K., and Nilsson J., "7.7 mJ pulses from a large core Yb^{3+}-doped, cladding pumped, Q-switched fibre laser", Conference of Lasers and Electro-optics, Baltimore USA, paper CtuQ5 (2001)